Freie Universität Berlin

Thermodynamic study of dendritic polyglycerol sulfate interacting with proteins

DISSERTATION

zur Erlangung des akademischen Grades des

Doktors der Naturwissenschaften (Dr. rer. nat.)

eingereicht im Fachbereich Biologie, Chemie, Pharmazie

der Freien Universität Berlin

vorgelegt von

Qidi Ran

aus Sichuan, China

June 2018

Declaration

This dissertation was performed from April 2014 to March 2018 in the group of Prof. Dr. Rainer Haag at the Institute of Chemistry and Biochemistry of the Freie Universität Berlin, in collaboration with the group of Prof. Dr. Matthias Ballauff at the Helmholtz-Zentrum Berlin.

Hereby I declare that this dissertation has never been submitted for any other degree or qualification. I certify that this dissertation is written by myself and the contents are original except citation of other people's work.

_____

Date and Signature

1st Reviewer: Prof. Dr. Rainer Haag, Freie Universität Berlin
2nd Reviewer: Prof. Dr. Matthias Ballauff, Helmholtz-Zentrum Berlin and Humboldt-Universität zu Berlin

Location of Defense: Room 36.07, Takustr. 3, 14195 Berlin
Date of Defense: 31.05.2018

Acknowledgements

First I would like to thank Prof. Dr. Rainer Haag for offering me a doctoral position in his group. My first lecture in Germany for a master degree was given by him and I remember his passion and clear thoughts as a lecturer. As the first supervisor for my thesis he gave me very pertinent and inspiring suggestions in everytime of my presentaion and our discussion. Moreover, he always encourages the group members to communicate with each other and help each other, which benefits not only in scientific thinking, but also in my future career.

Secondly, I sincerely thank Prof. Dr. Matthias Ballauff who co-supervised my research at the Helmholtz-Zentrum Berlin. I joined his group since my master lab course in 2012. That's when and ever since I learned from him that doing research should put the foot down and always think with logic. During my four-year thesis, he not only kept strict with experimental details, but also broadened my horizon with his knowledge and discussion on literature. Moreover, he taught me a lot about scientific writing.

I'm very thankful to my collaboration partners Prof. Dr. Joachim Dzubiella and Dr. Xiao Xu. They provided a deep understanding from the theory perspective, which complemented the experiments. We had many intense discussions on science which I will not forget. During our work together, I learned from them the diligence and enthusiasm to devote to one's interest.

I thank Dr. Pradip Dey, a former colleague in the Haag group, for synthesizing the polymer materials I used and being supportive during my writing. I thank Rohit Nikam from Prof. Dzubiella's group for doing the all-atom simulations in our publication.

Also I would like to acknowledge Prof. Dr. Yan Lu at Helmholtz-Zentrum Berlin who gave much support on scientific discussion and in the lab as well.

I'm grateful to my former colleague and good friend Dr. Shun Yu who gave me very helpful suggestions on my research.

Moreover, I appreciate all the colleagues in the Haag group and Ballauff group. I enjoyed every group activity and discussion with them. Especially, I thank our subgroup of Multivalency for providing such warm atomsphere and my Chinese friends in the Ballauff group who took care of me in daily life.

I want to thank Dr. Qiang Wei, a graduate from Haag group, who gave me much guidance and advices at the beginning of my thesis.

I acknowledge Dahlem Research School for financial support of my four-year research.

Finally, I deeply thank my parents and family far in China who are always supportive for my work and decisions. Especially, I thank my father for talking with me about my career and helping me get through all the hard moments in life.

Table of contents

1 Introduction

1.1 Polyelectrolytes in solution

1.1.1 Natural and synthetic polyelectrolytes

Polyelectrolytes are polymeric molecules with ionic and/or ionizable groups [1]. There are many natural polyelectrolytes in organisms that possess vital functions in biological activities (see Fig. 1). The most important species are nucleic acids (DNA and RNA) that carry and translate genetic information. Each monomer, i.e. nucleotide, has a phosphate group positioning outside along the helix, which renders nucleic acids highly negative. Another important class of polyelectrolytes are proteins that comprise negatively and positively charged amino acids. Proteins are versatile compounds in organisms that function as enzymes, antibodies, and carriers. The sequence and folding of a protein determine its isoelectric point and thus respective net charge at a specific pH. Fig. 1(b) shows the molecular structure of lysozyme at pH 7. The charged amino acids are not homogeneously distributed thus proteins cannot be treated as point charges but consist of both positive and negative patches. Even proteins with the same net charge can behave differently depending on the charge distribution. Moreover, there are many polymeric molecules with unconstrained structure. For example, heparin which is known as the biomolecule with the highest negative charge density [2] is a glycosaminoglycan with sulfate and carboxylate functional groups. The flexible structure and a specific

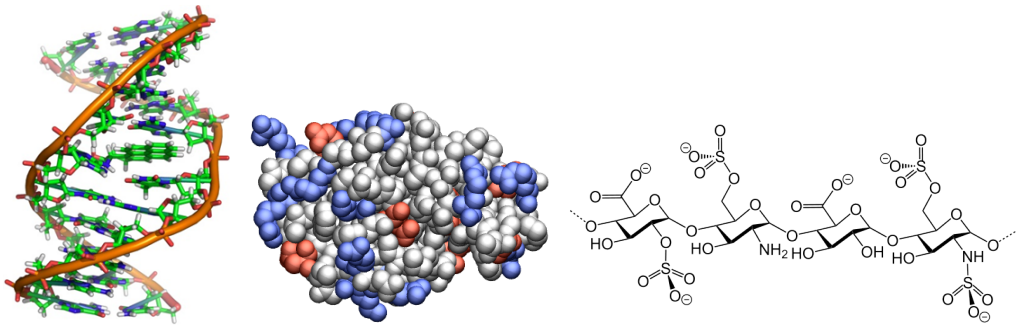

Figure 1: Examples of natural polyelectrolytes: (a) double-helix structure of deoxyribonucleic acid (DNA); (b) representation of lysozyme (PDB:2LZT) generated by the VMD software (coloring method: ResType; drawing method: VDW). Basic, acidic, and neutral amino acids are marked blue, red, and white beads, respectively; (c) chemical structure of the biomolecule heparin.

pentasaccharide sulfation sequence are responsible for its anticoagulant property via binding to stabilize the complex with antitrombin [3].

In the last decades synthetic polyelectrolytes have been developed with various structures including linear, branched, and complex nanoparticles [4–8]. Different functional groups confer charges on the polyelectrolyte surface. For example, polyvinylamine (PVAm), poly-L-Lysine (PLL), and polyethylenimine (PEI) are positive charged polymers with amine or imine functional groups. Poly(styrene sulfonate) (PSS) and poly(acrylic acid) (PAA) are negative with sulfonate and carboxylate side group, respectively. Negative polymers do not interrupt the structure of cell membrane. Furthermore, polymers with a charged surface can bind with biomolecules via electrostatic interaction as compared to neutral ones. Hence, they are designed with applications in biomedicine as therapeutic agents and drug carriers [9–11].

1.1.2 Counterion condensation

Ion distribution on the polyelectrolyte surface is an important characteristic that determines its surface potential and interaction with surrounding molecules. Charge renormalization by counterions is a fundamental concept for highly charged polyions. This phenomenon of counterion condensation was first formulated for charged cylinders by Manning in late sixties [12, 13] and observed in many polyelectrolyte solutions [14–20].

For a polyelectrolyte in ionic solution, the excess free energy of the system consists of small ion-small ion and polyion-small ion interactions in the Debye-Hückel approximation [21]. When the charge density is high enough, the unscreened Coulomb interaction between the polyion and small ions is strong. In that case, the counterions will "condense" on/in the polyion to weaken the polyion-small ion interaction, which brings a binding free energy and an entropy loss into the excess free energy of the system. The conterion condensation will take place until the total excess free energy of the system reaches the minimum [21], which corresponds to the following critical value for a rodlike polyelectrolyte

$$\xi = \frac{e^2}{\varepsilon k_{\mathrm{B}} T b} = 1. \tag{1}$$

ξ is the linear charge density parameter and b is the linear spacing between adjacent charges. The Bjerrum length $b = \frac{e^2}{\varepsilon k_B T}$ is then the critical charge spacing for a certain solvent at specific temperature. For instance, the Bjerrum length is $b = 7.135$Å in water at 25 °C [12]. When two monovalent backbone charges have a distance shorter than the Bjerrum length ($\xi > 1$), counterions bind to the backbone charges in sufficient degree until the "effective" charge density of the polyelectrolyte becomes one elementary charge per Bjerrum length [22]. On the contrary, when the charge spacing is larger than that ($\xi < 1$), no condensation occurs.

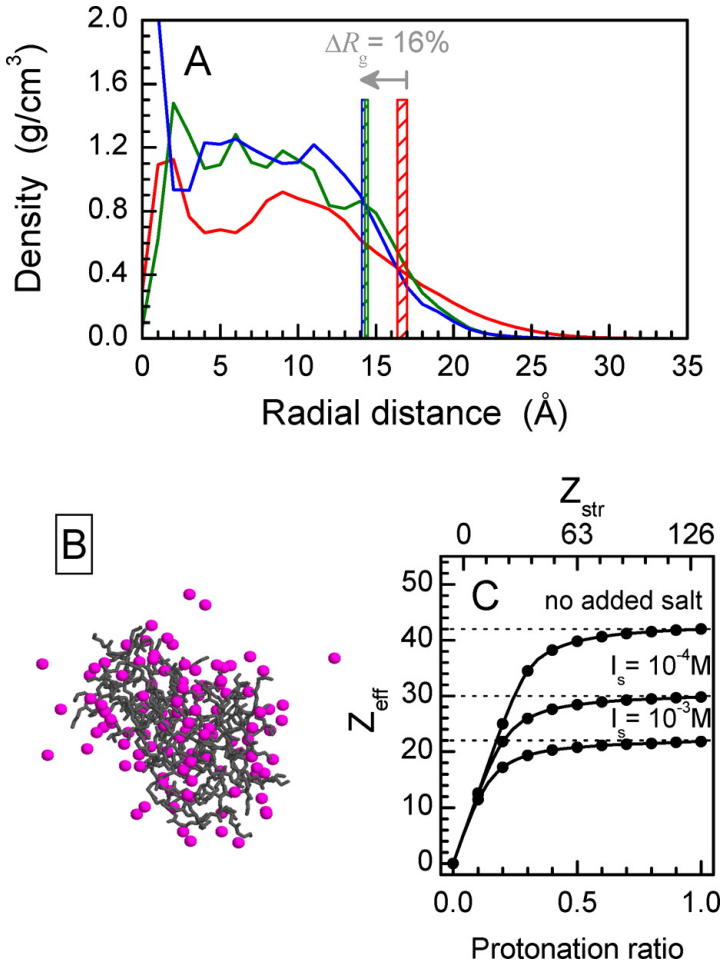

Figure 2: (A) Density of PAMAM-G4 scaffold along the radius by molecular dynamics simulations at non-charged (blue curve), half-charged (green), and all amines charged (red) states. The vertical bars mark the radius of gyration R_g for each protonation state. (B) Simulation snapshot of the fully charged PAMAM-G4 dendrimer with condensed counterions (magenta beads). (C) Estimated effective charge for PAMAM-G4 as a function of the protonation ratio and ionic strength [23].

Counterion condensation changes the properties of polyelectrolytes [24–26]. The molecular conformation, mobility, radius of gyration, and effective charge of dendrimers

with bound ions have been investigated by both experiments and computer simulations [14–16, 27–30]. Polyamidoamine (PAMAM) is a well-studied cationic dendrimer at neutral and low pH [31, 32]. Compared to neutral and partially charged dendrimers, the fully charged PAMAM-G4 dendrimer swells due to counterion uptake, which brings a larger R_g (see Fig. 2A). Besides, counterions penetrating from the dendrimer surface to the interior greatly reduce the effective charge from its structural charge with more added salt (see Fig. 2C). This effect of charge renormalization is more pronounced for higher generations [33].

Condensed counterions play important role in the interaction between polymeric electrolytes and biomolecules. The polycation PAMAM dendrimer is designed for gene delivery based on electrostatic attraction [34]. The penetration of counterions into the dendrimer interior affects the dynamics of the complex with DNA [35]. Moreover, the originally condensed counterions on both the nucleic acids and charged dendrimers are released upon the complexation [36]. The entropy gain due to counterion-release contributes to the complex formation, which will be further discussed below.

1.1.3 Dendritic polyglycerol sulfate

Among all the synthetic polyelectrolytes dendritic polymers have drawn special attention for their controlled synthesis and various functionalization of the surface. The molecular properties including size, shape, flexibility, density as well as their dependence on generation and solvent conditions have been explored for decades [37–41]. With special chemical physical properties and response to external stimuli dendrimers are now designed intensively as therapeutic agents, diagnostic probes, and drug carriers [5, 9, 11, 42–49].

Dendritic polyglycerol sulfate (dPGS), as branched mimic of heparin, is a negatively charged hydrophilic polymer with high cell compatibility [50]. It can be easily synthesized from a hyperbranched polyglycerol core and the degree of sulfation can be controlled for different purposes [48, 51–55]. The negative surface charges confer the polymer with anti-inflammatory potential by specific binding to positive patch on selectins [43, 54, 56, 57]. dPGS binds with L-selectin on the leukocytes and P-selectin on the endothelial cells, thus inhibits the recognition of selectins by complementary ligands and thus prevents the extravasation of leukocytes (see Fig. 3(a)). The inhibition

efficiency (IC_{50}) of dPGS to L-selectin in PBS is as low as 8 nM [56]. Based on the strong binding dPGS has been investigated as a potent candidate for bioimaging and drug delivery [47, 48, 58–60]. Fig. 3(b) shows a recent example where the dPGS shell provides the drug-loaded micelle with high targetability to tumor cells. Furthermore, the electrostatic interaction makes dPGS attractive to viruses with positively charged ligands on the surface, which inhibits the cell inflection [61, 62].

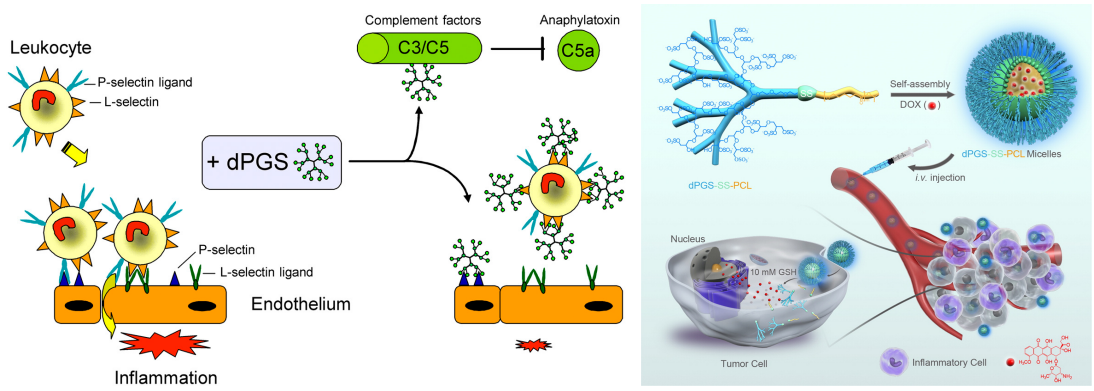

(a) (b)

Figure 3: (a) The anti-inflammatory effect of dPGS during disordered immune response [43]. dPGS binds to the adhesive proteins L- and P-selectins with high affinity thus inhibits the recognition of leukocytes by the endothelial cells. (b) Synthetic micelles with dPGS as the shell for active targeting to inflammation-related tumor tissues and local drug release [60].

To realize the applications *in vivo* it is essential to understand the interaction of dPGS with native biomolecules. Until now there is no systematic study on the binding process of dPGS with proteins. In this thesis we will study in detail the influence of size and environmental condition on the binding behavior.

1.2 Thermodynamics of polyelectrolyte-protein interaction

1.2.1 Driving forces for polyelectrolyte-protein interactions

Electrostatic interactions

For oppositely charged molecules, the electrostatic or Coulomb interaction contributes to the complex formation [63, 64]. DNA is an example for a strong biological polyelectrolyte. The condensation of DNA helix to the ultimate chromosome requires neutralization of the negative charges. Every eight histone proteins with positive charges

are packaged by DNA chain to reduce the strong repulsion within the chain and form a nucleosome which is the subunit of chromosome [65]. For non-specific binding between proteins and synthetic polyelectrolytes, the electrostatic attraction also plays substantial role. The binding affinity for the negative insulin with a positive polypropylene imine (PPI) dendrimer changes with pH and dendrimer generation [66] since the net charges of the protein and dendrimer are also changed.

Compared to point charges, the force between an inhomogeneously charged protein and a flexible polyelectrolyte is far more complicated. The effect of ionic strength on the binding affinity exhibited nonmonotonic dependence in many cases [67–70]. Namely, a maximum or plateau exists at low ionic strength I range 5$\sim$30 mM, which implies the interplay between unscreened and screened electrostatic interactions. There the protein can be treated not as point charge but as dipole with positive and negative domains. Computer modeling has shown that the electrostatic potential of negative proteins like insulin and bovine serum albumin is clearly divided into two separate regions (negative and positive) at neutral pH [70]. Seyrek *et al* used these proteins and also negative polyelectrolyte [70]. They found that the critical ionic strength I for maximum binding corresponds to the Debye length $\kappa^{-1} = \sqrt{\frac{\varepsilon_0 \varepsilon_r k_B T}{2 N_A e^2 I}}$ on the scale of the protein radius. At I lower than that, the screening length is long enough so that the repulsive long-range interaction diminishes the binding affinity. Afterwards the attractive short-range interaction between the polyanion and the positive patch in the protein coexists with the former. Finally the attractive part becomes predominant as I increases, thus the binding affinity changes monotonically with salt. Simply taking the protein as a dipole and the polyanion as a monople, the electrostatic interaction energy between them can be defined as the sum of attractive and repulsive terms [70, 71]. Nevertheless, the lack of atomistic details of both molecules makes the accurate prediction a formidable task. For proteins with multipolar charge distribution such as lysozyme in Fig. 1(b) it is even more difficult.

For charged molecules with hydrogen donor or acceptor, hydrogen bonding with the protein binding site as another part of electrostatic interaction may also contribute to the binding affinity [64, 72]. The carboxylate group and highly electronegative atoms on the inhibitor ligands could form hydrogen bonds with hydrogen donors on the side chain of aldose reductase [72]. The binding affinity changed with different nitro substituents

of the inhibitor. For some inhibitor derivatives, water molecules were also involved in hydrogen bonding with the protein and brought significant enthalpic contribution, however, this was compensated by an entropy penalty so that the total binding affinity did not change [72].

A rigorous evaluation of the electrostatics requires exact location of the charges on the protein and the molecular structure of the polyelectrolyte. So far this can only be attempted with computer simulations which, however, also have limitations such as absence of hydrogen bonding and hydrophobic interaction [73].

Counterion release

For a highly charged molecule, the binding affinity to another ligand changed monotonically with ionic strength, which was first observed for nucleotide-protein interactions [74–78]. The condensed counterions on the polyelectrolyte are released upon binding, which is dependent on the charge density and ionic strength [36, 79]. Based on the fundamental theory of counterion condensation [12], Record and Lohman established the relation between salt concentration and binding equilibrium [80, 81].

For the complexation of protein A and polyelectrolyte B, the apparent binding equilibrium is

$$[A] + [B] \overset{K_{\mathrm{eq}}}{\rightleftharpoons} [AB], \tag{2}$$

where

$$K_{\mathrm{eq}} = \frac{[AB]}{[A][B]}, \tag{3}$$

is the equilibrium constant. In the presence of counterion condensation on a highly charged polyelectrolyte, Δn_{ci} condensed ions are released upon binding of the protein and the protein becomes a multivalent counterion to the polyelectrolyte. With that the actual equilibrium is

$$[A] + [B] \overset{K_{\mathrm{tot}}}{\rightleftharpoons} [AB] + \Delta n_{\mathrm{ci}}[i], \tag{4}$$

where $[i]$ represents the bulk concentration of ions and

$$K_{\mathrm{tot}} = \frac{[AB][i]^{\Delta \mathrm{n_{ci}}}}{[A][B]} = K_{\mathrm{eq}}[i]^{\Delta \mathrm{n_{ci}}} \tag{5}$$

is the total binding constant. Thus the number of released ions is related to the binding constant by the Record-Lohman equation [81]

$$\frac{\mathrm{d}\ln K_{\mathrm{eq}}}{\mathrm{d}\ln[i]} = -\Delta n_{\mathrm{ci}}. \tag{6}$$

Counterion-release is a typical phenomenon that accompanies protein-polyelectrolyte interaction. Eq. 6 points out the underlying relation with salt concentration. Fig. 4 shows the logarithmic plots according to Eq. 6 [82]. The binding constant between a single-stranded homopolynucleotide poly(U) and a series of oligolysines was determined at different salt concentrations. The positive oligopeptides have different degrees of polymerization and thus the net charge ranges between +2 and +10. The binding constant is plotted as a function of the bulk concentration of potassium ion which serves as counterion for poly(U). All data points are located nicely on the fitted curves. The number of released ions is obtained from the slope according to Eq. 6, which increases with the net charge of the oligopeptide. For some protein-nucleic acid systems ion-uptake and ion-exchange may also occur [83, 84], which will not be explained here in detail.

Counterion-release is also directly observed by molecular dynamics simulation [86]. The released ions increase the entropy of the system, which becomes a driving force for binding. Considering the equilibrium between the constrained counterions on the polyelectrolyte surface and the ions in the bulk, the entropy gain of counterion-release can be evaluated in first approximation through [87]

$$\Delta G_{\mathrm{ci}} = -\Delta n_{\mathrm{ci}} RT \ln \frac{[ci]}{[i]}. \tag{7}$$

As mentioned above, this entropic contribution depends on the salt concentration $[i]$ and charge density which determines the concentration of locally condensed counterions $[ci]$.

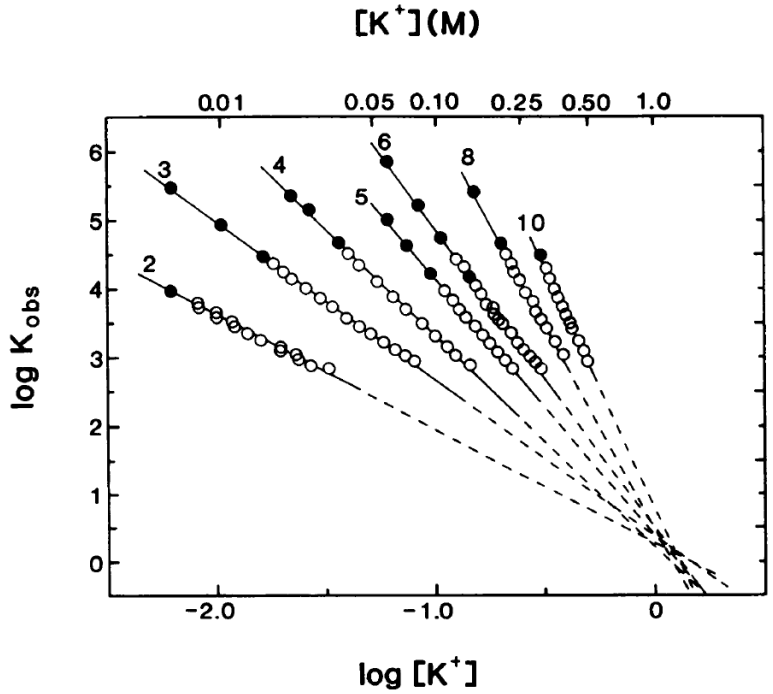

Figure 4: Salt dependence of the observed binding constant for a series of oligolysines binding with a single-stranded nucleic acid poly(U) [82]. At constant salt concentration, poly(U) was titrated into the oligopeptide solution. The fluorescence of trypsin in the oligopeptide sequence was quenched upon binding with poly(U). After equilibrium a 4 M salt solution was titrated to raise the salt concentration, meanwhile the dissociation of the oligopeptide from poly(U) increased the fluorescence signal (salt-back titrations). The binding constant was calculated from the fluorescence quenching according to their provided binding model [85]: •, data from titrations at constant salt concentration; ○, data from salt-back titrations [85]. The solid lines are fitted by Eq. 6. Dashed lines are extrapolations of the fitted lines. Each line refers to one oligolysine with specific net charge (+2, +3, +4, +5, +6, +8, +10).

Hydrophobic effect

For charged polyelectrolytes with hydrophobic segments, the hydrophobic interaction with a protein also contributes to the binding affinity. The key role is the hydrogen-bonding status of water molecules at the binding interface. The strength of a hydrogen bond depends sensitively on the chemical property of the molecules, and thus the displacement of water molecules during binding process is system-specific with either enthalpic or entropic signature. The classic hydrophobic effect refers to the approach of two hydrophobic surfaces. Water molecules are excluded from the interface [88–92], which brings entropy gain to the system analogous to counterion-release mechanism.

In late-stage optimization of binding affinity with proteins, many drug candidates are proposed to "lock" into the specific conformation of the protein receptor [93–96].

One strategy is linking lipophilic groups on the ligand to fill into the hydrophobic pocket in the protein [93, 96]. The well-ordered water molecules are released from the pocket. When the hydrophobic contact area increases, the binding affinity benefits from the entropy gain. Nonetheless, a concomitant enthalpic cost of the water movements always occurs [97].

1.2.2 Binding affinity of polyelectrolyte-protein interaction

The medical application of a polyelectrolyte drug or carrier requires consideration of its interaction with native biomolecules, typically proteins. Multiple techniques have been applied to characterize the polyelectrolyte-protein complexation such as atomistic force microscopy (AFM), light scattering, spectroscopy, calorimetry, quartz crystal microbalance (QCM), surface plasmon resonance (SPR), and microscale thermophoresis (MST) [98–100]. The secondary structure of the protein in the complex has drawn special attention since in many cases the hydrophobicity of the polyelectrolyte backbone leads to partial protein unfolding [101–105]. The hydrophobicity, polymer stiffness, charge sequence, and protein charge anisotropy aside from solution conditions are important determinants to the physicochemical properties of the complex [98]. Among them the energetics of the complexation process is a central issue for drug design and optimization [5, 97, 106, 107].

At equilibrium state of a binding process, the standard Gibbs free energy can be derived from the binding constant as [108]

$$\Delta G^\circ = -RT\ln K_{\mathrm{eq}} = \Delta H^\circ - T\Delta S^\circ. \tag{8}$$

ΔH° and ΔS° are the enthalpy and entropy change of an equilibrated reaction at standard state. The binding affinity or constant of a polyelectrolyte with protein relies on many factors. Different charged groups of the surface change the electrostatic interaction to high extent [5, 109]. Giri *et al* did a systematic study on the effect of different terminal groups and backbone [5]. On the one hand, the binding constant K_{eq} of human serum albumin (HSA) with PAMAM dendrimers was found highest with negative, medium with positive, and lowest with a neutral surface charge at physiological pH (7.4). On the other hand, the chemical structure of the dendrimer core altered K_{eq} to

different scales depending on the hydrophobicity. Solution condition also plays an important role. Temperature, pH, ionic strength, and ion species must all be taken into account [8, 70, 110–112]. The dependence of K_{eq} on these factors gives insights to the binding mechanism.

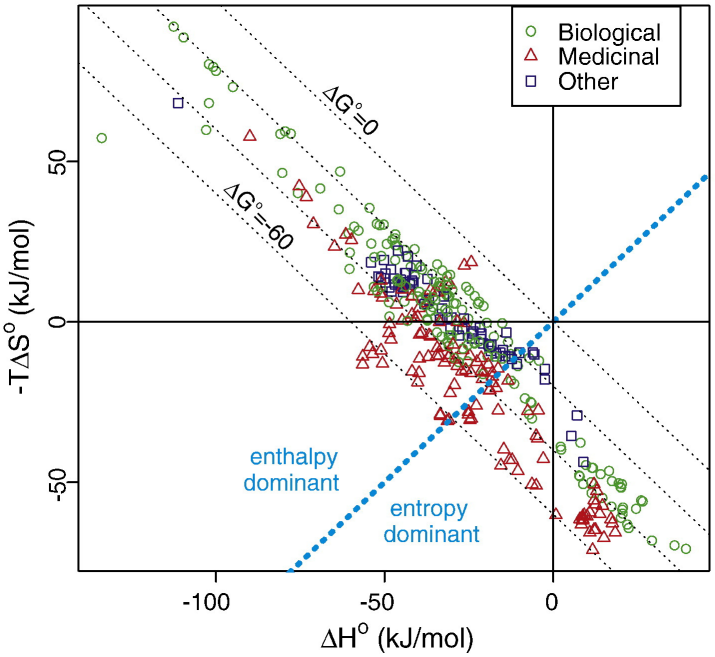

Figure 5: A summary of the thermodynamic parameters (binding enthalpy ΔH°, binding entropy ΔS°, and Gibbs free energy of binding ΔG°) for protein-ligand interaction held in the SCORPIO database [113]. Green circles are for biological ligands. Red triangles represent synthetic ligands designed for medicinal chemistry program. Interactions belong to neither category are noted as blue squares.

Up to now electrostatic and hydrophobic effects are recognized as the determinants of such interactions [5, 114]. Charge and water molecules influence the binding affinity and concomitantly the other thermodynamic parameters like enthalpy and entropy [97, 115]. According to literature, the Gibbs free energy of binding for non-specific protein interaction with a natural or synthetic ligand is located in the range of -15 – -60 kJ/mol [113]. Fig. 5 depicts the database which is separated into enthalpy and entropy dominant regions. For the same magnitude of ΔG° (each diagonal dashed line), the enthalpic and entropic contributions in the total binding free energy can be intrinsically different. To comprehend the enthalpy- or entropy-driven mechanism of binding, researchers have devoted much effort to find out the driving forces which will be the main task of this thesis.

1.2.3 van't Hoff and calorimetric enthalpies

van't Hoff plot

The binding constant K_{eq} can be measured at several temperatures with suitable intervals. The binding enthalpy ΔH° and binding entropy ΔS° can then be obtained from the change of K_{eq} according to Eq. 8. They are also called the van't Hoff enthalpy ΔH_{vH} and van't Hoff entropy ΔS_{vH} [108]. Work on protein-nucleic acid complexation showed that ΔH_{vH} changed markedly with temperature [116–118], which required the heat capacity change ΔC_{p} to be taken into account. For an interaction where ΔC_{p} is nonzero, the temperature dependence of binding enthalpy and entropy can be expressed as

$$\left(\frac{\partial \Delta H_{\mathrm{vH}}}{\partial T}\right)_{\mathrm{P}} = \Delta C_{\mathrm{p}} \tag{9}$$

and

$$\left(\frac{\partial \Delta S_{\mathrm{vH}}}{\partial T}\right)_{\mathrm{P}} = \frac{\Delta C_{\mathrm{p}}}{T}. \tag{10}$$

Both change with temperature is the basis of enthalpy-entropy compensation [119]. Taking the heat capacity change ΔC_{p} as a constant with T, ΔH_{vH} and ΔS_{vH} at any temperature are derived as

$$\Delta H_{\mathrm{vH}} = \Delta H_{\mathrm{vH,ref}} + \Delta C_{\mathrm{p}}(T - T_{\mathrm{ref}}) \tag{11}$$

and

$$\Delta S_{\mathrm{vH}} = \Delta S_{\mathrm{vH,ref}} + \Delta C_{\mathrm{p}} \ln\left(\frac{T}{T_{\mathrm{ref}}}\right), \tag{12}$$

where $\Delta H_{\mathrm{vH,ref}}$ and $\Delta S_{\mathrm{vH,ref}}$ are the binding enthalpy and entropy, respectively, at a reference temperature T_{ref}. With that the Gibbs free energy of binding can be rewritten as

$$\begin{aligned} \Delta G^{\circ} &= -RT \ln K_{\mathrm{eq}} \\ &= \Delta H_{\mathrm{vH,ref}} - T\Delta S_{\mathrm{vH,ref}} + \Delta C_{\mathrm{p}}\left[(T - T_{\mathrm{ref}}) - T\ln\left(\frac{T}{T_{\mathrm{ref}}}\right)\right] \end{aligned} \tag{13}$$

at a constant pressure. This temperature dependence of binding affinity is the nonlinear van't Hoff relation which is applied as follows: a reference temperature T_{ref} is chosen and fixed. The corresponding binding enthalpy $\Delta H_{\mathrm{vH,ref}}$, entropy $\Delta S_{\mathrm{vH,ref}}$, and heat capacity change ΔC_{p} are fit parameters [118].

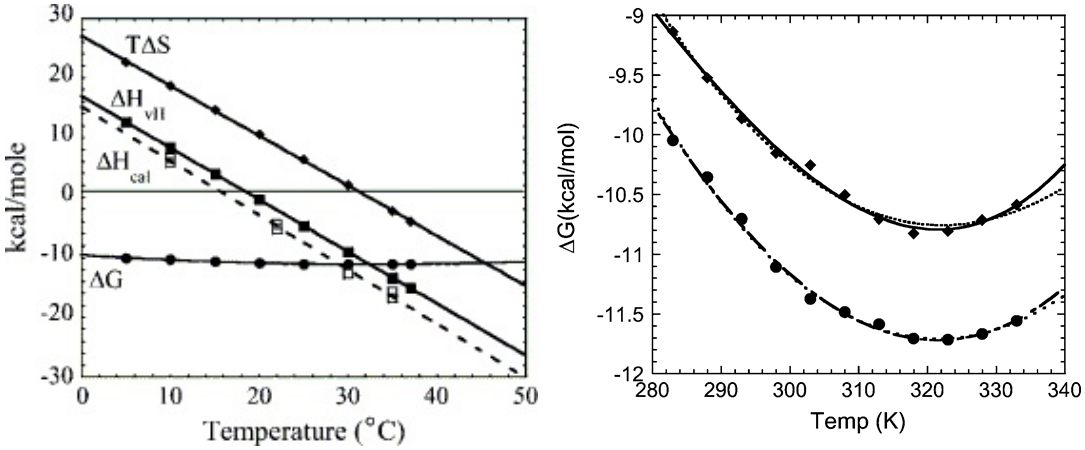

(a) (b)

Figure 6: (a) Nonlinear van't Hoff plot of Gibbs binding free energy ΔG on temperature to obtein the binding entropy $T\Delta S$ and binding enthalpy ΔH_{vH}. ΔH_{cal} is the calorimetric enthalpy measured by ITC [118]. (b) Nonlinear van't Hoff plot for DNA binding by two polymerases with (solid) and without (dashed) $\Delta\Delta C_{\mathrm{p}}$ parameter [120].

The nonlinear van't Hoff analysis is an efficient way to obtain the binding enthalpy and binding entropy. It is widely used by biochemists to analyze the enthalpic and entropic contributions in protein unfolding, enzyme activity, and protein-DNA binding [121–126]. Fig. 6(a) is a typical example referring to DNA binding of Klenow polymerase [118]. Within the temperature range, ΔG reaches the minimum at $\sim$30 °C, but slightly changes. ΔH_{vH} and ΔS both change from positive to negative with complete compensation. The binding process is thus entropy-driven at low temperature and enthalpy-driven at high temperature.

For some protein-DNA systems, ΔC_{p} was found to depend on temperature [120]. The temperature dependence is

$$\Delta C_{\mathrm{p}}(T) = \Delta C_{\mathrm{p,ref}} + \Delta\Delta C_{\mathrm{p}}(T - T_{\mathrm{ref}}) \tag{14}$$

with $\Delta\Delta C_\mathrm{p}$ a constant. Then Eq. 13 can be rewritten as [117]

$$\begin{aligned}\Delta G^\circ = \Delta H_{\mathrm{vH,ref}} + \Delta C_{\mathrm{p,ref}}(T - T_\mathrm{ref}) + \Delta\Delta C_\mathrm{p}[\frac{T^2 - T_\mathrm{ref}^2}{2} - T_\mathrm{ref}(T - T_\mathrm{ref})] \\ - T\Delta S_{\mathrm{vH,ref}} - T\Delta C_{\mathrm{p,ref}}\ln(\frac{T}{T_\mathrm{ref}}) - T\Delta\Delta C_\mathrm{p}[(T - T_\mathrm{ref}) - T_\mathrm{ref}\ln(\frac{T}{T_\mathrm{ref}})]\end{aligned} . \quad (15)$$

Fig. 6(b) shows the fittings with (solid) and without (dashed) a $\Delta\Delta C_\mathrm{p}$ parameter. Within the experimental temperature range the two fittings almost overlap with each other, which indicates that the resultant $\Delta\Delta C_\mathrm{p}$ is small [120].

The nonlinear van't Hoff plot unravels the temperature dependence of thermodynamic quantities and the underlying enthalpy-entropy compensation. The heat capacity change ΔC_p is brought by the solvent molecules [127]. The major contribution of the solvent to ΔC_p is the hydration/dehydration of the binding interface. Hydrophobic hydration has been profoundly studied by computer simulations compared to experiments [92, 128–131]. Briefly, transferring water to a hydrophobic surface is entropically favored and enthalpically unfavorable. It generates large positive ΔC_p and dehydration of a polar surface generates positive ΔC_p as well with much lower magnitude. Reversely, hydration of a polar surface and dehydration of an apolar surface correspond to negative ΔC_p. The scale of ΔC_p is totally dependent on the hydrophobicity of the binding surface. The minor contribution is from the electrostatic property. Postulating long-range electrostatic interaction, the heat capacity change arises from three parts: the near-ranged water dipoles, redistribution of mobile ions in the solvent upon binding, and the coupling between the dipoles and ions [127].

Linked equilibria

The binding enthalpy can be derived from the van't Hoff plot as mentioned above. Since the measured enthalpy by calorimetry is comprised of multiple heat effects, the agreement between the calorimetric and van't Hoff enthalpies is not to be expected and system-specific [116, 118, 132–134]. Fig. 6(a) compares the two. The calorimetric enthalpy is a bit more negative than the van't Hoff enthalpy indicating an effect of buffer dissociation. For some systems ΔH_vH and ΔH_cal differ widely from each other [6, 7]. The discrepancy can be traced back to linked equilibria including buffer ionization [116, 133], protein protonation [7, 135, 136], and possible conformational changes [117, 137].

Therefore the observed calorimetric enthalpy is the sum of all these contributions as [136]

$$\Delta H_{\mathrm{cal}} = \Delta H_{\mathrm{vH}} + \Delta H_{\mathrm{ion}} + \Delta H_{\mathrm{prot}} + \Delta H_{\mathrm{conf}}. \tag{16}$$

ΔH_{vH} is the intrinsic binding enthalpy according to van't Hoff analysis. ΔH_{ion} represents the ionization of buffer molecules. Each buffer has respective molar enthalpy $\Delta H^{\mathrm{o}}_{\mathrm{ion}}$ of proton dissociation [138], thus the total ionization enthalpy is proportional to the molar enthalpy as

$$\Delta H_{\mathrm{ion}} = \Delta n_{\mathrm{H^+}} \Delta H^{\mathrm{o}}_{\mathrm{ion}} \tag{17}$$

with positive $\Delta n_{\mathrm{H^+}}$ being the number of dissociated protons from the buffer. Calorimetry measurements done in two buffers with disparate $\Delta H^{\mathrm{o}}_{\mathrm{ion}}$ allow to determine the strength of buffer ionization since the other terms on the right side of Eq. 16 remain independent. Then the released protons are [7]

$$\Delta n_{\mathrm{H^+}} = \frac{\Delta H_{\mathrm{cal},1} - \Delta H_{\mathrm{cal},2}}{\Delta H^{\mathrm{o}}_{\mathrm{ion},1} - \Delta H^{\mathrm{o}}_{\mathrm{ion},2}}. \tag{18}$$

The released protons are loaded by the ionizable groups on the protein/polyelectrolyte. Then the protonation enthalpy ΔH_{prot} of free or bound protein/polyelectrolyte is [136]

$$\Delta H_{\mathrm{prot}} = \Delta n_{\mathrm{H^+}} \Delta H^{\mathrm{o}}_{\mathrm{prot}} \tag{19}$$

with $\Delta H^{\mathrm{o}}_{\mathrm{prot}}$ the protonation molar enthalpy of the charged group. Conformational change is temperature dependent so ΔH_{conf} also gives heat capacity change in the total

$$\Delta C_{\mathrm{p,cal}} = \Delta C_{\mathrm{p,vH}} + \Delta C_{\mathrm{p,ion}} + \Delta C_{\mathrm{p,prot}} + \Delta C_{\mathrm{p,conf}}, \tag{20}$$

which follows the same principle as ΔH_{cal}.

1.2.4 Enthalpy-entropy compensation

As for drug design, previous reports focused on the enthalpy change of protein binding acquiring the structural properties and the hydrogen-bonding enthalpies [113, 139–141].

Also the entropy gain in the hydrophobic effect attracts much attention as mentioned in section 1.2.1. In fact, being both hydrogen donor and receptor water molecules bring unusual complication to thermodynamic analysis and mutual influence on both enthalpy and entropy change in protein-drug binding.

Calorimetry has shown apparent evidence that the enthalpy and entropy change for a binding process depend strongly with temperature while the binding free energy barely changes [116, 118, 142–144]. This phenomenon of enthalpy-entropy compensation (EEC) has been observed in many biological and synthetic systems [145–147]. As seen in Fig. 7 of three different contexts, the enthalpy and entropy change parallelly with temperature. As a consequence, the overall binding free energy varies much less over a long range of temperature. Moreover, EEC was found among molecules with analogous chemical structures [72, 148, 149]. Whitesides *et al* investigated the binding thermodynamics between trypsin and eight inhibitors with different terminal groups [148]. Despite the different size, hydrophobicity, and binding modes, the eight ligands exhibited almost the same binding affinity. On the contrary, the enthalpic and entropic partition was significantly different. There too the enthalpic and entropic contributions by hydrogen bonding or hydrophobic effect completely compensate each other.

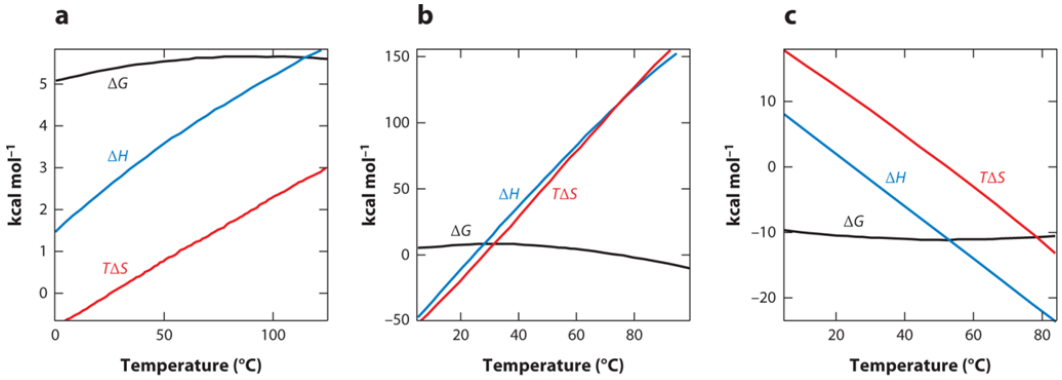

Figure 7: Enthalpy-entropy compensation as a general thermodynamic phenomenon observed in three example processes: (a) transfer of neopentane from its neat phase to water, (b) myoglobin unfolding, and (c) protein-protein association [150].

The molecular basis for enthalpy-entropy compensation is that water molecules at different ligand surfaces and in the bulk behave fundamentally differently. Thus the hydration/dehydration process brings enthalpy and entropy changes that have opposite sign and the same magnitude [119]. For instance, the tightly bound water at a polar

surface gains entropy when liberated from the surface and consumes enthalpy for the hydrogen-bond breakage [116]. By contrast, water at the apolar surface is more loosely constrained than water the bulk. Therefore, transfer from a hydrophobic surface to the bulk loses entropy and gains enthalpy [151]. One direct evidence is that the hydration site thermodynamics of binding ligands in a protein cavity was monitored [149], and the change of hydrogen bonding was found responsible for the enthalpy change of the interaction. Many reports focused on the enthalpy or entropy gain for higher binding affinity, however, their compensation has frustrated the efforts. Moreover, strong variation of enthalpy and entropy with temperature makes people hesitate to use thermodynamic data for rational drug design [134].

1.3 Isothermal titration calorimetry

Calorimetry which directly measures the enthalpy of a biochemical process is assistant for drug design [97, 134]. Isothermal titration calorimetry (ITC) gives the thermodynamic data of biological binding systems [152, 153] ever since it was introduced late last century [154]. Based on the standard Langmuir adsorption isotherm, the ITC device is able to obtain the binding constant K_{eq}, binding stoichiometry n, and apparent enthalpy change ΔH_{cal} with one measurement. The protein solution in the syringe is titrated stepwise into the cell filled with the polymer solution as shown in Fig. 8(a). The reference cell is filled with degassed water so no reaction occurs in it. The temperature of the two cells is kept the same by the heating circuit. The binding process absorbs or generates heat so that the heat flow between the two cells is different and recorded by the device, which corresponds to the peaks in the raw data (Fig. 8(b)). The interpretation of the heat signals is derived below.

Concerning a multi-site binding process, denote L as the ligand and R as the receptor. Conventionally the ligand is located in the syringe and titrated into the receptor solution. Then the binding reaction is

$$[L] + [RL_{m-1}] \rightleftharpoons [RL_m],\ 1 \leqslant m \leqslant n. \tag{21}$$

Eq. (21) describes the association of a free protein L and the complex RL_{m-1} consisting of one polyelectrolyte receptor and m-1 proteins in this case. n is the maximum binding

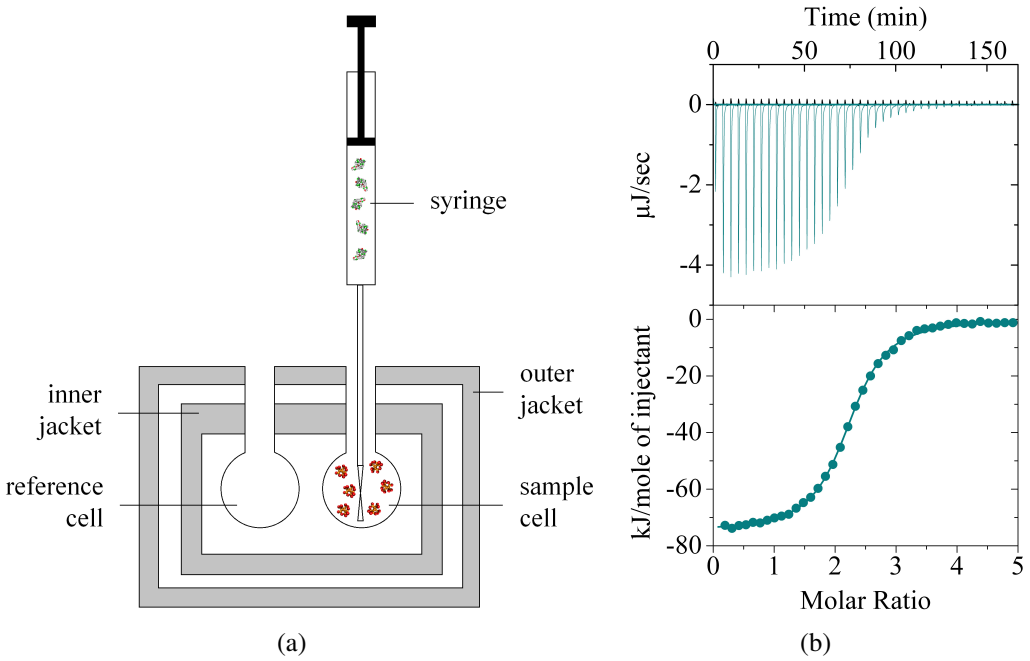

Figure 8: (a) Illustration of a MicroCal VP-ITC instrument. The lysozyme solution is located in the syringe and titrated into the dPGS solution in the cell. (b) Typical example of ITC raw data (upper panel) with adsorption (cyan) and dilution (grey) peaks, respectively. The integrated isotherm (lower panel) is obtained by substracting the dilution heat from the adsorption heat. The isotherm is fitted with the SSIS model.

number per receptor. Given the ligand (protein) coverage

$$\theta_m = \frac{[RL_m]}{[R]_{\text{tot}}} \tag{22}$$

with complex concentration $[RL_m]$ normalized by the total concentration $[R]_{\text{tot}}$ of the receptor, it makes

$$[L]_{\text{tot}} = [L] + [R]_{\text{tot}} \left(\sum_{m=1}^{n} m\theta_m \right). \tag{23}$$

$[L]_{\text{tot}}$ is the total concentration of the ligand containing free and bound species. The endothermic or exothermic binding process is triggered by the ligand uptake. Then the total heat goes

$$Q = [R]_{\text{tot}} V_{\text{tot}} \sum_{m=1}^{n} \Delta H_m \left(\sum_{p=m}^{n} \theta_p \right). \tag{24}$$

V_{tot} is the total volume of the mixture taken as the cell volume. ΔH_m is the enthalpy change for the m^{th} uptake.

Further data assessment requires a proper fitting model to the heat. The MicroCal ITC device provides optional models for independent binding, sequential binding, and competitive binding systems. The most straightforward and adopted is the single set of identical sites (SSIS) model which considering all the binding sites equivalent and independent, i.e. all the binding sites have the same binding constant and thermodynamic signature. Denote the total number of bound sites by N_{b} and number of total receptors by N_R, it gives the ligand coverage θ of total binding sites

$$\theta = \frac{N_{\text{b}}}{nN_R} \tag{25}$$

The number of microstates of the bound sites is

$$W = \frac{\zeta^{N_{\text{b}}}(nN_R)!}{N_{\text{b}}!(nN_R - N_{\text{b}})!} \tag{26}$$

as a solution to the combinatorial problem of placing N_{b} identical ligands on nN_R available sites. ζ is the partition function of a single bound ligand. W gives rise to the Boltzmann entropy $\frac{S}{k_{\text{B}}} = \ln W$, which is formulated into the system (canonical) Helmholtz free energy [114]

$$\beta F = \beta F_{\text{id}} - \frac{S}{k_{\text{B}}} + \beta N_{\text{b}} \Delta G^{\circ} \tag{27}$$

with

$$\beta = \frac{1}{k_{\text{B}} T} \tag{28}$$

making the energies dimentionless. The ideal gas free energy of unbound state is introduced as

$$\beta F_{\text{id}} = (N_L - N_{\text{b}}) \left[\ln\left(\frac{(N_L - N_{\text{b}})\Lambda^3}{V_{\text{tot}}} \right) - 1 \right] \tag{29}$$

with the number of total ligands N_L and the cubed thermal (de Broglie) wavelength Λ. The last term in the right side of Eq. (27) refers to the change of Gibbs free energy. As

for the SSIS model, ΔG° is in relation to the bound sites N_b, thus the minimization of the free energy corresponds to the differentiation

$$\frac{\partial F}{\partial N_\mathrm{b}} = 0. \tag{30}$$

Now with the unbound ligand concentration

$$[L] = \frac{(N_L - N_\mathrm{b})}{V_\mathrm{tot}} \tag{31}$$

and coverage θ in Eq. 25, the binding constant identical at all binding sites can be expressed in terms of coverage

$$K_\mathrm{eq} = \exp(-\beta \Delta G^\circ) = \frac{\theta}{(1-\theta)[L]}. \tag{32}$$

For the SSIS model Eq. 23 can be rephrased as

$$[L]_\mathrm{tot} = [L] + n[R]_\mathrm{tot}\theta. \tag{33}$$

Combining Eq. 32 with Eg. 33 gives a quadratic equation of θ

$$\theta^2 - \Big(1 + \frac{[L]_\mathrm{tot}}{n[R]_\mathrm{tot}} + \frac{1}{nK_\mathrm{eq}[R]_\mathrm{tot}}\Big)\theta + \frac{[L]_\mathrm{tot}}{n[R]_\mathrm{tot}} = 0. \tag{34}$$

Moreover, the molar enthalpies ΔH_m are identical, which briefs Eq. 24 as

$$Q = [R]_\mathrm{tot} V_\mathrm{tot} \Delta H_\mathrm{cal} n\theta. \tag{35}$$

Take the solution θ of Eq. 34 into Eq. 35. The total heat is expressed with the fit parameters n, ΔH_cal, and K_eq. In ITC measurements, the integration of the heat flow peaks with time (see Fig. 8(b)) refers to the total heat Q of each titration. Afterwards Q is normalized by the molar amount of titrated ligands to give the molar enthalpy change. To elucidate that, the differential heat is derived as

$$\frac{\partial Q}{\partial N_L} = \frac{1}{V_\mathrm{tot}} \frac{\partial Q}{\partial [L]_\mathrm{tot}} = \frac{\Delta H_\mathrm{cal}}{2} \left[1 + \frac{n - x - \frac{1}{K_\mathrm{eq}[R]_\mathrm{tot}}}{\sqrt{(n + x + \frac{1}{K_\mathrm{eq}[R]_\mathrm{tot}})^2 - 4nx}}\right]. \tag{36}$$

Eq. 36 is the exact fitting equation in Fig. 8(b). The abscissa is the molar ratio x denoted as

$$x = \frac{[L]_{\text{tot}}}{[R]_{\text{tot}}} \tag{37}$$

in the cell.

The convenient operation and data analysis of ITC makes it a useful tool for thermodynamic assessment. One limitation is that the detectable binding affinity is in the milimolar to nanomolar range. Also, one should be cautious to interpret the fitted K_{eq} for multi-site binding processes since the SSIS model does not consider the cooperativity or packing penalty.

2 Objective

Recently dendritic polyglycerol sulfate has been investigated as anti-inflammatory agent and drug delivery system [43, 60]. However, the fundamental knowledge of its interaction with serum proteins is still missing. Charged dendrimers are widely studied for biomedical applications whereas their binding mechanism with proteins is comparably less understood.

In this work, dPGS was set as a model to elucidate the driving forces for protein-polyelectrolyte interaction. Four dPGS with different sizes, i.e. G2, G4, G4.5, G5.5, are used. The model proteins are shown in Fig. 9. Human serum albumin (HSA) is the most abundant serum protein and delivers agents such as fatty acids and toxins in the human body [155]. It is a heart-shape protein with molecular weight of 66.5 kDa and a net charge of -14 *e* at physiological pH. Lysozyme is a well-studied enzyme protein. It has molecular weight of 14.3 kDa and a net charge of +8 *e* at pH 7.4, which is a good comparison to the negative HSA. The interaction between the proteins and dPGS of different sizes was measured experimentally by ITC at different temperatures and salt concentrations to obtain the thermodynamic parameters.

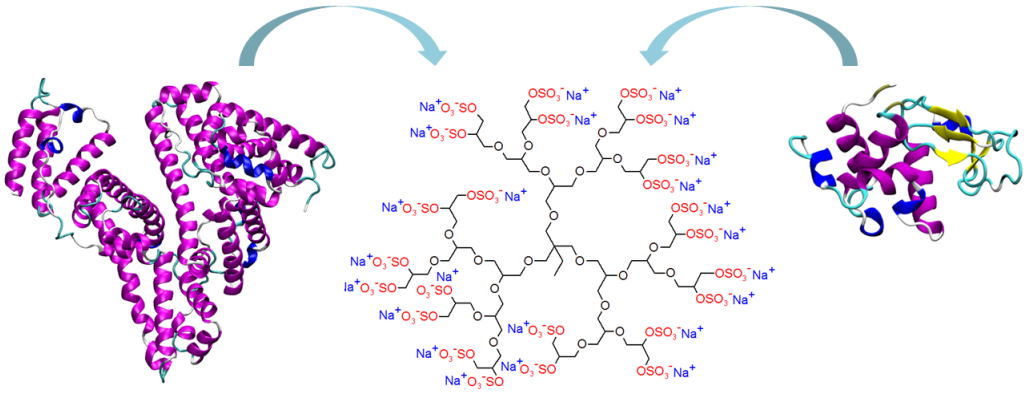

Figure 9: Scheme of the project: interaction between dPGS (-G2 as an example)(middle) and two model proteins HSA (left, PDB: 1N5U) and lysozyme (right, PDB: 2LZT) with different sizes and charges. The representations of the proteins are generated by the VMD software (coloring method: Secondary Structure; drawing method: NewCartoon).

The surface area of the polymer increases with size thus providing more binding sites to the proteins. The net charge of dPGS increases exponentially with the generation, however, the information on the surface potential and effective charge remains unknown due to counterion condensation. The effective charge is a crucial parameter that deter-

mines the Coulomb interaction with proteins. Therefore it is the first task to investigate the properties of dPGS in ionic solution by size and surface potential measurements.

Then HSA is chosen as a target protein to investigate the interaction with dPGS. Specially, the secondary structure of the protein at the bound state will be checked for potential *in vivo* applications of dPGS. Here we measure the interaction between HSA and dPGS of the second generation by ITC at different ionic strengths to elucidate the role of counterion-release in the driving force. The binding affinity will be compared to the molecular dynamics (MD) simulations with explicit salt and implicit water, which reveals the contribution of electrostatics. Besides, the temperature dependence of the binding affinity will lead to the binding enthalpy and entropy by van't Hoff analysis. Thus, the data allow us to analyze the role of the hydrophobic effect in the binding affinity, enthalpy, and entropy. Hence, the combination of experiments with simulations on dPGS-HSA interaction provides a fundamental understanding of the role of electrostatics and hydrophobic effects in protein binding.

It was reported that dPGS binds specifically to L- and P-selectins, but not E-selectin that does not contain a positively charged domain [43, 156]. Therefore, electrostatic interaction plays a crucial role in the binding selectivity. Here, we aim at a quantitative understanding of the driving forces for protein binding. Lysozyme is chosen as the model protein in ITC experiments for its comparable size to selectin and lower cost. dPGS of different sizes will be utilized to interact with lysozyme at 310 K and different ionic strengths. In this way, the strength of counterion-release in the complex formation can be revealed by Record-Lohman relation [80, 81]. Then we compare the binding affinity and binding number of dPGS-lysozyme complexation by ITC to the results by coarse-grained (CG) computer simulations. Equipped with both experiment and theory, we provide a quantitative understanding of the role of electrostatics and in particular the generation dependence of the binding affinity. With the verified simulation model, we can finally analyze the binding affinity and driving force of dPGS with selectins. Atomistic simulation will also be applied to dPGS-L-selectin complexation so that the contribution of water can be clearly distinguished.

Based on the above work, we extend the study on dPGS-lysozyme system to various temperatures and ionic strengths by ITC. Thus, the salt dependence of binding affinity leads to the extent of counterion-release, and the temperature dependence allows to

obtain the binding enthalpy and entropy at each condition by the nonlinear van't Hoff plot [116, 118]. The enthalpic and entropic contributions in the total free energy of binding can then be derived. Besides, thermodynamic data measured in different buffers give indication on the buffer/protein ionization upon binding. Thus, the comparison between van't Hoff enthalpy and calorimetric enthalpy will be discussed.

In all, the binding parameters of dPGS with HSA/lysozyme will be obtained by ITC at different conditions. A comprehensive thermodynamic analysis reveals the binding number, binding affinity, binding enthalpy and entropy. The salt and temperature dependence of all the parameters, that are related to electrostatic and hydrophobic effects, will be discussed in detail. Moreover, the combination of ITC with molecular dynamics simulation provides a good approach to understand the driving forces of protein-polyelectrolyte binding.

3 Publications and Manuscripts

3.1 Charged dendrimers revisited: Effective charge and surface potential of dendritic polyglycerol sulfate

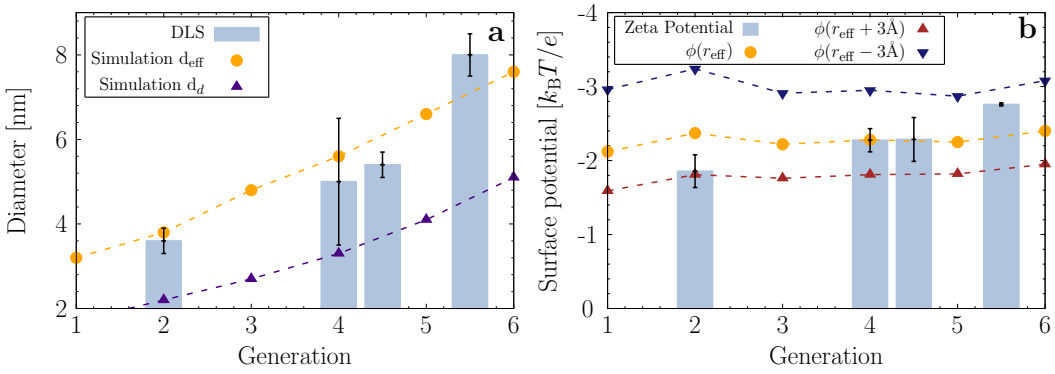

Xiao Xu, **Qidi Ran**, Rainer Haag, Matthias Ballauff, Joachim Dzubiella. *Macromolecules*, **2017**, 50 (12), 4759-4769 [20].

https://doi.org/10.1021/acs.macromol.7b00742

Author contributions

Xiao Xu designed the project, performed the simulations, and wrote the manuscript.

Qidi Ran performed the size and surface potential measurements of the synthesized dPGS and corrected the manuscript.

Rainer Haag discussed the project and provided suggestions.

Matthias Ballauff discussed the data and corrected the manuscript.

Joachim Dzubiella supervised the project, discussed the data, and corrected the manuscript.

3.2 Interaction of human serum albumin with dendritic polyglycerol sulfate: Rationalizing the thermodynamics of binding

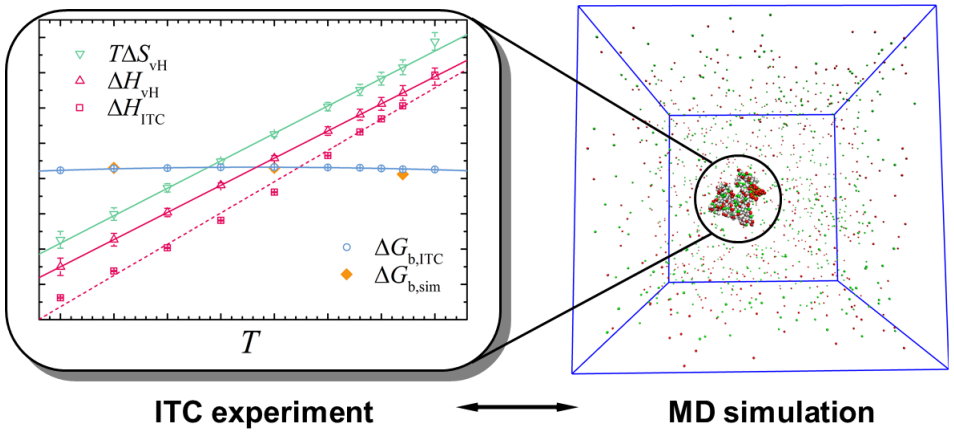

Qidi Ran, Xiao Xu, Pradip Dey, Shun Yu, Yan Lu, Joachim Dzubiella, Rainer Haag, Matthias Ballauff (Submitted).

Author contributions

Qidi Ran designed the project, performed the experiments, and wrote the manuscript.
Xiao Xu performed the simulations and corrected the manuscript.
Pradip Dey synthesized the dPGS polymers and corrected the manuscript.
Shun Yu and Yan Lu discussed the data and provided suggestions.
Joachim Dzubiella discussed the data and corrected the manuscript.
Rainer Haag and Matthias Ballauff supervised the project, discussed the data, and corrected the manuscript.

Interaction of human serum albumin with dendritic polyglycerol sulfate: Rationalizing the thermodynamics of binding

Qidi Ran,[1,2,3] Xiao Xu,[2,3,4] Pradip Dey,[1] Shun Yu,[2,4] Yan Lu,[2] Joachim Dzubiella,[2,3,4] Rainer Haag,[1,3,a)] and Matthias Ballauff[2,3,4,b)]

[1)] *Institute of Chemistry and Biochemistry, Freie Universität Berlin, Takustr. 3, 14195 Berlin, Germany*

[2)] *Institute of Soft Matter and Functional Materials, Helmholtz-Zentrum Berlin, Hahn-Meitner-Platz 1, 14109 Berlin, Germany*

[3)] *Multifunctional Biomaterials for Medicine, Helmholtz Virtual Institute, Kantstr. 55, 14513 Teltow-Seehof, Germany*

[4)] *Institut für Physik, Humboldt-Universität zu Berlin, Newtonstr. 15, 12489 Berlin, Germany*

We study the thermodynamics of the interaction between human serum albumin (HSA) and dendritic polyglycerol sulfate (dPGS) of different sizes (generations) by isothermal titration calorimetry (ITC) and computer simulations. The analysis by ITC revealed the formation of a 1:1 complex for the dPGS-G2 of second generation. The secondary structure of HSA remained unchanged in the presence of dPGS-G2 as shown by circular dichroism. For higher generations several HSA bound to one polymer (dPGS-G4: 2; dPGS-G5.5: 4). The free enthalpy of binding ΔG_b was determined at different temperatures and salt concentrations. The binding constant K_b exhibited a logarithmic dependence on the salt concentration thus indicating a marked contribution of counterion-release entropy to ΔG_b. The number of released counterions ($\sim$4) was found to be independent of temperature. In addition, the temperature dependence of ΔG_b was small whereas the enthalpy ΔH_ITC was found to vary strongly with temperature. The corresponding heat capacity change $\Delta C_\mathrm{p,ITC}$ for different generations were of similar values [8 kJ/(mol K)]. The nonlinear van't Hoff analysis of ΔG_b revealed a significant heat capacity change $\Delta C_\mathrm{p,vH}$ of similar magnitude [6 kJ/(mol K)] accompanied by a strong enthalpy-entropy compensation. ΔG_b obtained by molecular dynamics simulation with implicit water and explicit ions coincided with experimental results. The agreement indicates that the enthalpy-entropy compensation assigned to hydration effects is practically total and the binding affinity is fully governed by electrostatic interactions.

[a)] Electronic mail: haag@chemie.fu-berlin.de

[b)] Electronic mail: matthias.ballauff@helmholtz-berlin.de

I. INTRODUCTION

Charged dendritic polymers have been discussed for various biomedical applications, e.g. gene transfer, drug delivery and polymer therapeutics.[1–6] Dendritic polyglycerol sulfate (dPGS) is a synthetic hyperbranched polymer that closely resembles the respective perfect dendrimers.[7–9] It was found that dPGS is fully biocompatible and its use as anti-inflammatory drug is highly promising.[10,11] Recently, dPGS has also been identified as an excellent candidate for virus inhibition and drug delivery.[12–16] A meaningful application of a new agent requires consideration of its interaction with native proteins and in particular with human serum albumin (HSA) which is the most abundant plasma protein.[17] HSA plays a crucial role in the antioxidant capacity of human serum and provides multiple binding sites for ligands including fatty acids and many toxins.[18–23]

Up to now, there are comparably few studies dealing with the binding of charged dendrimers with HSA. At physiological pH the binding constant K_b of HSA with polyamidoamine (PAMAM) dendrimer was found to depend on the chemical structure of charged groups and also the hydrophobicity of the scaffold.[24] In many cases the complexation with a dendrimer led to partial destabilization of the protein due to hydrophobicity of the material.[25–30] Evidently, even a slight change of the secondary structure of HSA by a dendrimer may render its use as a drug questionable.[4] Also, partial unfolding may become a driving force for binding and one should pay special attention to this point. Electrostatic and hydrophobic interactions have been named as driving forces for binding.[24,29–32] However, there is no systematic study on the salt dependence of complex formation of HSA with charged dendrimers. Also, the effect of temperature was solely discussed with relation to the unfolding of bound proteins in the complex.[30,33] This is in contrast to the rich literature on the binding thermodynamics of proteins with biological polyelectrolytes.[31,34–39] In order to elucidate the driving forces, we require a quantitative knowledge of the balance of electrostatic and hydration-mediated effects leading to complex formation.

Previously, we employed isothermal titration calorimetry (ITC) and molecular dynamics simulations to analyze the interaction of HSA with a short chain of poly(acrylic acid) (PAA) containing 25 repeating units.[40] The simulations were coarse-grained with an implicit (continuum) treatment of water but retained the explicit action of salt ions and the hetereogeneous native charge distribution of the protein. Hence, hydration effects were only

included by dielectric screening while the full electrostatic interaction was considered still molecularly resolved. The binding constant determined by ITC agreed well with the value predicted by the simulations thus strongly indicating that the binding was fully governed by electrostatic interactions, which makes sense for a fully charged polyelectrolyte such as PAA. We found that the electrostatic binding was mostly dominated by the the well-known counterion-release mechanism:[41] A patch of charges on the protein surface becomes a multivalent counterion of the polyelectrolyte upon binding, thus releasing a part of the condensed counterions of the polyelectrolyte.[40,42–44] Approximately 3 counterions on the PAA chain were released upon complexation leading to a large favorable entropic contribution to the binding affinity.

More recently, we extended these combined experiment/simulation approaches to the interaction between dPGS and lysozyme which served as a well-defined model protein.[44] The association was found to be strong and several proteins were bound to dPGS. The number of bound proteins and experimental binding constants found by ITC could be completely rationalized in terms of the computer simulations based on our newly established coarse-grained model of dPGS.[9] A consistent comparison of binding free enthalpies taking into account the subtleties of cooperativity effects in the interpretation of ITC isotherms was revealed.[44] Owing to the high surface charge of dPGS it was not unexpected that there too we did not find any indication for hydration-mediated interactions, as considerably present in other dendrimer-protein binding systems.[24,30] Thus, the electrostatic interaction was the main driving force. Again the counterion-release mechanism was found to be the major contribution for binding, and linear (Debye-Hückel) electrostatic screening interactions were significant as well at 10 mM salt concentration. Hence, the combination of experiments with simulations led to a complete characterization of the electrostatic interaction between lysozyme and the charged dendrimer in terms of an empirical but simple separation in counterion release and screening effects.[44] However, this study was restricted to a single temperature and no full thermodynamic information was available.

In this work we extend the successful combination of molecular computer simulations with ITC to the investigation of the full association thermodynamics (affinity, enthalpy and entropy) between the important plasma protein HSA and dPGS. ITC is certainly the method of choice as it allows to determine the number of bound proteins and thermodynamic quantities at the same time.[39,45] The binding constant will be determined by ITC at different

temperatures and salt concentrations and again compared to simulations. Special attention is paid to the secondary structure of HSA in the bound state using circular dichroism (CD) spectroscopy. Any marked change would lead to a measurable heat signal which would disturb the thermodynamic analysis of the complex formation.[25]

The dependence of binding affinity on temperature can be used to obtain the binding enthalpy and entropy via a van't Hoff plot that takes into account the large specific heat observed for many comaparble systems.[35–37] In this way the various enthalpic and entropic contributions can be determined and compared to the free enthalpy of binding. In particular, we strive at an analysis of the marked enthalpy-entropy compensation[46] found for biological polyelectrolytes interacting with proteins.[47,48] The detailed molecular information on dPGS and HSA furnished by simulations can reveal the contribution of electrostatics to binding. Hence, this well-studied charged dendrimer[9] with HSA provides a model system that can lead to a better understanding of protein-polyelectrolyte interaction used in nanomedicine.[49–51]

II. MATERIALS AND METHODS

A. Materials

Human serum albumin (HSA) was purchased from Sigma-Aldrich (A3782) and used directly. HSA has a molecular weight of 66.5 kD and carries -14 e net charges under physiological pH.[40,52] The hydrodynamic radii of HSA and dPGS were measured by dynamic light scattering. The data are gathered in the supplementary information.

The chemical structure of a perfect dendrimer dPGS-G2 is illustrated in Fig. 1. dPGS is obtained by sulfation of a fractionated hyperbranched polyglycerol.[7,53] Thus, the synthetic dPGS is a dendritic polymer with low polydispersity and a degree of branching ∼60% compared to 100% for the perfect dendrimer.[7] Table I gives the molecular weight $M_{\mathrm{n,dPGS}}$ of dPGS. The degree of sulfation (DS) can be determined from the weight percentage of sulfur.[8,53] Here, the fully sulfated dPGS-G2, -G4, and -G5.5 were utilized while the main work was done on dPGS-G2. The generation of dPGS was assigned by comparing their molecular weight to the perfect dendrimer.[9]

The size and zeta potential of the used dPGS have been studied before in 10 mM salt

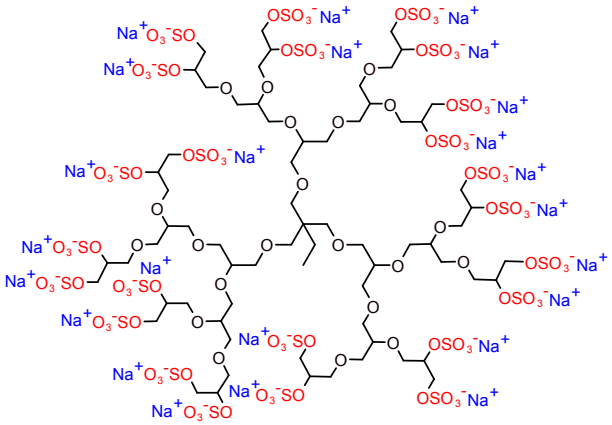

FIG. 1. Chemical structure of the dPGS-G2.

solution.[9] The results were directly compared to molecular computer simulations of the perfect dendrimers. With the agreement between experimental and simulation results, we could demonstrate that the idealized structure shown in Figure 1 provides a good rendition of the hyperbranched synthetic dPGS. The surface potential allowed us to deduct the effective charge $Q_{\mathrm{dPGS,eff}}$ of dPGS in the aqueous electrolyte solution at 10 mM salt concentration. Table I cites the most important parameters from this study.[9]

TABLE I. Properties of dPGS.[9] PDI: polydispersity index of the dPG core determined by gel permeation chromatography. DS: degree of sulfation determined from elemental analysis. N_{ter} represents the number of terminal sulfate groups. The number-averaged molecular weight $M_{\mathrm{n,dPGS}}$ was calculated from the respective dPG core $M_{\mathrm{n,dPG}}$ and sulfate groups. The effective net charge $Q_{\mathrm{dPGS,eff}}$ was taken from previous simulation of dPGS dendrimers with explicit counterions done at an ionic strength of 10mM.[9]

dPGS	G2	G4	G5.5
$M_{\mathrm{n,dPG}}$ [kD]	2.0	7.4	19.6
PDI	1.7	1.7	1.2
DS [%]	$\geq$98	$\geq$98	$\geq$98
N_{ter}	28	102	266
$M_{\mathrm{n,dPGS}}$ [kD]	4.9	17.8	46.7
$Q_{\mathrm{dPGS,eff}}$ [e]	-11	-19	-28

B. Isothermal titration calorimetry

The ITC measurements were performed with a VP-ITC instrument (MicroCal, GE Healthcare, Freiburg, Germany) with a cell volume of 1.43 ml and a syringe volume of 280 μl. All samples were dialyzed against buffer before measurements. Buffers with different ionic strengths were prepared by adding NaCl into 10 mM phosphate buffer with pH 7.4. For the forward titration HSA solution of 48 mg/ml was titrated into the dPGS-G2 solution. For all the reverse titrations the protein solutions were located in the cell and the dPGS solutions were in the syringe and titrated into the cell. Here, the initial concentration of HSA solution increased from 2 to 9 mg/ml with the generation of dPGS. The concentrations of dPGS samples were prepared according to the molar ratio (see supplementary information). The single set of identical sites (SSIS) model was chosen for the fitting of the ITC-isotherms by the Origin software (MicroCal, Inc.). A detailed discussion of the evaluation of the ITC-data has been given recently.[44]

C. Circular dichroism

CD measurements of HSA in the absence and presence of dPGS-G2 were carried out with a J-810 spectropolarimeter (Jasco, Hessen, Germany) equipped with a Peltier temperature controller. The spectra were recorded from 190 to 240 nm with a scan speed of 100 nm/min and a bandwidth of 1 nm using 0.1 cm quartz cells. The concentrations of HSA and dPGS-G2 were 4.5 μM and 25.2 μM, respectively, keeping the molar ratio comparable to the one used in the reverse ITC measurements. The c_s=25 mM phosphate buffer pH 7.4 was recorded as background which was subtracted from the sample spectra.

D. Coarse-grained computer simulation

As in our previous works,[40,44] we utilized implicit-water, explicit-salt coarse-grained (CG) simulations with the second-order stochastic dynamics (SD) integrator as provided in the GROMACS 4.5.4 software package.[54] The Langevin equation was integrated in 2 fs time steps with a friction time constant of $\tau_t = 1$ ps. The CG model of HSA was constructed by mapping each amino acid residue onto a single CG segment (bead). The structure of HSA in its native state was taken from the PDB data bank entry ID:1N5U. A structure-based,

Go-like model force field provided by the SMOG webtool for bimolecular simulations[55] was utilized to maintain the corresponding HSA native structure.[40] Only the CG beads referring to the acidic or alkaline amino acid residues at physiological pH were charged. To be precise, arginine and lysine were assigned with charge +1 e while aspartic acid and glutamic acid with -1 e. Thus, the overall net charge of HSA amounted to -14 e. The CG scheme of the dPGS with explicit ions and their parametrization was illustrated in our previous paper.[9] In short, the CG beads of the dPGS molecule represented individually the monomeric and the terminal groups. The terminal sulfate groups were charged each with -1 e. That gave the dPGS-G2 a net charge of -24 e and the degree of polymerization $N = 22$. The HSA-dPGS interaction included the charge-charge Coulomb interaction as well as the short-range Lennard-Jones (LJ) interaction with identical contact energy $\epsilon_{ij}^{inter} = 0.06\ k_BT$ for all pairwise HSA-dPGS CG beads as well as salt ions. Ions and HSA beads all had a LJ $\sigma = 0.4$ nm, while in dPGS the bead size varied by type.[9] The Lorentz-Bertelot mixing rules were applied.[9] Neutralizing counterions were added to the system as well as salt ions to adjust the ionic strength.

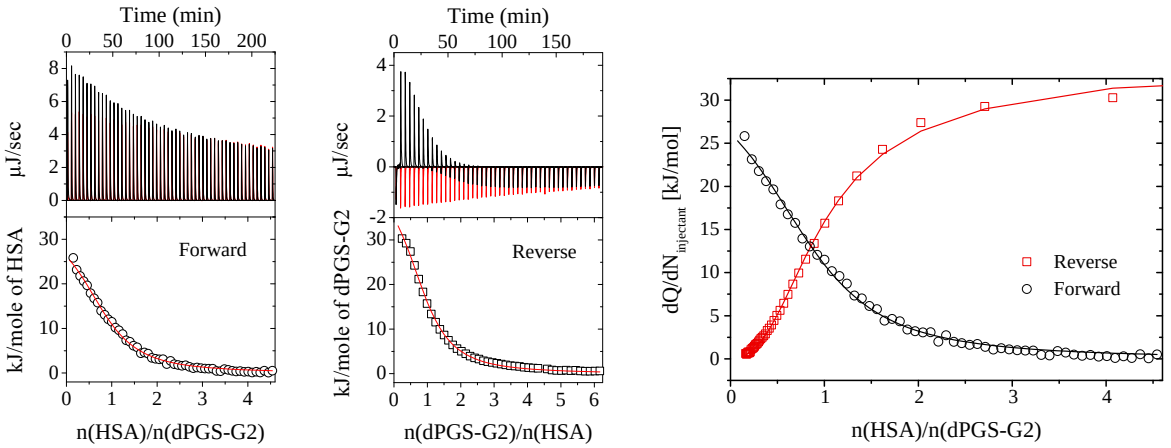

(a) (b) (c)

FIG. 2. The (a) forward and (b) reverse ITC isotherms for dPGS-G2-HSA interaction in c_s=25 mM phosphate buffer pH 7.4 at 310 K. The black and red peaks represent the adsorption and dilution heat, respectively. The black circles and squares are integrated heat change from the adsorption peaks after subtraction of the dilution peaks. The solid red curves are fitted enthalpy change by the SSIS model regarding to the molar ratio. (c) Comparison of the forward and reverse titration curves by unifying the molar ratio.

The simulations were performed in a cubic box with a side length of $L = 30$ nm with periodic boundary conditions in all three directions. The electrostatic interactions were calculated via Particle-Mesh-Ewald (PME)[56] summation where the long-range potential was evaluated in the reciprocal space using the Fast-Fourier Transform (FFT) with a grid spacing of 0.16 nm and the cubic interpolation of the fourth order. A cut-off radius of 4 nm was defined for both PME summation and short-range Lennard-Jones interactions. The choice of the cutoff was verified by reference simulations with an increased cutoff value $r_{\mathrm{cut}} = 6$ nm. The simulations were conducted at 283 K, 298 K and 310 K with the static dielectric constant of ϵ_r= 83.8, 78.3 and 74.1 for the continuum solvent, respectively. The PMF between HSA and dPGS was attained by using steered Langevin Dynamics (SLD)[54] as demonstrated before[40,57] with a steering velocity $v_{\mathrm{p}} = 0.2$ nm/ns and harmonic force constant $K = 2500$ kJ mol^{-1} nm^{-2}. Counterions that were within the dPGS effective radius released upon binding were defined as in our previous work.[44]

III. RESULTS AND DISCUSSION

A. Analysis by ITC

To investigate the reversibility of the binding process, HSA is titrated first into dPGS-G2 solution in a forward titration whereas a reverse titration is done by adding dPGS-G2 to a solution of HSA. Fig. 2(a)(b) show the heat flow (titration peaks) with time. Integration of these peaks leads to the ITC-isotherms for forward and reverse measurements as a function of the sample molar ratio n(syringe)/n(cell). As shown in the upper panel the adsorption peaks are endothermic in both titrations. The dilution of HSA adsorbs heat while dPGS releases heat upon dilution in the buffer. After subtraction of the heat of dilution, however, the adsorption curves are comparable as shown in the lower panel that represents the molar heat change for the injectant during titration. The solid lines present the fits of the single set of identical sites binding model.[58]

The fit by the SSIS binding model leads to the following parameters: The binding number N giving the number of bound HSA-molecules per dPGS-molecule, the binding constant K_{b}, and the calorimetric enthalpy ΔH_{ITC}. All data deriving from the forward and reverse titrations are listed in Table II. Both sets of data indicate clearly a 1:1 complex. Due to

TABLE II. Thermodynamic parameters of dPGS-G2 binding with HSA by forward and reverse ITC measurements in c_s=25 mM phosphate buffer pH 7.4 at 310 K.

	N	K_b [10^3 M^{-1}]	$\Delta G_{b,ITC}$ [kJ/mol]	ΔH_{ITC} [kJ/mol]
Forward	0.9±0.03	105±15.9	-29.8±0.4	34.1±1.4
Reverse	1.1±0.02	94.8±4.8	-29.5±0.1	42.4±0.3

possible systematic errors as, e.g. in concentrations, the fit parameters can differ from each other within 20% deviation for one to one binding.[59] If the binding number N is larger than one and the binding constants for all binding sites are distinguishable, the forward and reverse isotherms may exhibit different shapes and give different fits.[59–61] Here the forward and the reverse titrations give comparable binding constants K_b and free enthalpies of binding $\Delta G_{b,ITC}$ within the limits of error.

Figure 2(c) displays a comparison of the forward and the reverse titration curves, both as the function of the molar ratio n(HSA)/n(dPGS-G2). The two curves exhibit approximately a mirror symmetry and intersect at molar ratio ∼1. This is in full accord with the fit results of the titration curves by the SSIS model. An optimization of the starting points in the forward titration can be achieved by increasing the sample concentration.[58,62] However, in the forward titration [HSA] = 48 mg/ml almost reaches the limit of solubility. This problem can be avoided in the reverse titration since HSA in the cell requires much lower concentration and dPGS as injectant is highly soluble. Thus, the data obtained from the reverse titrations are superior. For this reason, the reverse titration was chosen for all the generations in the following measurements.

B. Secondary structure of bound HSA by circular dichroism

As mentioned above, a strong destabilization of the protein's secondary structure in a complex would rule out immediately the use of a dendritic structure as drug. Also, a partial unfolding of the protein upon binding to the polymer would give additional heat signals that disturb the analysis of the ITC data severely. Therefore we checked the secondary structure of HSA in the absence and presence of dPGS-G2 at four temperatures. Fig. 3(a) shows typical CD spectra for HSA which is a helix-rich protein. The two negative bands at 208 nm

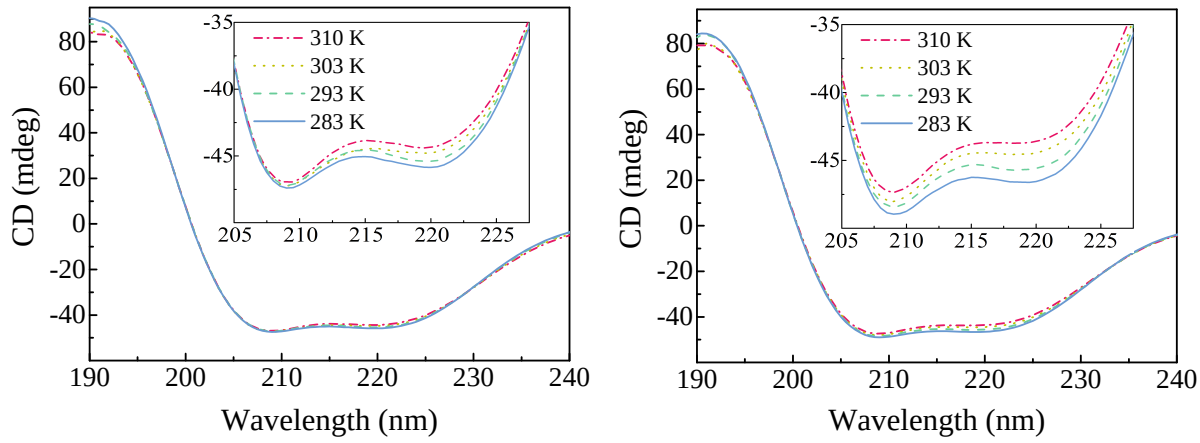

(a) (b)

FIG. 3. The CD spectra for HSA solution (a) without and (b) with dPGS-G2 in c_s=25 mM phosphate buffer pH 7.4 at different temperatures. The insets enlarge the bands characteristic for the α-helix at 208 nm and 222 nm wavelengths.

and 222 nm together with a positive band at 190 nm are characteristics for α-helices. We do not see any marked change of the spectra in Fig. 3(b) when adding a five-fold molar excess of dPGS to the solution of HSA (cf. the discussion of Figure 1 of ref.[25]). The CD spectra change hardly within the temperature range, only the peak at 190 nm slightly reduces and shifts to 191 nm. Also, no destabilization of HSA in the complex is seen when going from 283 K to 310 K. This can be seen from the two insets that display enlarged portions of the CD spectra. From these minor changes in Fig. 3(b) compared to (a) we conclude that dPGS-G2 does not notably disrupt the structure of HSA. This result is clearly opposite to CD spectra measured for other dendrimers containing hydrophobic parts where the binding leads to a severe change of the secondary structure.[25–30]

C. Counterion-release entropy contributions to protein binding

Figure 4(a) and (b) depict the ITC isotherms measured at different ionic strengths for dPGS-G2 at 310 K and 283 K. The fit parameters obtained by the SSIS model are summarized in Table III. The binding constant is decreasing with increasing ionic strength. At c_s=150 mM and 310K no heat signal could be detected. This shows that dPGS does not or very weakly interact with HSA under physiological condition.

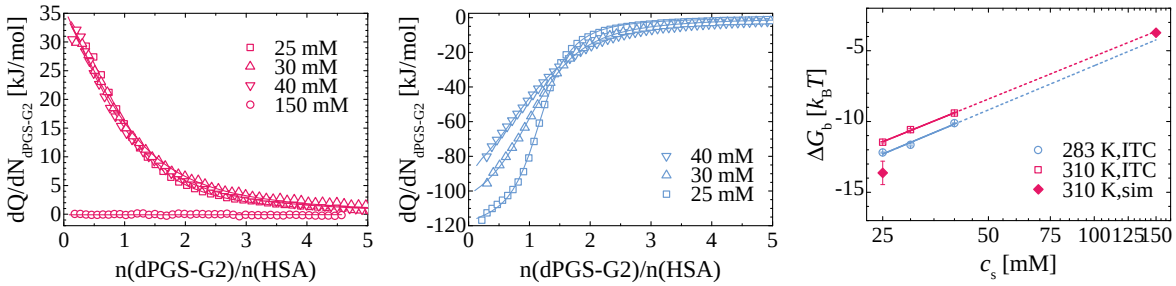

(a) (b) (c)

FIG. 4. ITC isotherms for dPGS-G2 binding with HSA at (a) 310 K and (b) 283 K in phosphate buffer pH 7.4 with different ionic strengths. (c) The salt dependence of the free enthalpy of binding by ITC and computer simulation according to Eq. 2. The fitted number of released counterions is 4.4±0.2 at 310 K and 4.5±0.6 at 283 K.

TABLE III. Thermodynamic parameters of dPGS-G2 binding with HSA in phosphate buffer pH 7.4 at different ionic strengths (see Fig. 4).

T [K]	c_s [mM]	N	K_b [10^3 M^{-1}]	$\Delta G_{b,ITC}$ [kJ/mol]	ΔH_{ITC} [kJ/mol]
310	25	1.1±0.02	94.8±4.8	-29.5±0.1	42.4±0.3
	30	1.2±0.03	39.0±2.5	-27.2±0.2	49.5±0.5
	40	1.3±0.03	12.1±0.8	-24.2±0.2	46.5±0.5
283	25	0.8±0.01	196±7.2	-28.7±0.1	-144.9±0.7
	30	0.9±0.01	114±2.9	-27.4±0.2	-133.6±0.5
	40	0.9±0.01	24.6±0.5	-23.8±0.1	-125.6±0.4

It is well-known that proteins and polyelectrolytes can bind through a counterion-release mechanism.[41] As we have argued previously,[40,42–44] a part of the condensed countions on the polyelectrolyte are replaced by a charged patch of the protein and released upon binding. The corresponding purely entropic gain in free enthalpy can be formulated in first approximation through

$$\Delta G_{ci} = -\Delta N_{ci} k_B T \ln(c_{ci}/c_s), \tag{1}$$

where c_{ci} and c_s are the concentrations of locally condensed counterions and the salt concentration in bulk, respectively. ΔN_{ci} is the number of released counterions. We hence describe the gain of free enthalpy by the equilibrium of a reservoir of strongly bound ions on the surface of the charged dendrimer and the ions in the bulk phase. $c_{ci} = 0.96$ M for dPGS-G2 derived from simulations[9] largely exceeds the salt concentration of 150 mM under physiolog-

ical condition. Counterion-release is therefore also operative at c_s=150 mM. Provided that counterion release/uptake plays an important role in the total binding affinity, the binding constant K_b will change with the salt concentration. Therefore the number ΔN_{ci} of released counterions follows as[41]

$$\frac{d\ln K_b}{d\ln c_s} = -\Delta N_{ci}. \tag{2}$$

Figure 4(c) displays plots of $\Delta G_b \propto \ln K_b$ against c_s in a semi-logarithmic scale. The number of released counterions ΔN_{ci} estimated from the slope is approximately 4 for both temperatures. The small dependence of ΔG_{ci} on temperature is to be expected from Eq. 1.

D. Coarse-grained computer simulations

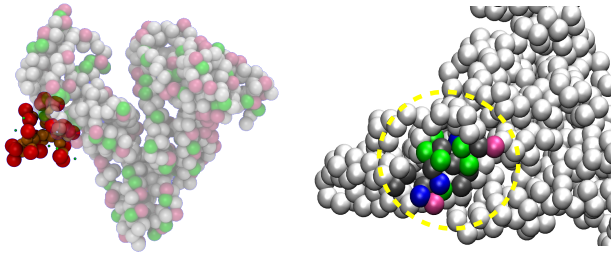

(a) (b)

FIG. 5. (a) Representative CG simulation snapshot of the dPGS-G2-HSA complex at ionic strength 25 mM. Neutral beads in the protein are colored white. Positive beads are green, and negative beads are pink. For dPGS-G2, the monomer beads are colored orange, and the terminal sulfate groups are red surrounded by small counterions (green). The Sudlow site II of HSA responsible for the binding of dPGS-G2 is enlarged in panel (b) which displays the positive amino acids (green) that directly participate in the binding. Hydrophobic and hydrophilic amino acids are colored black and blue, respectively.

In the following we discuss the results from the molecular computer simulations. Here the protein HSA was modeled in a coarse-grained fashion while retaining its heterogeneous charge structure[40] (see also Methods). A verified coarse-grained model of dPGS-G2 was worked out before.[9] As previously,[40,44] we simulate the binding process with explicit counterions but implicit water. We find that dPGS-G2 binds to the Sudlow site II on HSA. The structure of the complex is depicted in Fig. 5(a). It is interesting to note that a single PAA chain also binds to the Sudlow II site.[40] The corresponding site on the protein exhibits

a positive net charge as indicated in Fig. 5(b). This site interacts with dPGS-G2 bearing negative charges of high density. According to the simulation, the amino acids at the binding site that directly contact with dPGS are: positive: Arg410, Lys413, Lys534, Lys536, Lys538, Lys541, and negative: Glu492, Glu542. Therefore the patch features a net charge of +4 e. In the simulations the binding is of purely electrostatic nature as other attractive contributions such as hydrophobic or van der Waals are not considered.

From the simulations we obtain the potential of mean force (PMF) as a function of the HSA-dPGS center-of-mass distance r (see Fig. 6). The free enthalpy ΔG_{b} by simulation can be obtained from the difference between the zero reference state at far separation and the global minimum representing the bound state. The standard binding free enthalpy $\Delta G_{\mathrm{b,sim}}$ in the simulation is finally calculated by $\Delta G_{\mathrm{b,sim}} = \Delta G_{\mathrm{corr}} + \Delta G_{\mathrm{b}}$. $\Delta G_{\mathrm{corr}} = -k_{\mathrm{B}}T \ln(C^0 V_{\mathrm{b}})$ is the entropy correction arising from the accessible volume of the COM of dPGS at the bound state, which is different from the standard volume V^0=1/C^0=1 L/mol.[40,63] We find V_{b}=1.44 nm^3 from simulation quite consistent for all conditions (see supplementary information), which leads to $\Delta G_{\mathrm{corr}} = -0.14\ k_{\mathrm{B}}T$. With that, the resultant standard free enthalpy $\Delta G_{\mathrm{b,sim}}$ at c_{s}=25 mM agrees very well with the experimental data at 283 K and 298 K while it deviates at 310 K within 20 % (see Table IV and Fig. 4(c)). The good agreement thus demonstrates that the electrostatic interaction is the dominant driving force for the binding of HSA. In addition to this, there is only a weak dependence of the simulated $\Delta G_{\mathrm{b,sim}}$ on temperature. This too is in qualitative agreement with the experimental data discussed in the following section.

At low ionic strength both screened electrostatic (Debye-Hückel-like) interaction and counterion-release are expected to contribute to binding.[44] At high salt concentration c_{s}=150 mM, the screened electrostatic interaction between the polymer and the protein having the same charge becomes small and the entropy of counterion-release dominates. In this case, we find $\Delta G_{\mathrm{b,sim}}$ = -3.7 $k_{\mathrm{B}}T$. Figure 4(c) shows that this point is located next to the line extrapolated from the experimental data measured at lower ionic strengths. The simulation thus shows that HSA exhibits a very weak binding to dPGS-G2 at physiological condition consistent with the experimental data.

Fig. 7 displays the decrease of condensed ions on the dPGS surface (in reference to the unperturbed dendrimer far away from the protein) monitored in the simulation. As the dendrimer approaches the protein more counterions are released from the charged terminal

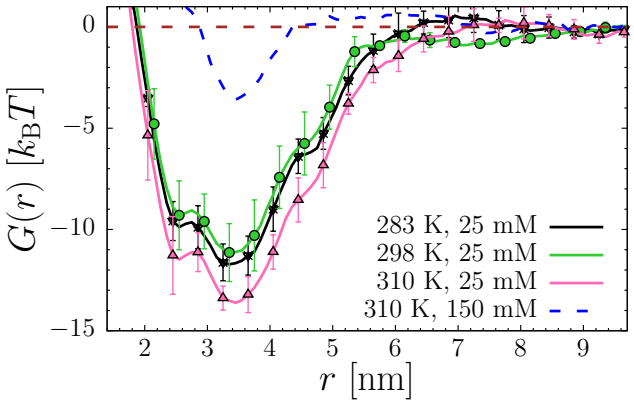

FIG. 6. The free enthalpy profile (or potential of mean force) $G(r)$ between dPGS-G2 and HSA versus their center-of-mass (COM) distance r from coarse-grained computer simulations at different ionic strengths and temperatures. The error bars come from 3 independent simulation runs.

groups of the dPGS. At the global minimum of the PMF, $r_0^1 = 3.5$ nm according to Fig. 6, about 2 ions are released. However, due to the small size and flexible branches of the dendrimer it may roll into the positive pocket of HSA and form a metastable state at shorter distance $r_0^2 = 2.4$ nm, which corresponds to the local minimum in Fig. 6 at all temperatures. There the number of released ions reaches 3. With that $\Delta N_{\rm ci}$ can be even larger at closer contact, which may occur in experiments though not fully favored in the simulations.

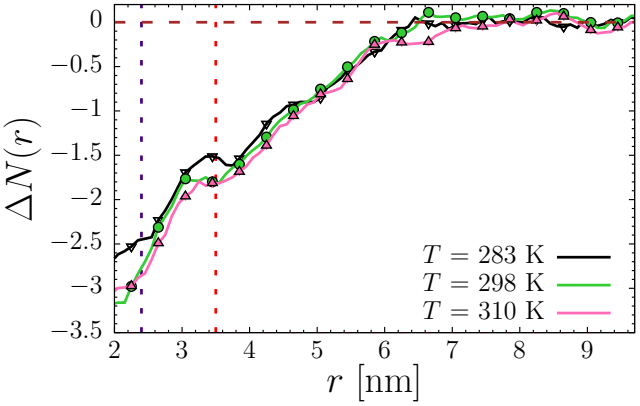

FIG. 7. The release of counterions $\Delta N(r)$ from the dPGS-G2 surface versus the center-of-mass (COM) distance r between the dendrimer and protein at different temperatures and $c_{\rm s} = 25$ mM. The red and purple dashed lines correspond to the local minima of $G(r)$ at distance $r_0^1 = 3.5$ nm and $r_0^2 = 2.4$ nm, respectively.

Both experiments and simulation demonstrate that the number of released ions is nearly

constant at different temperatures. Eq. 1 can then be used for an estimate of $\Delta G_{\rm ci}$: At 310 K and 25 mM salt concentration, the (purely entropic) free enthalpy gain $\Delta G_{\rm ci}$ from counterion release can be calculated as -3.6 $k_{\rm B}T$ per ion employing the concentration of condensed counterions $c_{\rm ci}$=0.96 M from simulation.[9] For 3∼4 released ions (according to both experiment and simulation) $\Delta G_{\rm ci}$ is thus within the range of -11 to -15 $k_{\rm B}T$. The total free enthalpy of binding $\Delta G_{\rm b,ITC}$ from experiment is -11.5 $k_{\rm B}T$ (-29.5 kJ/mol). Hence, we conclude that counterion-release is the major driving force for our system within the errors of the methods. Screened electrostatic interactions just contribute a minor part. This is in accord with our recent study on dPGS binding with the positive protein lysozyme, where counterion-release also plays a dominant role at low salt concentration accompanied in most cases by a small part of simple screened electrostatic interactions.[44]

Together with the previous study on the binding of lysozyme to dPGS[44], the present investigation suggests that the interaction of highly charged macromolecules with proteins can be understood in a semi-quantitative fashion by coarse-grained simulation taking into account water only implicitly. This would in turn mean that other possible interactions related, e.g. to the binding or release of water molecules plays only a minor role in these systems. In order to elucidate this point further, the enthalpies and entropies of binding are determined experimentally next and related to the free enthalpy of binding.

E. Dependence on temperature

The ITC binding isotherms of dPGS with HSA at different temperatures are shown in Fig. 8. All the fit parameters including the binding number N, binding constant $K_{\rm b}$, and calorimetric enthalpy $\Delta H_{\rm ITC}$ are summarized in Table IV. N increases from 1 for dPGS-G2 to ca. 4 for dPGS-G5.5 due to the larger surface area of the dendritic structure. The binding affinity decreases with increasing generation slightly, probably due to higher effective charge[9] and increased electrostatic repulsion of the dPGS to HSA bearing a negative charge as well. For $N > 1$ the repulsion between the bound proteins also comes into play, which leads to a negative cooperativity of binding.

The enthalpy $\Delta H_{\rm ITC}$ measured directly by ITC increases drastically from negative to positive for all the generations as shown in Figure 8(d). Hence, the slope of these curves defining the heat capacity $\Delta C_{\rm p,ITC}$ is of appreciable magnitude for all dPGS under consideration here

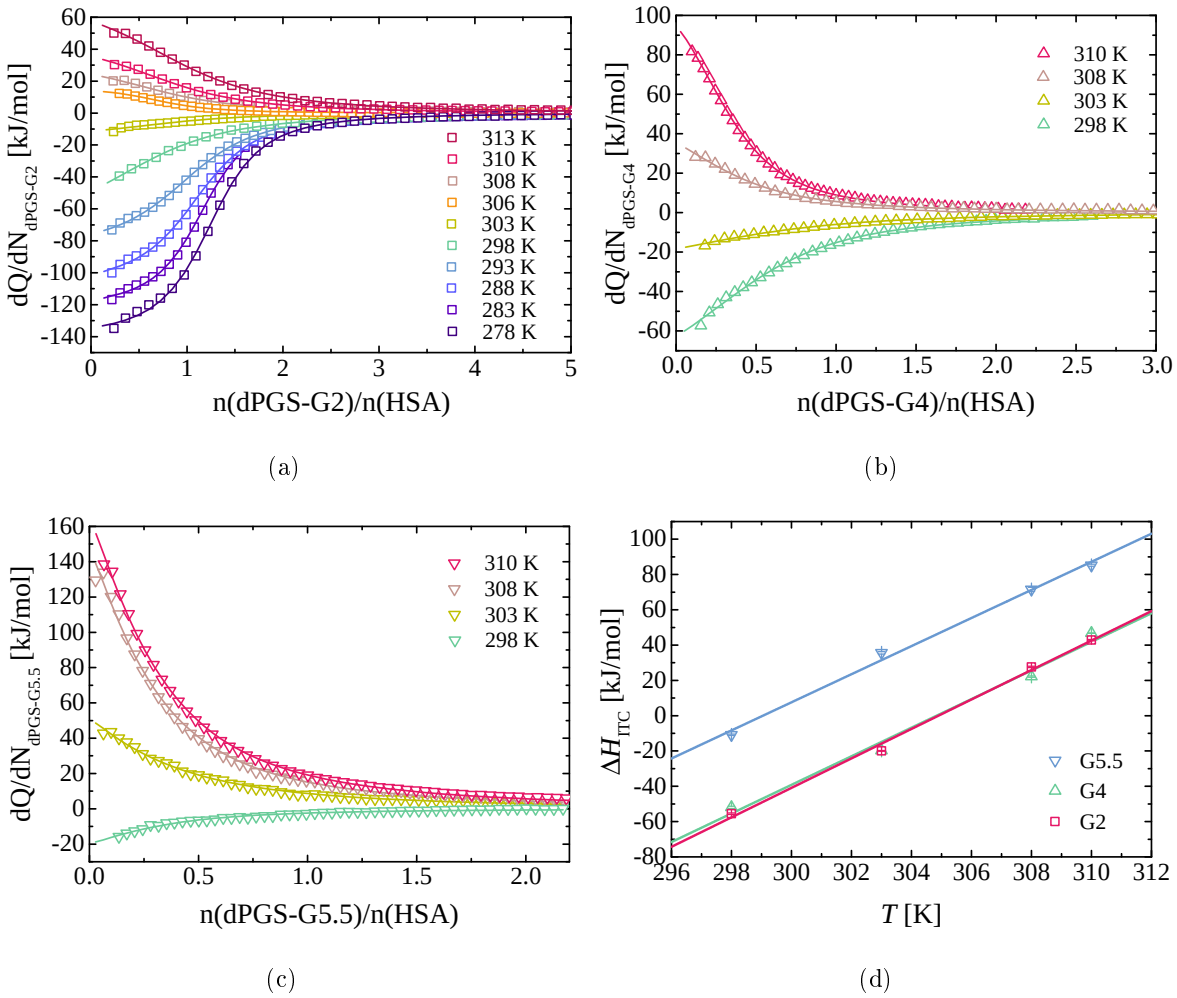

FIG. 8. ITC isotherms for (a) dPGS-G2, (b) -G4, (c) -G5.5 binding with HSA in c_s=25 mM phosphate buffer pH 7.4 at different temperatures. The solid lines are fitted by the SSIS model. (d) The temperature dependence of the observed enthalpy for all the generations from 298 K to 310 K. The heat capacity changes $\Delta C_{p,ITC}$ obtained from the slopes are 8.3±0.4 kJ/(mol K), 8.1±0.6 kJ/(mol K), and 8.0±0.4 kJ/(mol K) for G2, G4 and G5.5, respectively.

($\Delta C_{p,ITC}$: 8.3±0.4 kJ/(mol K), 8.1±0.6 kJ/(mol K), and 8.0±0.4 kJ/(mol K) for G2, G4 and G5.5, respectively.). Compared to the strong dependence of ΔH_{ITC} on temperature, the free enthalpy $\Delta G_{b,ITC}$ changes only slightly with temperature for all generations. Similar findings have been made in studies of the interaction between proteins and nucleic acids.[35–38,64] Here we analyze this dependence on temperature for the binding of HSA to dPGS-G2 where a 1:1. complex is formed. Hence, all possible complications arising from the interaction of several bound proteins (negative cooperativity; see the discussion of this point in ref.[44]) do

TABLE IV. Thermodynamic parameters of dPGS binding with HSA in c_s=25 mM phosphate buffer pH 7.4. HSA was the ligand and dPGS was the receptor. ΔH_{vH}, ΔS_{vH}, and $\Delta C_{p,vH}$ are fit parameters from Fig. 9.

dPGS	T [K]	N	K_b [10^3 M^{-1}]	$\Delta G_{b,ITC}$ [kJ/mol]	$\Delta G_{b,sim}$ [kJ/mol]	ΔH_{ITC} [kJ/mol]	ΔH_{vH} [kJ/mol]	$T\Delta S_{vH}$ [kJ/mol]	$\Delta C_{p,vH}$ [kJ/(mol K)]
G2	278	0.8±0.01	617±31	-30.8±0.1		-175.2±0.8	-140.1±9.8	-109.4±9.6	6.2±0.5
	283	0.8±0.01	196±7.2	-28.7±0.1	-27.9±2.2	-144.9±0.7	-109.3±7.2	-80.3±7.1	
	288	0.9±0.01	133±4.9	-28.2±0.1		-118.6±0.6	-78.5±4.8	-50.6±4.8	
	293	0.9±0.01	75.1±3.1	-27.3±0.1		-87.5±0.5	-47.7±2.8	-20.5±2.9	
	298	1.3±0.03	57.4±3.3	-27.1±0.1	-27.9±3.5	-55.5±2.1	-16.9±2.9	10.3±2.8	
	303	1.1±0.05	54.9±8.7	-27.5±0.4		-19.9±0.2	13.9±4.8	41.5±4.8	
	306	1.3±0.02	54.9±3.7	-27.8±0.2		12.7±0.1	32.4±6.3	60.5±6.3	
	308	1.2±0.04	73.1±6.1	-28.7±0.2		27.6±0.3	44.7±7.3	73.2±7.3	
	310	1.1±0.02	94.8±4.8	-29.5±0.1	-35.1±2.1	42.4±0.3	57.0±8.3	86.1±8.4	
	313	1.0±0.01	92.3±4.0	-29.8±0.1		77.2±0.5	75.5±9.8	105.5±10.0	
G4	298	1.8±0.1	38.0±3.2	-26.1±0.2		-52.0±0.6			
	303	1.6±0.1	28.6±3.6	-25.8±0.3		-19.8±0.3			
	308	2.7±0.2	30.7±3.8	-26.5±0.3		22.2±0.4			
	310	2.8±0.1	22.7±0.5	-25.9±0.1		46.8±0.1			
G5.5	298	3.9±0.8	8.2±2.8	-23.3±0.9		-10.8±0.4			
	303	4.4±0.6	4.6±0.9	-21.2±0.5		35.6±0.7			
	308	5.0±0.4	6.5±0.9	-22.5±0.4		71.6±1.2			
	310	4.2±0.1	8.1±0.4	-23.2±0.1		85.2±0.6			

not intervene.

In the following, the temperature dependence of $\Delta G_{b,ITC}$ of the binding of HSA to dPGS-G2 is analyzed in terms of a non-linear van't Hoff plot that takes into account a large heat capacity $\Delta C_{p,vH}$:[65]

$$\begin{aligned} \Delta G_b &= -RT\ln K_b \\ &= \Delta H_{vH,ref} - T\Delta S_{vH,ref} + \Delta C_{p,vH}[(T - T_{ref}) - T\ln(\frac{T}{T_{ref}})]. \end{aligned} \tag{3}$$

The analysis according to Eq. 3 is done as follows: The given temperature is chosen as reference temperature T_{ref} and the corresponding binding enthalpy $\Delta H_{vH,ref}$, entropy $\Delta S_{vH,ref}$, and heat capacity change $\Delta C_{p,vH}$ are obtained as fit parameters. Fig. 9 displays the corresponding plot. The values ΔH_{vH}, ΔS_{vH} and $\Delta C_{p,vH}$ for dPGS-G2 by this fit are listed in Table IV. The fit results shows that using a constant (T-independent) $\Delta C_{p,vH}$ is a good approximation throughout the present range of temperature.

Fig. 10 summarizes the main results of this analysis. ΔH_{vH} is found to change strongly

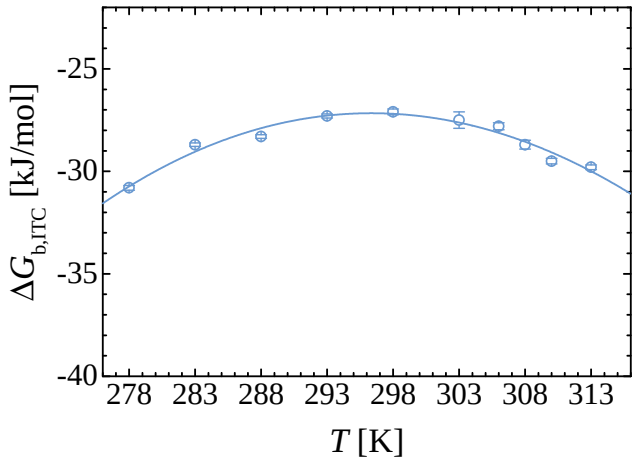

FIG. 9. The nonlinear van't Hoff analysis for dPGS-G2-HSA interaction according to Eq. 3.

with temperature similar to ΔH_{ITC}. The rather small difference between ΔH_{vH} and ΔH_{ITC} is most likely due to linked equilibria, e.g. proton dissociation or association of buffer.[34,35] Lines of ΔH_{vH} and $T\Delta S_{\mathrm{vH}}$ against temperature run perfectly in parallel. The marked compensation of enthalpy and entropy at different temperatures is a typical phenomenon for hydration effects commonly observed in biomolecular association processes.[39,40,46,48,64,66] Concomitantly, ΔG_{b} varies only very slightly with temperature on this scale.

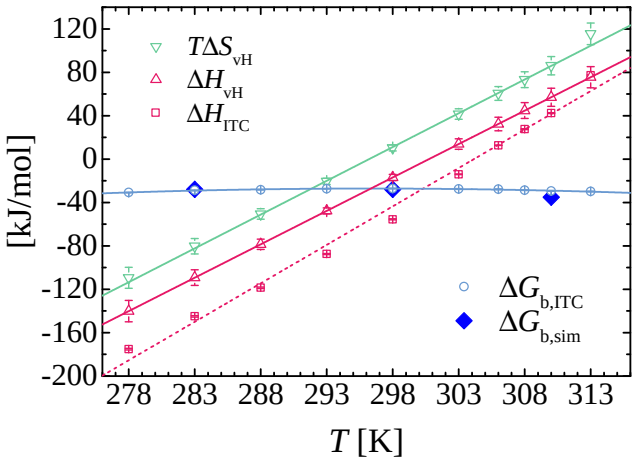

FIG. 10. The enthalpic (ΔH_{vH}) and entropic ($T\Delta S_{\mathrm{vH}}$) contributions in the total free enthalpy of binding for dPGS-G2-HSA interaction according to the van't Hoff analysis. The measured calorimetric enthalpy ΔH_{ITC} is compared to the binding enthalpy. The simulated $\Delta G_{\mathrm{b,sim}}$ agrees with experimental value $\Delta G_{\mathrm{b,ITC}}$ at different temperatures.

As already discussed above, the agreement of ΔG_{b} obtained by experiments and simulations with implicit water indicates that the electrostatic terms dominate the whole binding affinity. Hence, we are led to the conclusion that the compensation of enthalpy and entropy related to hydration is nearly total in the present case. This is in accord with the notion that water molecules involved in the contact area dominate the strong enthalpy-entropy compensation but barely contribute to the binding affinity.[67,68] Computer simulations have shown that the hydration of a hydrophobic surface can generate a large positive heat capacity change.[69,70] A markedly positive ΔC_{p} was also found when studying the interaction of nucleic acids with proteins and was traced back to the hydration of nonpolar surface and/or dehydration of polar surface.[35,67] Here, since dPGS binds to a charged site with a hydrophilic entry and a hydrophobic interior pocket (see Fig. 5(b)), both processes can be involved. We hence conclude that hydration effects lead to marked contributions to the measured enthalpy which is mostly cancelled out by a concomitant entropic term. Thus only electrostatic terms, mainly counterion release, contribute significantly to the measured free enthalpy of binding. A a consequence, the enthalpies measured directly by ITC may not tell us much about the driving forces for binding but the analysis must comprise the entire free ethalpy of binding ΔG_b (cf. also the discussion of this point in ref.[48] and further references given there).

IV. CONCLUSION

We presented a study on the binding between the highly charged dendritic polymer dPGS of different generations and HSA by varying both the temperature and the ionic strength. The entire set of data strongly suggests that the binding affinity is governed by electrostatic factors. In particular, we find from both experiment and simulation that the binding is dominated by counterion release. ITC measurements done at different temperatures indicate strong enthalpy-entropy compensation. All hydration contributions to the enthalpy are thus cancelled out by a concomitantly large entropic contribution.

The present study furthermore suggests that the good agreement of theory and ITC-data is a more general feature, at least for highly charged macromolecular structures. Further studies along these lines are under way. Evidently, simulations are extremely useful when discussing hydrophilic or charged polymeric materials in general as drugs or drug delivery agents. Thus, the present combination of calorimetry and computer simulations may be

helpful to understand the interaction of more complicated carrier systems[49–51] with blood proteins.

ACKNOWLEDGMENTS

The author X. Xu was funded by the China Scholarship Council. The Helmholtz Virtual Institute for Multifunctional Biomaterials for Medicine and the International Research Training Group IRTG 124 funded by the German Science Foundation are gratefully acknowledged for financial support.

REFERENCES

[1]E. G. Timoshenko, Y. A. Kuznetsov, and R. Connolly, J. Chem. Phys. **117**, 9050 (2002).

[2]C. C. Lee, J. A. MacKay, J. M. Fréchet, and F. C. Szoka, Nat. Biotechnol. **23**, 1517 (2005).

[3]Y. Cheng, L. Zhao, Y. Li, and T. Xu, Chem. Soc. Rev. **40**, 2673 (2011).

[4]J. Khandare, M. Calderón, N. M. Dagia, and R. Haag, Chem. Soc. Rev. **41**, 2824 (2012).

[5]N. T. Pourianazar, P. Mutlu, and U. Gunduz, J. Nanopart. Res. **16**, 2342 (2014).

[6]J. Bugno, H.-j. Hsu, and S. Hong, Biomater. Sci. **3**, 1025 (2015).

[7]R. Haag, A. Sunder, and J.-F. Stumbé, J. Am. Chem. Soc. **122**, 2954 (2000).

[8]H. Türk, R. Haag, and S. Alban, Bioconjugate Chem. **15**, 162 (2004).

[9]X. Xu, Q. Ran, R. Haag, M. Ballauff, and J. Dzubiella, Macromolecules **50**, 4759 (2017).

[10]J. Khandare, A. Mohr, M. Calderón, P. Welker, K. Licha, and R. Haag, Biomaterials **31**, 4268 (2010).

[11]J. Dernedde, A. Rausch, M. Weinhart, S. Enders, R. Tauber, K. Licha, M. Schirner, U. Zügel, A. von Bonin, and R. Haag, Proc. Natl. Acad. Sci. **107**, 19679 (2010).

[12]D. Maysinger, D. Gröger, A. Lake, K. Licha, M. Weinhart, P. K.-Y. Chang, R. Mulvey, R. Haag, and R. A. McKinney, Biomacromolecules **16**, 3073 (2015).

[13]T. Schneider, P. Welker, K. Licha, R. Haag, and G. Schulze-Tanzil, BMC musculoskeletal disorders **16**, 387 (2015).

[14]J. Vonnemann, C. Sieben, C. Wolff, K. Ludwig, C. Böttcher, A. Herrmann, and R. Haag, Nanoscale **6**, 2353 (2014).

[15]J. Vonnemann, S. Liese, C. Kuehne, K. Ludwig, J. Dernedde, C. Böttcher, R. R. Netz, and R. Haag, J. Am. Chem. Soc. **137**, 2572 (2015).

[16]A. Sousa-Herves, P. Würfel, N. Wegner, J. Khandare, K. Licha, R. Haag, P. Welker, and M. Calderón, Nanoscale **7**, 3923 (2015).

[17]A. G. Gornall, C. J. Bardawill, and M. M. David, J. Biol. Chem. **177**, 751 (1949).

[18]S. Sugio, A. Kashima, S. Mochizuki, M. Noda, and K. Kobayashi, Protein Eng. **12**, 439 (1999).

[19]P. Ascenzi and M. Fasano, IUBMB Life **61**, 1118 (2009).

[20]M. Fasano, S. Curry, E. Terreno, M. Galliano, G. Fanali, P. Narciso, S. Notari, and P. Ascenzi, IUBMB Life **57**, 787 (2005).

[21]H. Mandula, J. M. R. Parepally, R. Feng, and Q. R. Smith, J. Pharmacol. Exp. Ther. **317**, 667 (2006).

[22]O. K. Abou-Zied and N. Al-Lawatia, ChemPhysChem **12**, 270 (2011).

[23]J. Nilvebrant and S. Hober, Comput. Struct. Biotechnol. J. **6**, 1 (2013).

[24]J. Giri, M. S. Diallo, A. J. Simpson, Y. Liu, W. A. Goddard III, R. Kumar, and G. C. Woods, ACS Nano **5**, 3456 (2011).

[25]H.-M. Zhang, K. Lou, J. Cao, and Y.-Q. Wang, Langmuir **30**, 5536 (2014).

[26]B. Klajnert, L. Stanisławska, M. Bryszewska, and B. Pałecz, Biochim. Biophys. Acta **1648**, 115 (2003).

[27]E. Froehlich, J. Mandeville, C. Jennings, R. Sedaghat-Herati, and H. Tajmir-Riahi, J. Phys. Chem. B **113**, 6986 (2009).

[28]J. Mandeville and H. Tajmir-Riahi, Biomacromolecules **11**, 465 (2010).

[29]S. Sekowski, A. Buczkowski, B. Palecz, and T. Gabryelak, Spectrochim. Acta A **81**, 706 (2011).

[30]P. Chanphai, E. Froehlich, J. Mandeville, and H. Tajmir-Riahi, Colloids Surf. B **150**, 168 (2017).

[31]S. Lindman, I. Lynch, E. Thulin, H. Nilsson, K. A. Dawson, and S. Linse, Nano Lett. **7**, 914 (2007).

[32]L. Giehm, C. Christensen, U. Boas, P. M. Heegaard, and D. E. Otzen, Biopolymers **89**, 522 (2008).

[33]M. Ciolkowski, B. Pałecz, D. Appelhans, B. Voit, B. Klajnert, and M. Bryszewska, Colloids Surf. B **95**, 103 (2012).

[34]N. Welsch, A. L. Becker, J. Dzubiella, and M. Ballauff, Soft Matter **8**, 1428 (2012).

[35]A. Niedzwiecka, J. Stepinski, E. Darzynkiewicz, N. Sonenberg, and R. Stolarski, Biochemistry **41**, 12140 (2002).

[36]K. Datta and V. J. LiCata, Nucleic Acids Res. **31**, 5590 (2003).

[37]K. Datta, A. J. Wowor, A. J. Richard, and V. J. LiCata, Biophys. J. **90**, 1739 (2006).

[38]A. J. Wowor, K. Datta, H. S. Brown, G. S. Thompson, S. Ray, A. Grove, and V. J. LiCata, Biophys. J. **98**, 3015 (2010).

[39]S. Geschwindner, J. Ulander, and P. Johansson, J. Med. Chem. **58**, 6321 (2015).

[40]S. Yu, X. Xu, C. Yigit, M. van der Giet, W. Zidek, J. Jankowski, J. Dzubiella, and M. Ballauff, Soft Matter **11**, 4630 (2015).

[41]M. T. Record, C. F. Anderson, and T. M. Lohman, Q. Rev. Biophys. **11**, 103 (1978).

[42]K. Henzler, B. Haupt, K. Lauterbach, A. Wittemann, O. Borisov, and M. Ballauff, J. Am. Chem. Soc. **132**, 3159 (2010).

[43]C. Yigit, J. Heyda, M. Ballauff, and J. Dzubiella, J. Chem. Phys. **143**, 064905 (2015).

[44]X. Xu, Q. Ran, P. Dey, R. Nikam, R. Haag, M. Ballauff, and J. Dzubiella, Biomacromolecules **19**, 409 (2018).

[45]A. Velazquez-Campoy and E. Freire, Nat. Protoc. **1**, 186 (2006).

[46]D. F. Evans and H. Wennerstrom, *Colloidal domain* (Wiley-Vch, 1999) pp. 279–286.

[47]V. Lafont, A. A. Armstrong, H. Ohtaka, Y. Kiso, L. Mario Amzel, and E. Freire, Chem. Biol. Drug Des. **69**, 413 (2007).

[48]J. D. Chodera and D. L. Mobley, Annu. Rev. Biophys. **42**, 121 (2013).

[49]T. Cedervall, I. Lynch, M. Foy, T. Berggård, S. C. Donnelly, G. Cagney, S. Linse, and K. A. Dawson, Angew. Chem. Int. Ed. **46**, 5754 (2007).

[50]D. Walczyk, F. B. Bombelli, M. P. Monopoli, I. Lynch, and K. A. Dawson, J. Am. Chem. Soc. **132**, 5761 (2010).

[51]A. Salvati, A. S. Pitek, M. P. Monopoli, K. Prapainop, F. B. Bombelli, D. R. Hristov, P. M. Kelly, C. Åberg, E. Mahon, and K. A. Dawson, Nat. Nanotechnol. **8**, 137 (2013).

[52]B. Meloun, L. Moravek, and V. Kostka, FEBS Lett. **58**, 134 (1975).

[53]F. Paulus, D. Steinhilber, P. Welker, D. Mangoldt, K. Licha, H. Depner, S. Sigrist, and R. Haag, Polym. Chem. **5**, 5020 (2014).

[54]B. Hess, C. Kutzner, D. Van Der Spoel, and E. Lindahl, J. Chem. Theory Comput. **4**, 435 (2008).

[55]J. K. Noel, P. C. Whitford, K. Y. Sanbonmatsu, and J. N. Onuchic, Nucleic Acids Res. **38**, W657 (2010).

[56]U. Essmann, L. Perera, M. L. Berkowitz, T. Darden, H. Lee, and L. G. Pedersen, J. Chem. Phys. **103**, 8577 (1995).

[57]C. Yigit, M. Kanduc, M. Ballauff, and J. Dzubiella, Langmuir **33**, 417 (2016).

[58]L. MicroCal, MicroCal, LLC, Northampton, MA (2004).

[59]M. W. Pantoliano, R. A. Horlick, B. A. Springer, D. E. Van Dyk, T. Tobery, D. R. Wetmore, J. D. Lear, A. T. Nahapetian, J. D. Bradley, and W. P. Sisk, Biochemistry **33**, 10229 (1994).

[60]A. M. Spuches, H. G. Kruszyna, A. M. Rich, and D. E. Wilcox, Inorg. Chem. **44**, 2964 (2005).

[61]J.-P. E. Grolier and J. M. Del Río, J. Solution Chem. **44**, 987 (2015).

[62]T. Wiseman, S. Williston, J. F. Brandts, and L.-N. Lin, Anal. Biochem. **179**, 131 (1989).

[63]M. K. Gilson and H.-X. Zhou, Annu Rev Biophys Biomol Struct. **36**, 21 (2007).

[64]R. Talhout, A. Villa, A. E. Mark, and J. B. Engberts, J. Am. Chem. Soc. **125**, 10570 (2003).

[65]J. R. Horn, D. Russell, E. A. Lewis, and K. P. Murphy, Biochemistry **40**, 1774 (2001).

[66]W.-Y. Chen, H.-M. Huang, C.-C. Lin, F.-Y. Lin, and Y.-C. Chan, Langmuir **19**, 9395 (2003).

[67]D. Ben-Amotz and R. Underwood, Acc. Chem. Res. **41**, 957 (2008).

[68]B. Breiten, M. R. Lockett, W. Sherman, S. Fujita, M. Al-Sayah, H. Lange, C. M. Bowers, A. Heroux, G. Krilov, and G. M. Whitesides, J. Am. Chem. Soc. **135**, 15579 (2013).

[69]K. A. Silverstein, A. Haymet, and K. A. Dill, J. Am. Chem. Soc. **120**, 3166 (1998).

[70]M. Lukšič, T. Urbic, B. Hribar-Lee, and K. A. Dill, J. Phys. Chem. B **116**, 6177 (2012).

Supporting information for: Interaction of human serum albumin with dendritic polyglycerol sulfate: Rationalizing the thermodynamics of binding

Qidi Ran,[1,2,3] Xiao Xu,[2,3,4] Pradip Dey,[1] Shun Yu,[2,4] Yan Lu,[2] Joachim Dzubiella,[2,3,4] Rainer Haag,[1,3,a)] and Matthias Ballauff[2,3,4,b)]

[1)] *Institute of Chemistry and Biochemistry, Freie Universität Berlin, Takustr. 3, 14195 Berlin, Germany*

[2)] *Institute of Soft Matter and Functional Materials, Helmholtz-Zentrum Berlin, Hahn-Meitner-Platz 1, 14109 Berlin, Germany*

[3)] *Multifunctional Biomaterials for Medicine, Helmholtz Virtual Institute, Kantstr. 55, 14513 Teltow-Seehof, Germany*

[4)] *Institut für Physik, Humboldt-Universität zu Berlin, Newtonstr. 15, 12489 Berlin, Germany*

[a)]Electronic mail: haag@chemie.fu-berlin.de

[b)]Electronic mail: matthias.ballauff@helmholtz-berlin.de

I. DYNAMIC LIGHT SCATTERING

The surface area of dPGS dendrimer grows with generation according to the size measurement. It was performed with a Zetasizer Nano ZS instrument (ZEN 3500, Malvern Instruments, Herrenberg, Germany) equipped with a 18 mW He-Ne laser (λ=633 nm). The hydrodynamic diameter by volume was measured by dynamic light scattering (DLS) in UV-transparent disposable cuvettes (VWR, Germany) at a back scattering angle of 173°. Each compound was dissolved in 10 mM phosphate buffer (adding NaCl to adjust ionic strength to 25 mM) pH 7.4 at concentration of 2 mg/ml and was filtered through 0.8 μm polyethersulfone syringe filter (PALL, USA). Prior to measurement, the sample was equilibrated for 2 min at 37° and measured with 10 scans each lasting for 10 s. The stated values are the mean of three independent measurements.

TABLE I. Hydrodynamic size of HSA and dPGS used.

	HSA	dPGS-G2	dPGS-G4	dPGS-G5.5
D_h [nm]	6.6±0.1	3.5±0.3	5.8±0.8	7.1±0.3

II. ITC RAW DATA

TABLE II. Initial concentrations of HSA and dPGS in ITC measurements at 25 mM ionic strength and 310 K.

Titration	Cell	Syringe
Forward	[dPGS-G2]= 0.03 [mM]	[HSA]= 0.72 [mM]
Reverse	[HSA]= 0.03 [mM]	[dPGS-G2]= 0.93 [mM]
	[HSA]= 0.10 [mM]	[dPGS-G4]= 1.06 [mM]
	[HSA]= 0.10 [mM]	[dPGS-G5.5]= 1.07 [mM]

The binding affinity of dPGS with HSA decreases with polymer generation, whereas the binding number increases. Therefore the molar ratio in ITC measurements with reverse titration decreases. The initial sample concentrations at 310 K are listed in Table II and

the isotherms for dPGS-G4 and -G5.5 are shown in Fig. 1. The dilution heat for dPGS is more exothermic for higher generation as shown in the titration peaks of the raw data.

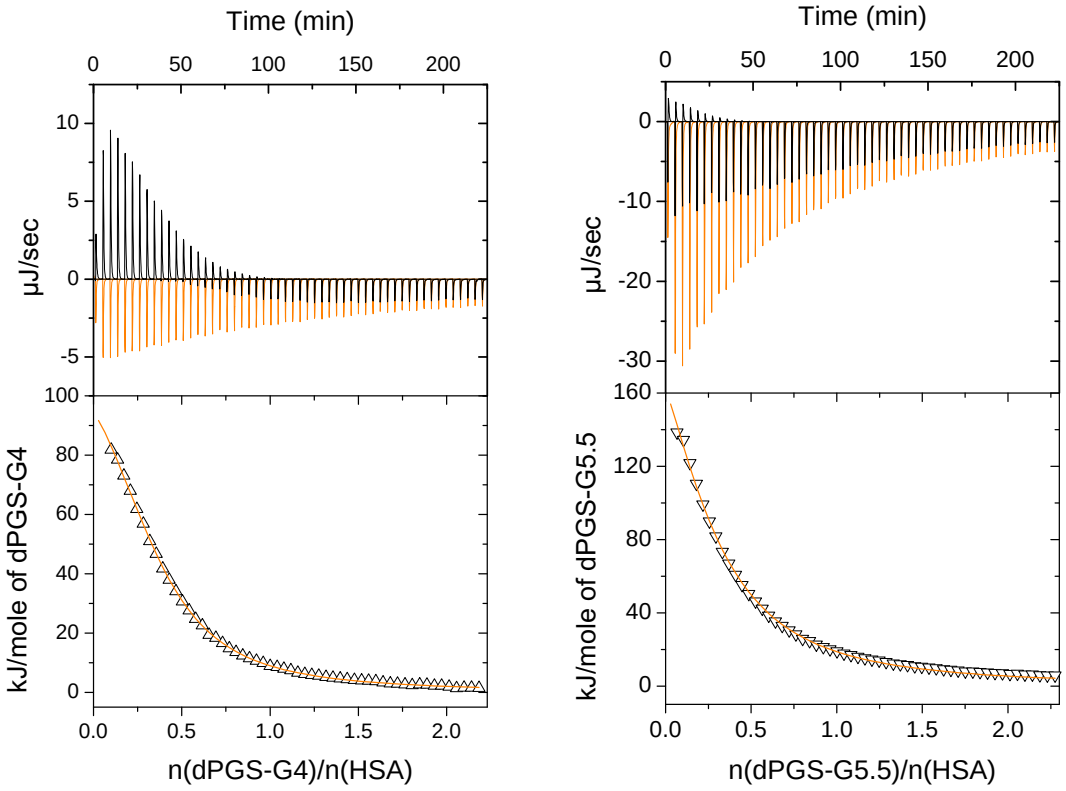

(a) (b)

FIG. 1. ITC isotherms for (a) dPGS-G4 and (b) -G5.5 binding to HSA (reverse titration) in phosphate buffer pH 7.4 at 25 mM ionic strength and 310 K. The black and orange peaks in the upper panel represent the adsorption and dilution heat of dPGS, respectively. The dilution heat is substracted from the adsorption heat. The resultant black triangles in the lower panel are the integrated molar heat for each titration regarding to the injectant. The orange lines are fitted by the single sets of identical sites model.

III. ACCESSIBLE BINDING VOLUME

In order to measure the accessible binding volume of the dPGS-G2 molecule, simulations regarding to the HSA-dPGS complexation in equilibrium are conducted. We plot the $r_{x,y}$ corresponding to the x,y-coordinate of the dPGS-G2 center-of-mass (COM) for each simula-

tion frame in Fig. 2. Namely, the trajectory of the dPGS-G2 COM in simulation is projected at the xy-plane. With that, it is found that for all temperatures and salt concentrations the dPGS is roughly confined in a spherical region. We calculate the standard derivation $\Delta r = \sqrt{1/(3N_s) \cdot \{\sum_{i=1}^{N_s}[(r_x^i - \mu_x)^2 + (r_y^i - \mu_y)^2 + (r_z^i - \mu_z)^2]\}}$ of the $r_{x,y,z}$ series with respect to the respective mean value $\mu_{x,y,z}$. Here, N_s is the number of the sample points and $r_{x,y,z}^i$ refers to the x, y, and z coordinate of the sample point measured at the ith simulation frame. Δr is considered as the radius of the spherical binding volume of dPGS COM, which follows with the binding volume $V_\mathrm{b} = 4\pi\Delta r^3/3$. For all cases, $\Delta r \approx 0.7$ nm is found consistent, which finally leads to the volume $V_\mathrm{b} = 1.44$ nm^3.

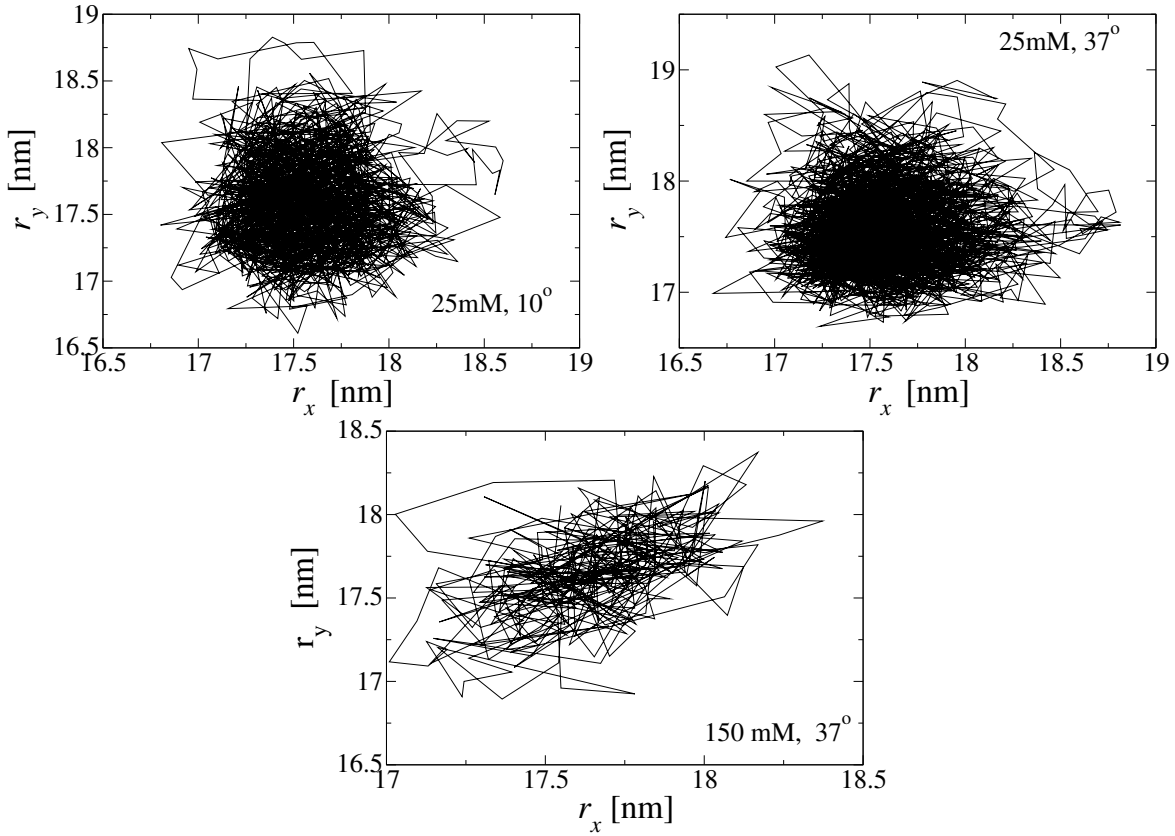

FIG. 2. The projection of the G2-dPGS COM in the xy plane. From left to right, the measure is taken at 25 mM-10°C, 25 mM-37°C, 150 mM-37°C, respectively.

3.3 Counterion-release entropy governs the inhibition of serum proteins by polyelectrolyte drugs

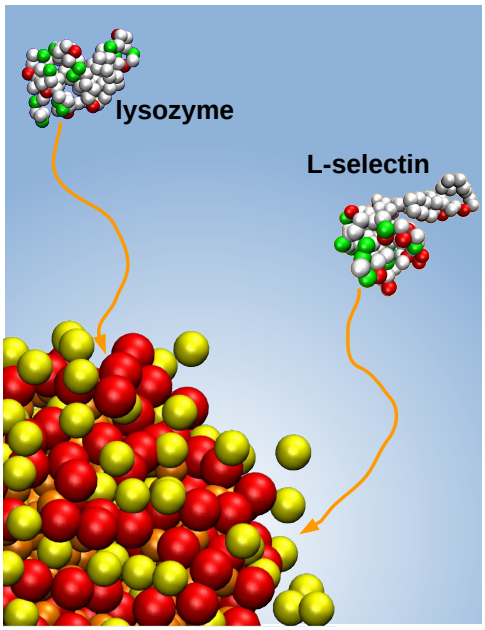

Xiao Xu, **Qidi Ran**, Pradip Dey, Rohit Nikam, Rainer Haag, Matthias Ballauff, Joachim Dzubiella. *Biomacromolecules*, **2018**, 19 (2), 409-416 [157].
https://doi.org/10.1021/acs.biomac.7b01499

Author contributions

Xiao Xu designed the project, performed the coarse-grained simulations, and wrote the manuscript.

Qidi Ran designed the project, performed the ITC experiments, and corrected the manuscript.

Pradip Dey synthesized the dPGS polymers.

Rohit Nikam performed the all-atom simulations.

Rainer Haag discussed the data, provided suggestions, and corrected the manuscript.

Matthias Ballauff discussed the data, provided scientific guidelines, and corrected the manuscript.

Joachim Dzubiella supervised the projexct, discussed the data, and corrected the manuscript.

3.4 Thermodynamics of the binding of lysozyme to a dendritic polyelectrolyte: Counterion-release versus hydration

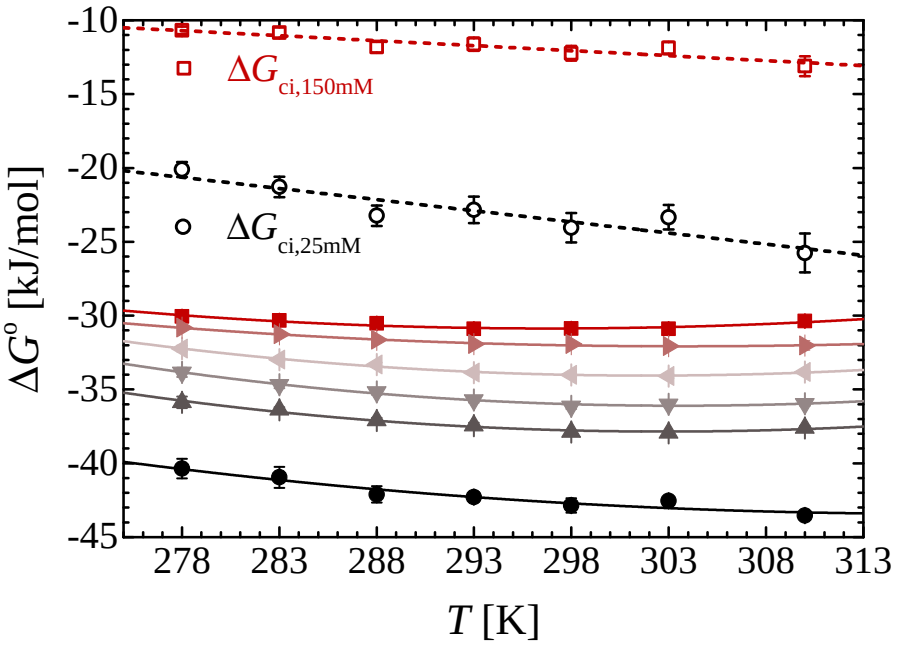

Qidi Ran, Xiao Xu, Joachim Dzubiella, Rainer Haag, Matthias Ballauff (To be submitted).

Author contributions

Qidi Ran designed the project, performed the ITC experiments, and wrote the manuscript.
Xiao Xu performed the simulations and corrected the manuscript.
Joachim Dzubiella discussed the data and corrected the manuscript.
Rainer Haag and Matthias Ballauff supervised the project, discussed the data, and corrected the manuscript.

Thermodynamics of the binding of lysozyme to a dendritic polyelectrolyte: Counterion release versus hydration

Qidi Ran,[1,2,3] Xiao Xu,[2,3,4] Joachim Dzubiella,[2,3,4] Rainer Haag,[1,3,a)] and Matthias Ballauff[2,3,4,b)]

[1)] *Institute of Chemistry and Biochemistry, Freie Universität Berlin, Takustr. 3, 14195 Berlin, Germany*

[2)] *Institute of Soft Matter and Functional Materials, Helmholtz-Zentrum Berlin, Hahn-Meitner-Platz 1, 14109 Berlin, Germany*

[3)] *Multifunctional Biomaterials for Medicine, Helmholtz Virtual Institute, Kantstr. 55, 14513 Teltow-Seehof, Germany*

[4)] *Institut für Physik, Humboldt-Universität zu Berlin, Newtonstr. 15, 12489 Berlin, Germany*

The interaction between dendritic polyglycerol sulfate (dPGS) of the second generation and lysozyme was studied by isothermal titration calorimetry (ITC) at different temperatures and salt concentrations. Analysis by ITC showed that 2∼3 lysozyme molecules were bound to each dPGS. The resulting binding constant K_b and the Gibbs free enthalpy ΔG^o decreased markedly with increasing salt concentration but was nearly independent of temperature. The salt dependence of K_b led to the conclusion that ca. 3 counterions bound to dPGS were released upon complex formation. The gain in entropy by this counterion-release scales logarithmically with salt concentration and is the main driving force for binding. The temperature dependence of ΔG^o was analyzed by the nonlinear van't Hoff plot taking into account a finite heat capacity change $\Delta C_\mathrm{p,vH}$. This evaluation led to the binding enthalpy ΔH_vH and the binding entropy ΔS_vH. Both quantities varied strongly with temperature and even changed sign, but they compensated each other throughout the entire range of temperature. Coarse-grained computer simulations with explicit salt and implicit water were used to obtain the binding free energies that agreed with ITC results. Thus, electrostatic factors were the driving forces for binding whereas all hydration contributions leading to the strongly varying ΔH_vH and ΔS_vH canceled out. The calorimetric enthalpy ΔH_ITC measured directly by ITC differed largely from ΔH_vH. ITC measurements done in two buffer systems with different ionization enthalpies revealed that binding was linked to buffer ionization and a partial protonation of the protein.

[a)] Electronic mail: haag@chemie.fu-berlin.de

[b)] Electronic mail: matthias.ballauff@helmholtz-berlin.de

I. INTRODUCTION

The interaction of proteins with polyelectrolytes is a long-standing subject in biochemistry, drug design, and materials science:[1–5] On the one hand, many biopolymers as e.g. DNA are highly charged and interact with proteins via electrostatic forces.[6] On the other hand, proteins may form complexes with natural or synthetic polyelectrolytes of opposite charge ("complex coacervates" cf. ref.[2,3]) that have found applications as food colloids.[5] Central to this field is the investigation of the equilibrium binding constant between a given protein and a polyelectrolyte in order to explore the various thermodynamic factors that lead to binding. Isothermal titration calorimetry (ITC) has become a pivotal technique to explore the thermodynamics of binding of polyelectrolytes and ligands in general to proteins.[7,8] The heat signal measured directly by ITC can be converted to the binding constant K_b the temperature dependence of which may then yield the enthalpy and entropy of binding ΔH_b and ΔS_b, respectively.[9–11] The total heat ΔH_ITC also furnished by ITC need not agree with ΔH_b since linked equilibria may also contribute to the heat signal.[12,13] It is thus evident that ITC can be used to explore the full thermodynamics of binding between polyelectrolytes and proteins. However, the use of these data for the design of drugs may be difficult and in parts questionable.[14] Additional information furnished by computer simulations using coarse-grained and molecular models would clearly be helpful to clarify the details of binding in order to use these data for drug design and for predicting the binding constants of polyelectrolytes to a given protein.

We have recently shown that ITC data can directly be combined with molecular dynamics (MD) simulations.[16] As model polyelectrolyte we used the dendritic polyglycerol sulfate(dPGS). The scaffold of these dPGS dendrimers is made up from a hyperbranched polyglycerol core. Sulfate groups attached to all terminals render these molecules very hydrophilic and highly charged. dPGS has been shown to be promising drug and carrier recently[17–23]. It has also been the subject of a comprehensive study by computer simulation[24] and can be considered a well-controlled model polyelectrolyte. Fig. 1 displays the chemical structure of a dPGS. The synthesized dPGS with hyperbranched structure[25] comes close to the perfect dPGS dendrimer of generation 2 (see the discussion in ref.[24]).

In our recent study, ITC and computer simulations with implicit water were used to study the binding of lysozyme to dPGS of different generations.[16] This investigation demonstrated

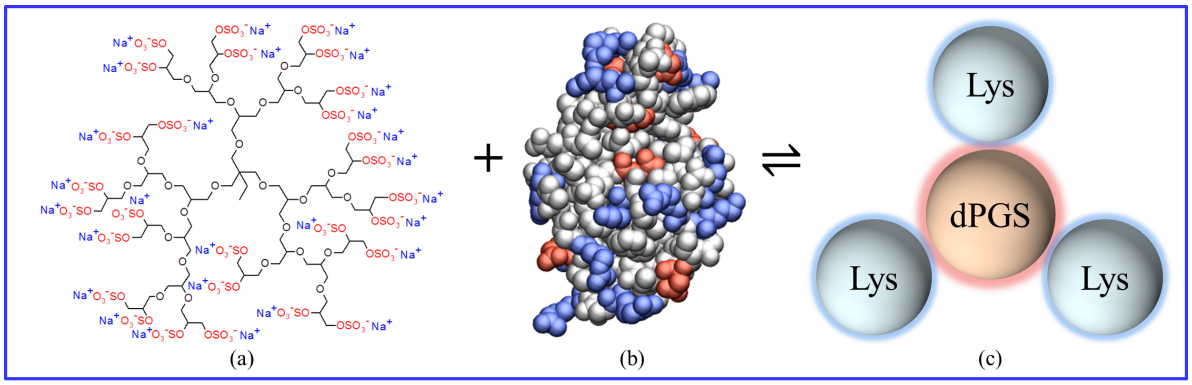

FIG. 1. (a) Chemical representative of dPGS. (b) The molecular structure of lysozyme (PDB ID: 2LZT).[15] The blue, red, and white beads represent positive, negative, and neutral amino acids, respectively. (c) Sketch of the dPGS-Lys complex taking all molecules as spheres. The overall positive lysozymes and negative dPGS are characterized with blue and red surfaces, respectively. The stoichiometry of complexation is ∼3 at 310 K and 10 mM salt purely driven by electrostatic interaction.[16]

that the interaction of the dPGS dendrimers with proteins can be traced back mainly to electrostatic effects. The main part of the electrostatic interaction was shown to be counterion-release: A part of the counterions condensed to the polyelectrolyte dPGS[24] is released upon binding of the protein. The released counterions increase the entropy of the system. The decrease of Gibbs free enthalpy ΔG° scales therefore with $\ln c_{\mathrm{s}}$ where c_{s} denotes the salt concentration in the solution.[6,26] In addition to this, the screened (linear) electrostatic attraction on the Debye-Hückel (DH) level between the negatively charged dPGS and the positively charged lysozyme plays a role at low concentration of added salt.[16] We found that the binding constant derived from MD-simulations with explicit ions but implicit water fully agreed with the experimental values derived by ITC. The same result was obtained in a recent study of the binding of poly(acrylic acid) to HSA by both ITC and computer simulations.[27] These findings led to the conclusion that electrostatic terms dominate the binding of charged polymers to proteins to a large extend.

To elucidate this point further, we have recently performed a comprehensive thermodynamic investigation of the binding of HSA to dPGS by ITC.[28] The binding constant K_{b} was measured at different temperatures at low salt concentration. In addition to this, the dependence of the binding constant on salt concentration was determined. Here the analysis of the

binding constant K_b of the 1:1-complex of HSA and dPGS-G2 demonstrated that the free enthalpy of binding depends hardly on temperature. However, both the enthalpy and entropy have been found to vary strongly with temperature but compensate each other. This enthalpy-entropy compensation (EEC) has been observed in many systems by now[14,29–33] and is related to a high value of the heat capacity change ΔC_{p}. It is clearly seen also in systems of biological relevance.[9–11]

Here we extend these investigations to the binding of dPGS-G2 to lysozyme using again a systematic variation of both the salt concentration and the temperature. In this way the electrostatic factors contributing to binding can be separated from hydrophilic/hydrophobic hydration/dehydration. In addition to these experimental studies, we extend our previous MD-simulations of the system dPGS/lysozyme.[16] Special attention is laid to the direct comparison of experimental data to data obatined by simulations. The EEC can hence be studied in detail for this system which will allow us to discuss the role of thermodynamic quantities for predicting the interaction of proteins with highly charged macromolecules. In this context it is revealing to consider the various contributions to the enthalpy ΔH_{ITC} measured directly by ITC. The entire set of data will allow us a comprehensive discussion of the use of thermodynamic data when discussing and predicting thermodynamic equilibria between proteins and highly charged macromolecules.

II. MATERIALS AND METHODS

A. Materials

The protein lysozyme from chicken egg white with molecular weight 14.3 kDa was purchased from Alfa Aesar (J60701) and used directly. dPGS of second generation (dPGS-G2) was synthesized according to literature.[25,34] The properties of dPGS-G2 are collected in Table I. More details are given in our previous work.[16,24]

B. Isothermal titration calorimetry

10 mM sodium phosphate dibasic (Na_2HPO_4) and 1.8 mM potassium phosphate monobasic (KH_2PO_4) were dissolved into solution and the pH was adjusted to 7.4 at R.T. by adding 1 M NaOH. To prepare a buffer with different ionic strengths additional NaCl was added into

TABLE I. Chemical properties of dPGS. $M_{\mathrm{n,dPGS}}$: number-averaged molecular weight of dPGS; PDI: polydispersity index; DS: degree of sulfation of the terminal groups; N_{ter}: total number of terminal sulfate groups.

Label	$M_{\mathrm{n,dPGS}}$ [kD]	PDI	DS [%]	N_{ter}
dPGS	4.9	1.7	$\geq$98	28

the buffer individually.

Isothermal titration calorimetry was used to evaluate the thermodynamics of dPGS-protein binding. The measurements were performed by a MicroCal VP-ITC instrument (GE Healthcare, Freiburg, Germany) with a syringe volume 280 μl and a cell volume 1.43 ml. The interaction was measured at 6 ionic strengths each with 7 temperatures. A solution of lysozyme was located in the syringe and titrated stepwise into the cell filled with dPGS solution. The dilution heat was obtained by titrating a lysozyme solution of the same concentration into pure buffer. Fig. 2 displays typical examples of experimental ITC-curves. At higher salt concentration the binding affinity became smaller and the sample concentrations had to be increased to obtain a sigmoidal isotherm[35]. Our previous analysis showed that an increase of the sample concentration did not change the resulting binding constant (see Table S1 of ref.[16]). Table II gathers the sample concentrations used for the respective concentration of salt.

TABLE II. Protein concentration c_{Lys} and dPGS concentration c_{dPGS} in ITC measurements at different ionic strength c_{s}. The sample concentrations are the same for different temperatures at one ionic strength.

c_{s} [mM]	25	50	75	100	125	150
c_{Lys} [mM]	0.11	0.24	0.56	0.87	1.31	1.36
c_{dPGS} [μM]	2.4	10.3	22.5	35.1	57.8	69.9

The raw data were analyzed with the Origin 7.0 (MicroCal) software and the single set of identical sites (SSIS) model was chosen to fit the isotherm. SSIS model assumes that all the binding sites are equivalent and independent. The thermodynamic data here are compared with previous ITC measurements at 310 K in a different buffer (3-(N-morpholino)propanesulfonic acid; MOPS).[16]

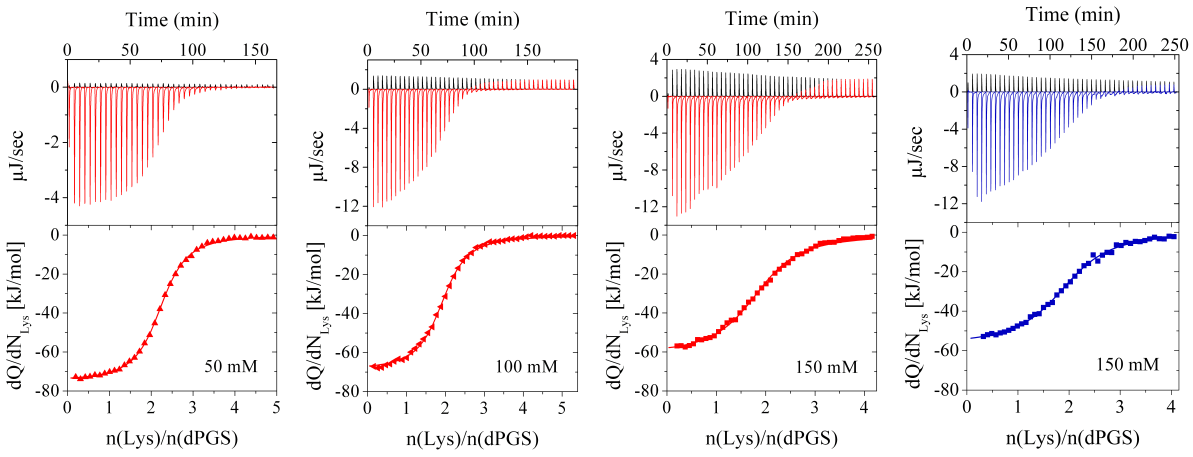

FIG. 2. ITC isotherms in phosphate buffer pH 7.4 at ionic strength (a) 50 mM, (b) 100 mM, and (c) 150 mM and 310 K. (d) shows the isotherm in MOPS buffer at 150 mM and 310 K cited from ref.[16]. The black peaks in the upper panels represent the dilution heat of lysozyme into respective buffer which will be substracted from the adsorption heat. The signal gets stronger at higher ionic strength due to higher sample concentration. The red and blue peaks are the adsorption heat into dPGS solutions. The symbols in the lower panel are the integrated molar heat for each titration related to the added protein. The solid curves are fitted by the SSIS model.

C. Molecular dynamics simulation

Coarse-grained (CG) simulations with implicit water and explicit salt were performed as described in our previous work.[16,27] The simulation used the stochastic dynamics (SD) integrator in GROMACS 4.5.4 software package.[36] The CG model of dPGS-G2 dendrimer was established by us before and used directly here.[24] The CG model of Lysozyme (PDB: 2LZT) was constructed taking each amino acid residue as a single CG bead maintained by a structure-based Go-model force field.[37] At physiological pH dPGS-G2 and lysozyme had net charge of -24 e and +8 e, respectively.[16] The binding between lysozyme and dPGS-G2 was conducted at 293 K and 310 K each with two salt concentrations 25 mM and 150 mM. The potential of mean force (PMF) was obtained using steered Langevin Dynamics (SLD)[36] with steering velocity $v_{\mathrm{p}} = 0.2$ nm/ns and harmonic force constant $K = 2500$ kJ mol^{-1} nm^{-2}. All paramerization was the same as in our previous work.[16]

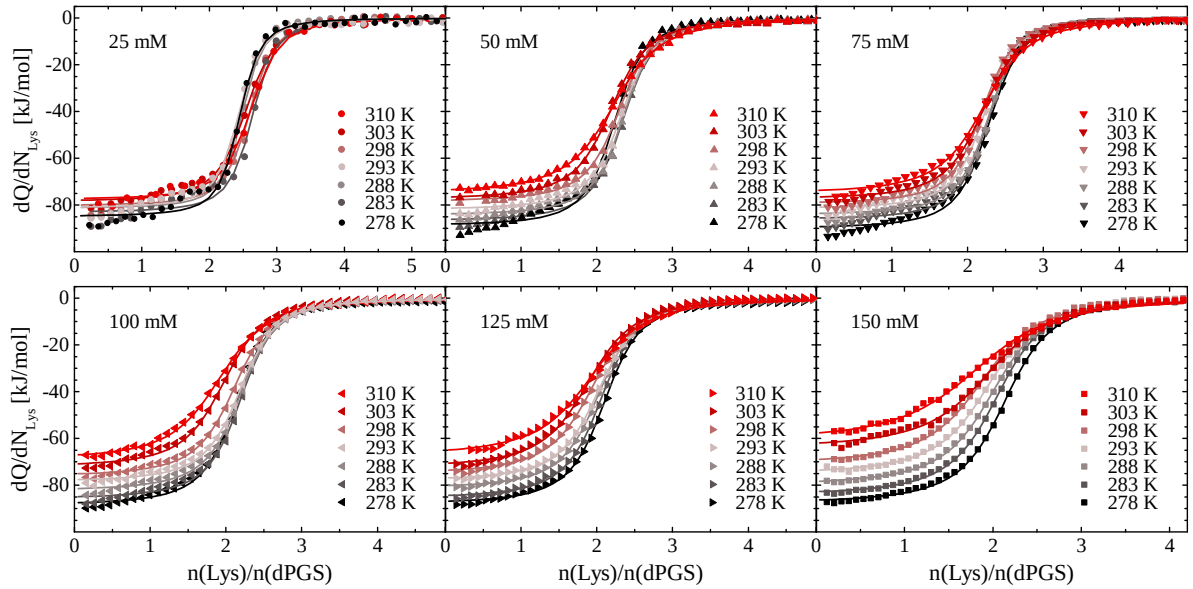

FIG. 3. ITC isotherms for dPGS-G2 binding with lysozyme in phosphate buffer pH 7.4 with ionic strengths: 25 mM, 50 mM, 75 mM, 100 mM, 125 mM, 150 mM at different temperatures. The solid lines present the fits by the SSIS model.

III. RESULTS AND DISCUSSION

The complex formation of lysozyme with dPGS of different generations was studied recently by ITC and computer simulations at 310 K and 10 mM salt concentration.[16] Lysozyme has an effective charge of +8 e at physiological pH. The synthetic dPGS-G2 bears -28 e total charges while its effective charge is -11 e in solution due to counterion condensation.[24] Fig. 1 sketches the adsorption process for dPGS-G2. We found that approximately three lysozyme molecules and one dPGS form a complex with $K_\mathrm{b} \sim 10^8$ M^{-1} at 10 mM salt.[16] The sulfate terminal groups bind with positive patch on the protein thereby releasing ca. 3 counterions bound to dPGS. In the present work, all binding experiments are done in phosphate buffer whereas the experiments in ref.[16] were done in MOPS buffer. Here we chose the phosphate buffer because the adjusted pH hardly changes with temperature.[38] In addition, the use of different buffers will allow us to discern possible heat contributions from the buffer aside from binding[12,13].

The raw data of the titration peaks and the respective isotherms at 310 K and c_s=50 mM, 100 mM, 150 mM are shown in Fig. 2. The interaction is exothermic under all conditions. All the parameters including binding number N, binding constant K_b, and ITC enthalpy ΔH_ITC

could be obtained very well by fitting the data with the SSIS model.[7] Fig. 3 gives a survey of all ITC isotherms together with the respective fits referring to all salt concentrations and temperatures under consideration here. Table III summarizes all fit parameters obtained from the ITC-experiments. The number N of bound lysozyme molecules decreases slightly with salt concentration but stays approximately constant with temperature. In the present salt concentration of 25 mM it is found slightly smaller than previously observed 3 – 4 in 10 mM MOPS buffer.[16] The binding affinity of lysozyme with dPGS decreases with salt concentration as expected. Table III furthermore shows that the binding free enthalpy ΔG^{o} hardly changes with temperature but decreases significantly with increasing ionic strength.

A. Electrostatic and steric contributions to the binding affinity

In our previous study we discussed the electrostatic contributions to the binding constant. Based on a comparison of ITC-data with MD-simulations, we found that the binding between dPGS and lysozyme was mainly driven by counterion-release.[16] Simulations of the highly charged dPGS dendrimers[24] demonstrated that there is a thin shell or Stern layer of condensed counterions on the surface of the dendrimers. From this a surface concentration of condensed counterions c_{ci} can be estimated (see Table S3 of ref.[16]). In case of G2, $c_{\mathrm{ci}} = 0.96$ M is much higher than the salt concentrations in bulk used here in the ITC-runs. When lysozyme is bound to dPGS, the positive patch on the surface of the protein becomes a multivalent counterion to the dendrimer. A concomitant number of the condensed counterions of dPGS is thereby released into the bulk solution. The corresponding gain of entropy follows as

$$\Delta G_{\mathrm{ci}} = -T\Delta S_{\mathrm{ci}} = -\Delta N_{\mathrm{ci}} k_{\mathrm{B}} T \ln(c_{\mathrm{ci}}/c_{\mathrm{s}}), \tag{1}$$

where c_{ci} and c_{s} are the concentrations of local condensed counterions and bulk salt, respectively, and ΔN_{ci} is the number of released counterions.[16,39] From this it follows that the binding constant is related to ΔN_{ci} if counterion-release is a dominant driving force:[6,26]

$$\frac{\mathrm{d}\ln K_{\mathrm{b}}}{\mathrm{d}\ln c_{\mathrm{s}}} = -\Delta N_{\mathrm{ci}}. \tag{2}$$

Fig. 4 presents the dependence of the binding constant on salt concentration. The number of released counterions ranges between 2.5 and 2.7 (data referring to other temperatures are shown in the SI), which is in accord with our previous result where $\Delta N_{\mathrm{ci}} = 3.1$ in MOPS buffer at 310 K.[16] The released counterions from the dPGS surface upon binding can also

TABLE III. Thermodynamic properties of lysozyme binding to dPGS-G2 in phosphate buffer pH 7.4 at different conditions. N, K_b, and ΔH_{ITC} are fitting parameters by ITC. ΔG^o is calculated according to Eq. 6. ΔH_{vH}, ΔS_{vH} and $\Delta C_{p,vH}$ are the binding enthalpy, entropy, and heat capacity change fitted by Eq. 6.

c_s [mM]	T [K]	N	K_b [10^5 M^{-1}]	ΔG^o [kJ/mol] (k_BT)	ΔH_{ITC} [kJ/mol]	ΔH_{vH} [kJ/mol]	$T\Delta S_{vH}$ [kJ/mol]	$\Delta C_{p,ITC}$ [kJ/(mol K)]	$\Delta C_{p,vH}$ [kJ/(mol K)]
25	278	2.4±0.02	384±99	-40.4±0.7 (-17.5)	-84.9±0.8	3.5±12.3	43.9±12.0	0.22±0.02	-1.20±0.75
	283	2.6±0.03	362±110	-41.0±0.7 (-17.4)	-83.1±0.9	-2.5±8.7	38.6±8.7		
	288	2.4±0.02	433±100	-42.1±0.6 (-17.6)	-81.3±0.7	-8.5±5.5	33.3±5.6		
	293	2.4±0.01	345±48	-42.3±0.3 (-17.4)	-81.3±0.7	-14.4±3.6	27.8±3.6		
	298	2.5±0.02	325±65	-42.9±0.5 (-17.3)	-80.4±0.6	-20.4±4.9	22.3±4.9		
	303	2.5±0.01	216±20	-42.5±0.3 (-16.9)	-78.6±0.5	-26.4±8.0	16.6±8.0		
	310	2.5±0.01	217±20	-43.5±0.2 (-16.9)	-77.7±0.5	-34.8±12.9	8.6±13.1		
50	278	2.2±0.02	55.1±9.3	-35.9±0.4 (-15.5)	-88.9±0.7	11.7±4.8	47.4±4.7	0.43±0.03	-1.99±0.29
	283	2.3±0.01	51.7±3.9	-36.4±0.2 (-15.5)	-86.8±0.5	1.7±3.4	38.2±3.4		
	288	2.3±0.01	53.7±4.1	-37.1±0.2 (-15.5)	-84.4±0.5	-8.3±2.2	28.8±2.2		
	293	2.3±0.01	47.5±3.7	-37.5±0.2 (-15.4)	-82.1±0.5	-18.2±1.4	19.3±1.4		
	298	2.3±0.01	43.8±1.9	-37.9±0.1 (-15.3)	-78.6±0.3	-28.2±1.9	9.6±1.9		
	303	2.2±0.01	34.7±1.7	-37.9±0.1 (-15.1)	-77.5±0.4	-38.2±3.1	-0.3±3.1		
	310	2.2±0.01	21.7±1.1	-37.6±0.1 (-14.6)	-74.9±0.2	-52.2±5.0	-14.4±5.1		
75	278	2.3±0.02	22.8±3.1	-33.8±0.3 (-14.6)	-90.1±0.5	16.4±3.8	50.2±3.8	0.46±0.02	-2.06±0.24
	283	2.2±0.01	25.2±2.2	-34.7±0.2 (-14.7)	-86.2±0.6	6.1±2.7	40.7±2.7		
	288	2.2±0.01	23.9±1.9	-35.2±0.2 (-14.7)	-84.3±0.5	-4.2±1.7	31.1±1.7		
	293	2.2±0.01	23.3±1.7	-35.7±0.2 (-14.7)	-81.7±0.5	-14.5±1.1	21.2±1.1		
	298	2.2±0.01	21.7±1.5	-36.1±0.2 (-14.6)	-79.5±0.4	-24.8±1.5	11.2±1.5		
	303	2.2±0.01	16.1±0.9	-36.0±0.1 (-14.3)	-77.6±0.4	-35.1±2.5	1.0±2.5		
	310	2.2±0.01	11.5±0.6	-36.0±0.1 (-14.0)	-75.1±0.4	-49.5±4.0	-13.6±4.1		
100	278	2.1±0.01	11.4±1.0	-32.2±0.2 (-13.9)	-88.5±0.4	11.0±3.0	43.2±3.0	0.63±0.02	-1.89±0.19
	283	2.2±0.01	12.2±0.7	-33.0±0.1 (-14.0)	-85.8±0.4	1.6±2.2	34.5±2.1		
	288	2.2±0.01	11.0±0.6	-33.3±0.1 (-13.9)	-82.4±0.4	-7.9±1.4	25.6±1.4		
	293	2.2±0.01	10.9±0.5	-33.9±0.1 (-13.9)	-78.6±0.4	-17.3±0.9	16.5±0.9		
	298	2.1±0.01	9.2±0.4	-34.0±0.1 (-13.7)	-76.3±0.3	-26.7±1.2	7.3±1.2		
	303	2.0±0.01	7.6±0.4	-34.1±0.1 (-13.5)	-72.2±0.4	-36.2±2.0	-2.1±2.0		
	310	1.9±0.01	5.0±0.2	-33.8±0.1 (-13.1)	-69.1±0.4	-49.4±3.2	-15.5±3.2		
125	278	2.1±0.01	6.2±0.4	-30.8±0.2 (-13.3)	-88.0±0.3	-3.4±2.0	27.4±1.9	0.65±0.02	-1.11±0.12
	283	2.1±0.01	5.9±0.2	-31.3±0.1 (-13.3)	-85.6±0.2	-9.0±1.4	22.3±1.4		
	288	2.0±0.01	5.5±0.1	-31.6±0.1 (-13.2)	-81.4±0.2	-14.6±0.9	17.1±0.9		
	293	2.0±0.01	4.9±0.1	-31.9±0.1 (-13.1)	-78.3±0.2	-20.1±0.6	11.7±0.6		
	298	2.0±0.01	4.0±0.2	-31.9±0.1 (-12.9)	-75.2±0.3	-26.7±0.8	6.3±0.8		
	303	1.9±0.01	3.4±0.2	-32.1±0.1 (-12.7)	-72.5±0.4	-31.3±1.3	0.8±1.3		
	310	2.0±0.02	2.5±0.3	-32.0±0.3 (-12.4)	-67.2±0.6	-39.1±2.1	-7.0±2.1		
150	278	2.1±0.01	4.4±0.02	-30.1±0.1 (-13.0)	-87.6±0.2	-3.2±4.3	26.8±4.2	0.88±0.04	-1.47±0.27
	283	2.1±0.01	4.0±0.09	-30.3±0.1 (-12.9)	-84.2±0.2	-10.5±3.1	19.8±3.1		
	288	2.0±0.01	3.4±0.08	-30.5±0.1 (-12.7)	-79.9±0.2	-17.9±1.9	12.8±2.0		
	293	2.0±0.01	3.2±0.1	-30.9±0.1 (-12.7)	-75.2±0.3	-25.2±1.3	5.6±1.3		
	298	1.9±0.01	2.6±0.1	-30.9±0.1 (-12.5)	-71.0±0.4	-32.3±1.7	-1.7±1.7		
	303	2.0±0.01	2.1±0.1	-30.9±0.1 (-12.3)	-64.0±0.4	-39.9±2.8	-9.1±2.8		
	310	1.9±0.01	1.3±0.07	-30.4±0.1 (-11.8)	-60.9±0.5	-50.2±4.5	-19.9±4.6		

be monitored by computer simulations[16] and the results agree with experiments (see SI). Since c_{ci} equals to 0.96 M at 310 K for dPGS-G2,[24] Eq. 1 predicts ΔG_{ci} at 25 mM salt concentration to be -9.8 k_BT. It hence presents a major contribution in the total binding free enthalpy. The solid lines in Fig. 4 referring to different temperatures are approximately

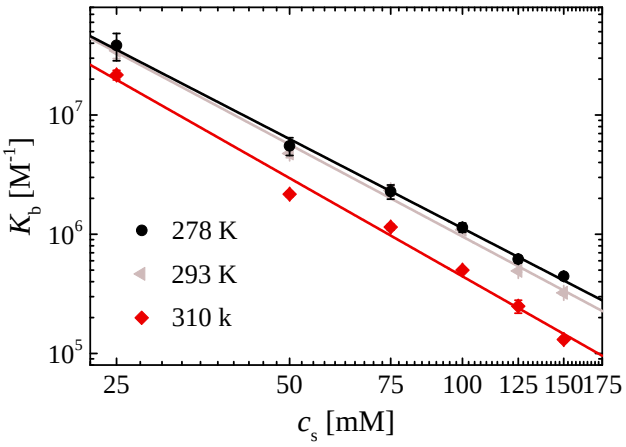

FIG. 4. The dependence of binding constant on salt concentration for three different temperatures. The number of released counterions ΔN_{ci} from the slope of these lines fitted according to Eq. 2 is 2.5±0.1 at 278 K, 2.6±0.1 at 293 K, and 2.7±0.1 at 310 K in phosphate buffer. ΔN_{ci} measured in MOPS buffer at 310 K was 3.1±0.1.[16]

parallel so the number of released counterions does not depend on temperature within the limits of error. It thus demonstrates that counterion-release does not contribute to the heat capacity ΔC_p on this level of approximation.

In addition to counterion-release, there is a Debye-Hückel (DH) attraction ΔG_{ele} between dPGS and the bound lysozyme. Moreover, there is an electrostatic repulsion between bound proteins. Considering all the charged beads individually, the pairwise charge-charge interaction on the Debye-Hückel level was determined by computer simulation.[16] The resultant overall electrostatic interaction between lysozyme and dPGS-G2 decreases slightly with the number of bound proteins. For the first three bound proteins at c_s=10 mM, the attraction was found similar to be -26 kJ/mol (-10 k_BT) (see Fig. 2D in ref.[16]).

Steric repulsion between the bound lysozymes enters as a third term. This packing penalty is non-existent for the first uptake and positive for the subsequent proteins. It becomes a limiting factor when the packing of the proteins leads to a more or less full coverage of the surface. For the situation encountered for G2 where 4 lysozymes are bound, simulations showed this term to be of minor importance.[16]

The findings above lead to the conclusion that the binding free enthalpy of subsequent lysozymes is not a constant but decreases with the number of bound proteins. The Langmuir model which is the basis of the SSIS fitting, on the other hand, assumes that each bound

protein is attached independently and the free enthalpy of binding is equivalent for all bound proteins.

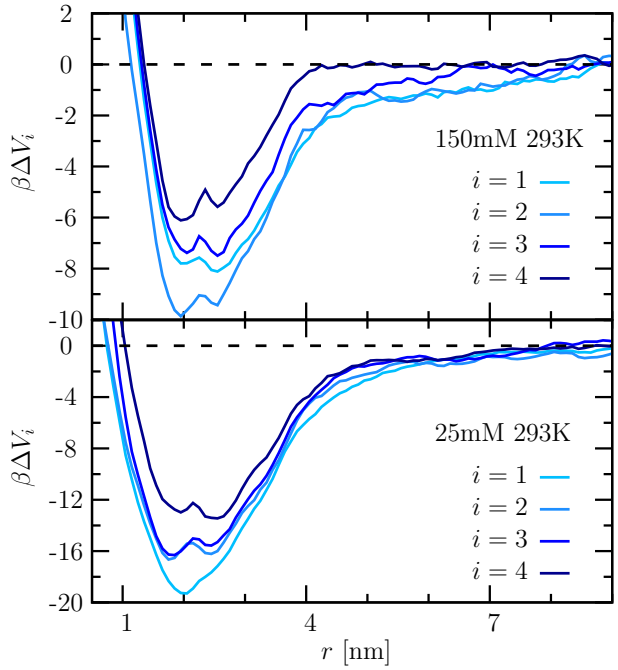

FIG. 5. The potential of mean force (PMF) curves βV_i for the complexation between dPGS-G2 and lysozyme versus the dPGS-lysozyme center of mass distance r. V_i is in the unit of $k_\mathrm{B}T$ ($\beta = 1/k_\mathrm{B}T$). The binding coordination number i ranges from 1 to 4 as indicated in the graph. The simulation was done at $T = 293$ K and salt concentration $c_\mathrm{s} = 25$ mM (lower panel) and 150 mM (upper panel).

To elucidate the cooperativity in a multivalent binding, we measured the complexation of lysozyme with dPGS-G2 for different coordination numbers i by MD simulations. Fig. 5 shows the PMF profile at 293 K and two salt concentrations. The respective local minimum reveals the binding distance r_b and binding free enthalpy $\Delta G_\mathrm{b}^\mathrm{sim}$ at the given coordination number. The complexation between dPGS and the first bound lysozyme is purely driven by electrostatic effects with a binding free enthalpy -27 $k_\mathrm{B}T$ at 10 mM salt (see the discussion of Fig. 2C in ref.[16]). The magnitude of $\Delta G_\mathrm{b}^\mathrm{sim}$ decreases with i, which indicates a negative cooperativity caused by electrostatic repulsion and steric hindrance.

To account for this negative cooperativity, we recently developed a new way of comparing ΔG_b between the simulation and the ΔG^0 stemming from ITC experiments:[16] In canonical

simulations, the concentration c_{bound} of bound and non-interacting ligands follows as[16]

$$c_{\mathrm{bound}} = \frac{i}{V_{\mathrm{b}}} = c_{\mathrm{free}} \exp(-\beta \Delta G_{\mathrm{b}}), \tag{3}$$

where c_{free} is the concentration of free (unbound) ligands and V_{b} refers to the effective volume in which the bound ligands are confined. ΔG_{b} defines the transfer free enthalpy from bulk to the bound state, which can be taken directly from the minimum of the PMF profile.[16] We now assume that the binding complex consists of i lysozyme ligands bound in a shell on the surface of dPGS which are idealized as sphere. Hence, the binding volume $V_{\mathrm{b}} = 4\pi(r_{\mathrm{b}})^2\delta_{\mathrm{b}}$. We take the binding distance $r_{\mathrm{b}} = 2.5$ nm at saturation together with the thickness of the spherical binding shell $\delta_{\mathrm{b}} = 1$ nm.

In the Langmuir model used for the evaluation of the experiments the protein coverage θ is defined as

$$\theta = \frac{i}{N} = c_{\mathrm{free}} K_{\mathrm{b}} (1 - \theta), \tag{4}$$

with $K_{\mathrm{b}} = v_0 \exp(-\beta \Delta G^{\mathrm{o}})$ the binding constant related to the Langmuir binding enthalpy ΔG^{o} in Table III. Here the volume prefactor v_0 is defined to be 1 liter/mol. Combination of Eq. 3 with 4 leads to the "simulation-referenced" Langmuir *free enthalpy* by

$$\Delta G_{\mathrm{b}}^{\mathrm{ITC}} = \Delta G^{\mathrm{o}} - k_{\mathrm{B}}T \ln(1 - \theta^*) - k_{\mathrm{B}}T \ln(v_0 N / V_{\mathrm{b}}), \tag{5}$$

which leads to a direct comparison between the experimental ITC-curves and the simulations discussed previously.[16] The degree of coverage θ^* is obtained from the inflection point of the ITC-isotherms where n(Lys)/n(dPGS) $= N$ and is smaller than unity.[16]

We apply this method to the present data and find θ^* at four different conditions (see SI). $\Delta G_{\mathrm{b}}^{\mathrm{ITC}}$ at the inflection point can then be calculated with Eq. 5 and compared to $\Delta G_{\mathrm{b}}^{\mathrm{sim}}$ in Fig. 6. We find a full agreement between simulation and ITC experiment for all conditions. Thus, the experimental results can be rationalized very well in terms of the simulations.

It is interesting to note that the data taken at higher salt concentration exhibit a much lower dependence on θ (squares in Fig. 6) than the ones obtained for lower salt concentrations (circles). This means that the binding affinity at $c_{\mathrm{s}} = 150$ mM shows much weaker negative cooperativity, which can be traced back to the weaker DH interaction in the presence of more salt. At the same time, the simulations confirm a weak dependence of ΔG^{o} on temperature consistent with the experimental data.

A meaningful comparison of ΔG^{o} measured at different conditions requires that θ^* remains constant under all conditions. Table III shows that the number N of bound lysozymes measured for a given salt concentration does not depend on temperature. Therefore the present

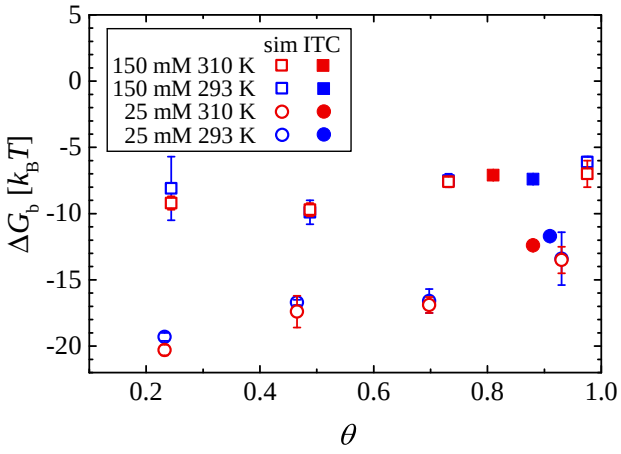

FIG. 6. The binding free enthalpy $\Delta G_{\mathrm{b}}^{\mathrm{sim}}$ versus the protein coverage $\theta = i/N^{\mathrm{sim}}$, where i is the binding coordination number and N^{sim} is the binding stoichiometry from simulations. $\Delta G_{\mathrm{b}}^{\mathrm{sim}}$ by simulations at different conditions are depicted by the empty symbols. These results are compared with the "simulation-referenced" Langmuir *free enthalpy* $\Delta G_{\mathrm{b}}^{\mathrm{ITC}}$ according to Eq. 5 at θ^*, denoted by the filled points.

set of data can be used to discuss the dependence on temperature without restrictions. There are small changes of N for a given temperature when going from low salt concentrations to higher ones. however, this change can be disregarded in good approximation. Hence, the data gathered in Table III allow us to discuss the dependence of ΔG^{o} both on salt concentration and temperature which is done in the following.

B. Enthalpy-entropy compensation

As discussed above, the accuracy of the obtained ΔG^{o} is fully sufficient for a meaningful analysis of the dependence on T. Previous work on complex formation of proteins with nucleic acids has clearly revealed that the binding enthalpy depends markedly on temperature,[10,11] which shows that the heat capacity change ΔC_{p} is of appreciable magnitude. Therefore the binding free enthalpy must be rendered in terms of the nonlinear van't Hoff relation[10,40]

$$\begin{aligned} \Delta G^{\mathrm{o}} &= -RT\ln K_{\mathrm{b}} \\ &= \Delta H_{\mathrm{vH,ref}} - T\Delta S_{\mathrm{vH,ref}} + \Delta C_{\mathrm{p,vH}}[(T - T_{\mathrm{ref}}) - T\ln(\frac{T}{T_{\mathrm{ref}}})], \end{aligned} \tag{6}$$

where $\Delta H_{\mathrm{vH,ref}}$ and $\Delta S_{\mathrm{vH,ref}}$ are the binding enthalpy and entropy, respectively, at a given reference temperature T_{ref}.

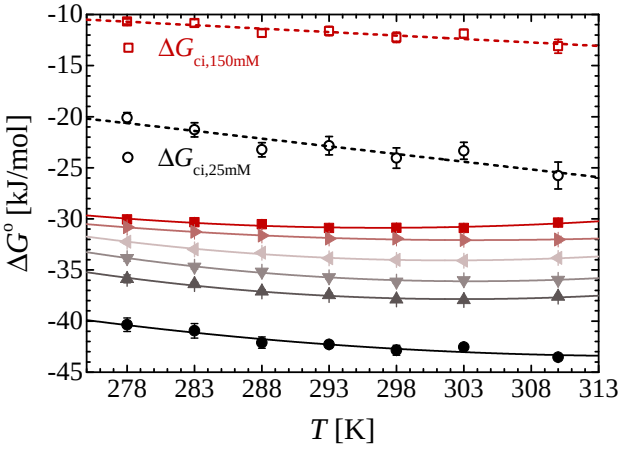

FIG. 7. Nonlinear van't Hoff analysis for dPGS-Lys complexation at different ionic strengths according to Eq. 6: 25 mM (●), 50 mM (▲), 75 mM (▼), 100 mM (◀), 125 mM (▶), 150 mM (■). The counterion-release entropy gain $\Delta G_{\rm ci}$ is calculated with $\Delta N_{\rm ci}$ according to Eq. 1.

The analysis of the data shown in Fig. 7 according to Eq. 6 is done as follows: The given temperature is chosen as reference temperature $T_{\rm ref}$ and the corresponding binding enthalpy $\Delta H_{\rm vH,ref}$, entropy $\Delta S_{\rm vH,ref}$, and heat capacity change $\Delta C_{\rm p,vH}$ are obtained as fit parameters. This procedure is done for all temperatures under consideration here. The values $\Delta H_{\rm vH}$, $\Delta S_{\rm vH}$ and $\Delta C_{\rm p,vH}$ obtained for all temperatures by this fit are listed in Table III. Here $\Delta C_{\rm p,vH}$ has been treated as a freely floating parameter but the fit results are constant for each salt concentration.

The curvature in Fig. 7 which is due to the heat capacity $\Delta C_{\rm p,vH}$ of appreciable magnitude is similar and the data are of sufficient precision to determine this quantity. $\Delta C_{\rm p,vH}$ is constant in this range of temperature and approximately -2 kJ/(mol K) for all the ionic strengths. Both $\Delta H_{\rm vH}$ and $\Delta S_{\rm vH}$ change strongly with temperature whereas $\Delta G^{\rm o}$ is nearly a constant. This insensitivity of $\Delta G^{\rm o}$ to T necessarily leads to a marked enthalpy-entropy compensation considering a large $\Delta C_{\rm p,vH}$.

Fig. 7 also contains the part $\Delta G_{\rm ci}$ calculated for 25mM and 150 mM salt by Eq. 1. The magnitude of $\Delta G_{\rm ci}$ varies linearly with temperature, which is obvious from Eq. 1: $\Delta S_{\rm ci} = \Delta N_{\rm ci} k_{\rm B} \ln(c_{\rm ci}/c_{\rm s})$ does not depend on T if one disregards small change of $c_{\rm ci}$ with temperature. The difference between $\Delta G_{\rm ci}$ and $\Delta G^{\rm o}$ is mainly due to the electrostatic interaction $\Delta G_{\rm ele}$ as discussed above and in ref.[16]. At constant temperature e.g. 293 K, this electrostatic part can be read off to be -19 kJ/mol at both 25 mM and 150 mM salt from Fig. 7. It does

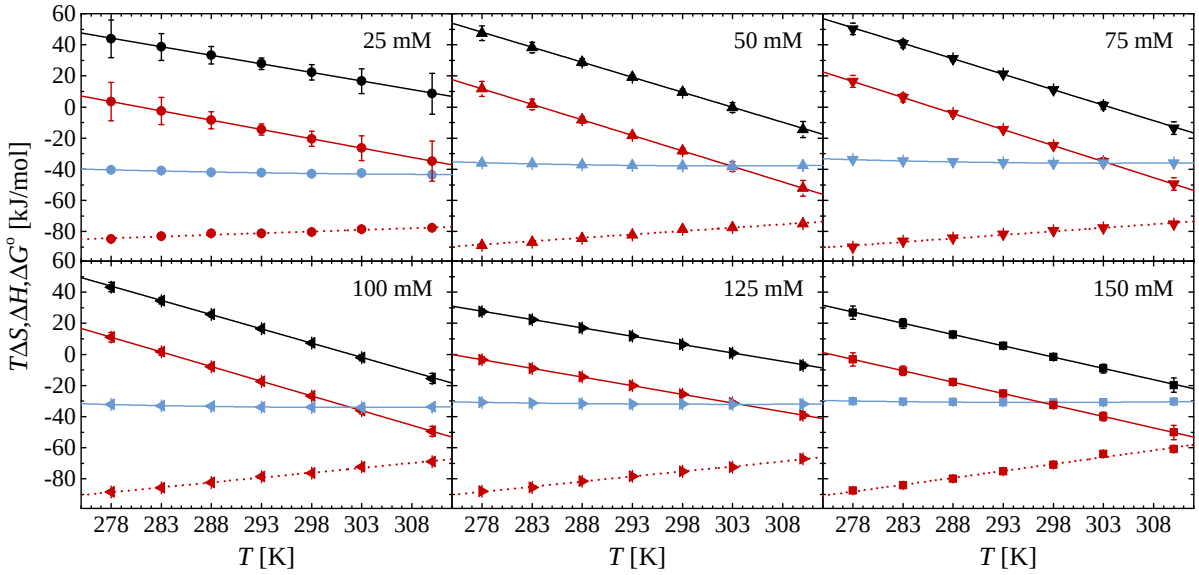

FIG. 8. The entropic ($T\Delta S_{\mathrm{vH}}$,black) and enthalpic (ΔH_{vH},red) contributions in total binding free enthalpy (ΔG^{o},blue) at different ionic strengths. The calorimetric enthalpy ΔH_{ITC} (dashed red) is plotted as a comparison to ΔH_{vH}.

not vanish with added salt as expected for a simple DH-interaction. Thus, the analytical modeling of the electostatic interaction between the protein adhering directly to the dendritic polyelectrolyte requires a more detailed decription containing higher order multipole terms. It should be noted, however, that the simulation carries along all necessary contributions since it fully agrees with the experimental data.

Fig. 8 depicts the entropic and enthalpic contributions in the total binding free enthalpy at all ionic strengths. It demonstrates directly the entropy-enthalpy compensation (EEC). ΔH_{vH} and ΔS_{vH} may even change sign in several cases in Fig. 8 whereas ΔG^{o} depends much weaker on temperature. It is thus evident that the EEC is leading to a nearly constant free enthalpy of binding since ΔH_{vH} and $T\Delta S_{\mathrm{vH}}$ run strictly parallel within the present window of temperature. Thus, for the present system the enthalpic and entropic changes with temperature due to hydration seem to cancel out each other nearly completely. In general, EEC is a commonly observed phenomenon for binding of polyelectrolytes with proteins[30,31,41]. This effect has widely frustrated the use of thermodynamic data for drug design.[14]. The present discussion underscores this problem and accentuates that one should strive to calculate ΔG^{o} rather than enthalpic or entropic contributions individually.

Fig. 8 shows clearly that ΔH_{vH} deviates markedly from the directly measured ΔH_{ITC}, which is different from the dPGS-HSA binding system in our previous study.[28] It is well-known that ΔH_{ITC} measured directly in the calorimetry experiment need not agree with the binding enthalpy ΔH_{vH}.[14,40,42–44] Explanations for this finding are based on the fact that ΔH_{ITC} may also contain contributions of linked equilibria such as ionization or conformational changes of the protein or ligand. The next section will discuss the measured enthalpy in more detail.

C. Binding enthalpy versus calorimetric enthalpy

TABLE IV. Enthalpy contributions of linked equilibria for dPGS-Lys complexation in phosphate buffer at 310 K. $\Delta H_{\mathrm{ITC}}^{\mathrm{MOPS}^*}$ is taken from previous measurements[16]. According to ref[38], the dissociation enthalpy $\Delta H^{\mathrm{o}}_{\mathrm{ion,MOPS}}$ and $\Delta H^{\mathrm{o}}_{\mathrm{ion,phos}}$ are 22.67 kJ/mol and 2.88 kJ/mol, respectively, at 310 K neglecting the salt dependence. $\Delta n_{\mathrm{H^+}}$ can then be obtained according to Eq. 10 and $\Delta H_{\mathrm{ion}} = \Delta n_{\mathrm{H^+}} \Delta H^{\mathrm{o}}_{\mathrm{ion,phos}}$ in phosphate buffer. ΔH_{prot} is calculated with Eq. 8. The protonation enthalpy $\Delta H^{\mathrm{o}}_{\mathrm{prot}}$ for arginine and lysine is -46 kJ/mol according to the literature.[45] Thus, the protonation enthalpy in this system can be calculated according to $\Delta H^{*}_{\mathrm{prot}} = \Delta n_{\mathrm{H^+}} \Delta H^{\mathrm{o}}_{\mathrm{prot}}$.

c_{s} [mM]	$\Delta H_{\mathrm{ITC}}^{\mathrm{phos}}$ [kJ/mol]	$\Delta H_{\mathrm{ITC}}^{\mathrm{MOPS}^*}$ [kJ/mol]	$\Delta n_{\mathrm{H^+}}$	ΔH_{ion} [kJ/mol]	ΔH_{prot} [kJ/mol]	$\Delta H^{*}_{\mathrm{prot}}$ [kJ/mol]
25	-77.7±0.5	-65.4±0.4	0.62±0.03	1.8±0.1	-44.7±12.5	-29
50	-74.9±0.2	-65.2±0.2	0.49±0.02	1.4±0.1	-24.1±4.9	-23
75	-75.1±0.4	-66.4±0.3	0.44±0.03	1.3±0.1	-26.9±3.7	-20
100	-69.1±0.4	-64.6±0.3	0.22±0.02	0.6±0.1	-20.3±2.9	-10
125	-67.2±0.6	-60.0±0.2	0.36±0.03	1.0±0.1	-29.±1.6	-17
150	-60.9±0.5	-56.7±0.5	0.21±0.04	0.6±0.1	-11.3±4.1	-10

The directly measured ΔH_{ITC} rises with both temperature and salt concentration (see Table III). Fig. 9 displays ΔH_{ITC} as the function of temperature at different salt concentrations. In general, the linear dependence of enthalpy ΔH_{ITC} on temperature corresponds to a heat capacity change $\Delta C_{\mathrm{p,ITC}}$ as

$$\Delta H_{\mathrm{ITC}} = \Delta H_{\mathrm{ITC},0} + \Delta C_{\mathrm{p,ITC}}(T - T_0). \tag{7}$$

The exothermic process is accompanied with a positive heat capacity change (see Fig. 9). Notably, $\Delta C_{\mathrm{p,ITC}}$ increases with salt concentration similar to findings made for a protein-DNA binding system[46]. The value increases with ionic strength thus suggesting an exothermic

process that is repressed by ions (see the discussion of this point in ref.[46]). Compared to $\Delta C_{\mathrm{p,ITC}}$, the intrinsic part $\Delta C_{\mathrm{p,vH}}$ has opposite sign and does not depend on ionic strength within the limits of error. This is indicative of linked equilibria that compensate $\Delta C_{\mathrm{p,vH}}$ and gives overall positive $\Delta C_{\mathrm{p,ITC}}$.

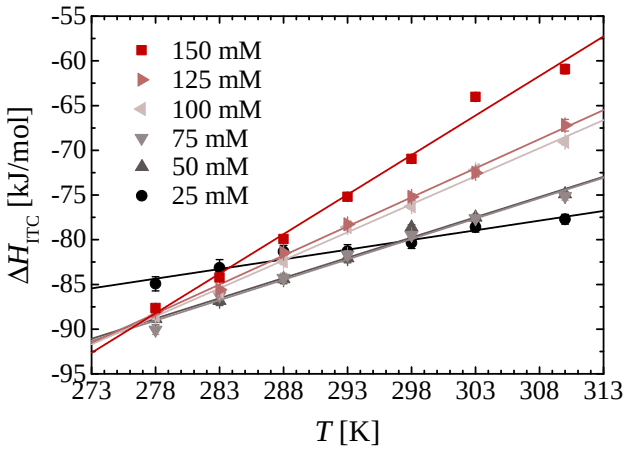

FIG. 9. The temperature dependence of calorimetric enthalpy for dPGS-Lys complexation at different ionic strengths. The heat capacity change according to ITC experiments can be derived from the slope. $\Delta C_{\mathrm{p,ITC}}$ increases monotonically from 0.22±0.02 kJ/(mol K) at c_{s}=25mM to 0.88±0.04 kJ/(mol K) at c_{s}=150 mM.

According to Kozlov and Lohman, the observed enthalpy change by calorimetry can be split up into several contributions as[12]

$$\Delta H_{\mathrm{ITC}} = \Delta H_{\mathrm{vH}} + \Delta H_{\mathrm{prot}} + \Delta H_{\mathrm{ion}}. \tag{8}$$

Thus, the calorimetric enthalpy contains the binding enthalpy ΔH_{vH}, the protonation enthalpy of free or bound protein/ligand ΔH_{prot}, and the ionization (deprotonation) enthalpy of the buffer $\Delta H_{\mathrm{ion}} = \Delta n_{\mathrm{H^+}} \Delta H^{\mathrm{o}}_{\mathrm{ion}}$ with positive $\Delta n_{\mathrm{H^+}}$ being the number of protons supplied by the buffer. $\Delta H^{\mathrm{o}}_{\mathrm{ion}}$ is the molar enthalpy of buffer deprotonation. Similarly, the temperature dependence gives the observed $\Delta C_{\mathrm{p,ITC}}$ as[12]

$$\Delta C_{\mathrm{p,ITC}} = \Delta C_{\mathrm{p,vH}} + \Delta C_{\mathrm{p,prot}} + \Delta C_{\mathrm{p,ion}}. \tag{9}$$

Here $\Delta C_{\mathrm{p,vH}}$ is due to binding. The electrostatic contribution to ΔC_{p} is relatively small.[47] The hydration or dehydration of nonpolar and polar solute gives large heat capacity change with different signs.[48]

Binding experiments done in two different buffer solutions with distinguishable $\Delta H^{\circ}_{\rm ion}$ allow us to calculate the caloric effect of buffer ionization since the first two terms at the right side of Eq. 8 remain unchanged. Here we compare the measured $\Delta H_{\rm ITC}$ in MOPS obtained previously at 310 K and different ionic strengths[16] and phosphate buffer done here. From these data the number of released protons at 310 K can be derived as

$$\Delta n_{\rm H^+} = \frac{\Delta H^{\rm MOPS}_{\rm ITC} - \Delta H^{\rm phos}_{\rm ITC}}{\Delta H^{\circ}_{\rm ion,MOPS} - \Delta H^{\circ}_{\rm ion,phos}}. \tag{10}$$

The buffer ionization enthalpies for dPGS-Lys interaction at 310 K in phosphate buffer are summarized in Table IV taking the data obtained with the MOPS buffer as reference.[16] $\Delta n_{\rm H^+}$ protons are released from the buffer and it decreases with salt concentration. The positive ionization enthalpy thus decreases with salt and is relatively small. Then the large discrepancy between $\Delta H_{\rm ITC}$ and $\Delta H_{\rm vH}$ must be traced back to a negative $\Delta H_{\rm prot}$. The protonation enthalpy can also be estimated with $\Delta n_{\rm H^+}$ and given $\Delta H^{\circ}_{\rm prot}$, however, it depends on the species of amino acid.[45] Here we roughly estimate the protonation enthalpy with $\Delta H^{\circ}_{\rm prot}$ of lysine and arginine from the literature.[45] The values in Table IV are in a comparable range with the calculation according to Eq. 8, which indicates that positive residues at the binding site may be protonated and the protonation brings a large negative contribution to the measured enthalpy.

It should be kept in mind that the binding of several lysozyme molecules to a single dPGS is characterized by a notable negative cooperativity, in particular when the binding takes place at low ionic strength. This could be see directly from simulations and from inspection of Fig. 6. Hence, all thermodynamic quantities will depend on the number of bound lysozymes and refer to the situation where $\theta = \theta^*$, that is, near the inflection point of the ITC titration curve. The measured enthalpy $\Delta H_{\rm ITC}$, on the other hand, derives from the ITC-isotherm at low degree of coverage θ. Therefore $\Delta H_{\rm ITC}$ is expected to be larger in magnitude in cases where negative cooperativity comes into play.

IV. CONCLUSION

We presented a systematic thermodynamic study on complexation of dPGS-G2 with lysozyme. In particular, we measured the dependence of the binding constant on temperature and ionic strength. The dependence on salt concentration clearly revealed counterion-release

as driving force while the dependence on temperature demonstrated strong enthalpy-entropy compensation. Together with the simulation work on the dPGS-lysozyme binding, the present thermodynamic analysis shows that the enthalpic and the entropic contributions compensate each other over the entire range of temperature to give a nearly constant ΔG^{o} driven solely by electrostatic factors. Hence, in case of the present hydrophilic dendritic system the driving force, namely counterion-release with electrostatic attraction, is responsible for binding while all contributions due to hydration cancel out in good approximation.

ACKNOWLEDGMENTS

The author X. Xu was funded by the China Scholarship Council. The Helmholtz Virtual Institute for Multifunctional Biomaterials for Medicine and the International Research Training Group IRTG 124 funded by the German Science Foundation are gratefully acknowledged for financial support.

REFERENCES

[1]N. Miura, P. L. Dubin, C. Moorefield, and G. Newkome, Langmuir **15**, 4245 (1999).

[2]C. Cooper, P. Dubin, A. Kayitmazer, and S. Turksen, Curr. Opin. Colloid Interface Sci. **10**, 52 (2005).

[3]A. B. Kayitmazer, D. Seeman, B. B. Minsky, P. L. Dubin, and Y. Xu, Soft Matter **9**, 2553 (2013).

[4]Q. Wei, T. Becherer, S. Angioletti-Uberti, J. Dzubiella, C. Wischke, A. T. Neffe, A. Lendlein, M. Ballauff, and R. Haag, Angew. Chem. Int. Ed. **53**, 8004 (2014).

[5]W. Xiong, C. Ren, M. Tian, X. Yang, J. Li, and B. Li, Food Hydrocolloids **73**, 41 (2017).

[6]M. T. Record, C. F. Anderson, and T. M. Lohman, Q. Rev. Biophys. **11**, 103 (1978).

[7]L. MicroCal, MicroCal, LLC, Northampton, MA (2004).

[8]A. Velazquez-Campoy and E. Freire, Nat. Protoc. **1**, 186 (2006).

[9]A. Niedzwiecka, J. Stepinski, E. Darzynkiewicz, N. Sonenberg, and R. Stolarski, Biochemistry **41**, 12140 (2002).

[10]K. Datta and V. J. LiCata, Nucleic Acids Res. **31**, 5590 (2003).

[11]K. Datta, A. J. Wowor, A. J. Richard, and V. J. LiCata, Biophys. J. **90**, 1739 (2006).

[12]A. G. Kozlov and T. M. Lohman, Proteins **41**, 8 (2000).

[13]N. Welsch, A. L. Becker, J. Dzubiella, and M. Ballauff, Soft Matter **8**, 1428 (2012).

[14]S. Geschwindner, J. Ulander, and P. Johansson, J. Med. Chem. **58**, 6321 (2015).

[15]M. Ramanadham, L. Sieker, and L. Jensen, Acta Crystallogr. B Struct. Sci. **46**, 63 (1990).

[16]X. Xu, Q. Ran, P. Dey, R. Nikam, R. Haag, M. Ballauff, and J. Dzubiella, Biomacromolecules **19**, 409 (2018).

[17]J. Dernedde, A. Rausch, M. Weinhart, S. Enders, R. Tauber, K. Licha, M. Schirner, U. Zügel, A. von Bonin, and R. Haag, Proc. Natl. Acad. Sci. **107**, 19679 (2010).

[18]J. Khandare, A. Mohr, M. Calderón, P. Welker, K. Licha, and R. Haag, Biomaterials **31**, 4268 (2010).

[19]M. Weinhart, D. Gröger, S. Enders, S. B. Riese, J. Dernedde, R. K. Kainthan, D. E. Brooks, and R. Haag, Macromol. Biosci. **11**, 1088 (2011).

[20]T. Schneider, P. Welker, K. Licha, R. Haag, and G. Schulze-Tanzil, BMC musculoskeletal disorders **16**, 387 (2015).

[21]A. Boreham, J. Pikkemaat, P. Volz, R. Brodwolf, C. Kuehne, K. Licha, R. Haag, J. Dernedde, and U. Alexiev, Molecules **21**, 22 (2015).

[22]D. Maysinger, D. Gröger, A. Lake, K. Licha, M. Weinhart, P. K.-Y. Chang, R. Mulvey, R. Haag, and R. A. McKinney, Biomacromolecules **16**, 3073 (2015).

[23]A. Sousa-Herves, P. Würfel, N. Wegner, J. Khandare, K. Licha, R. Haag, P. Welker, and M. Calderón, Nanoscale **7**, 3923 (2015).

[24]X. Xu, Q. Ran, R. Haag, M. Ballauff, and J. Dzubiella, Macromolecules **50**, 4759 (2017).

[25]R. Haag, A. Sunder, and J.-F. Stumbé, J. Am. Chem. Soc. **122**, 2954 (2000).

[26]M. T. Record, T. M. Lohman, and P. De Haseth, J. Mol. Biol. **107**, 145 (1976).

[27]S. Yu, X. Xu, C. Yigit, M. van der Giet, W. Zidek, J. Jankowski, J. Dzubiella, and M. Ballauff, Soft Matter **11**, 4630 (2015).

[28]Q. Ran, X. Xu, P. Dey, S. Yu, Y. Lu, J. Dzubiella, R. Haag, and M. Ballauff, (2018).

[29]R. Lumry and S. Rajender, Biopolymers **9**, 1125 (1970).

[30]M. R. Eftink, A. Anusiem, and R. L. Biltonen, Biochemistry **22**, 3884 (1983).

[31]A. Cooper, C. M. Johnson, J. H. Lakey, and M. Nöllmann, Biophys. Chem. **93**, 215 (2001).

[32]F. Sedlmeier, D. Horinek, and R. R. Netz, J. Chem. Phys. **134**, 02B604 (2011).

[33]J. D. Chodera and D. L. Mobley, Annu. Rev. Biophys. **42**, 121 (2013).

[34]H. Türk, R. Haag, and S. Alban, Bioconjugate Chem. **15**, 162 (2004).

[35]T. Wiseman, S. Williston, J. F. Brandts, and L.-N. Lin, Anal. Biochem. **179**, 131 (1989).

[36]B. Hess, C. Kutzner, D. Van Der Spoel, and E. Lindahl, J. Chem. Theory Comput. **4**, 435 (2008).

[37]J. K. Noel, P. C. Whitford, K. Y. Sanbonmatsu, and J. N. Onuchic, Nucleic Acids Res. **38**, W657 (2010).

[38]H. Fukada and K. Takahashi, Proteins **33**, 159 (1998).

[39]K. Henzler, B. Haupt, K. Lauterbach, A. Wittemann, O. Borisov, and M. Ballauff, J. Am. Chem. Soc. **132**, 3159 (2010).

[40]J. R. Horn, D. Russell, E. A. Lewis, and K. P. Murphy, Biochemistry **40**, 1774 (2001).

[41]G. Klebe, Nat. Rev. Drug Discov. **14**, 95 (2015).

[42]H. Naghibi, A. Tamura, and J. M. Sturtevant, Proc. Natl. Acad. Sci. **92**, 5597 (1995).

[43]D. Haidacher, A. Vailaya, and C. Horváth, Proc. Natl. Acad. Sci. **93**, 2290 (1996).

[44]A. L. Becker, N. Welsch, C. Schneider, and M. Ballauff, Biomacromolecules **12**, 3936 (2011).

[45]M. A. Marini, R. L. Berger, D. P. Lam, and C. J. Martin, Anal. Biochem. **43**, 188 (1971).

[46]A. G. Kozlov and T. M. Lohman, J. Mol. Biol. **278**, 999 (1998).

[47]K. Gallagher and K. Sharp, Biophys. J. **75**, 769 (1998).

[48]V. V. Loladze, D. N. Ermolenko, and G. I. Makhatadze, Protein Sci. **10**, 1343 (2001).

Supporting Information for: Thermodynamics of the binding of lysozyme to a dendritic polyelectrolyte: Counterion-release versus hydration

Qidi Ran,[1,2,3] Xiao Xu,[2,3,4] Joachim Dzubiella,[2,3,4] Rainer Haag,[1,3,a)] and Matthias Ballauff[2,3,4,b)]

[1)] *Institute of Chemistry and Biochemistry, Freie Universität Berlin, Takustr. 3, 14195 Berlin, Germany*

[2)] *Institute of Soft Matter and Functional Materials, Helmholtz-Zentrum Berlin, Hahn-Meitner-Platz 1, 14109 Berlin, Germany*

[3)] *Multifunctional Biomaterials for Medicine, Helmholtz Virtual Institute, Kantstr. 55, 14513 Teltow-Seehof, Germany*

[4)] *Institut für Physik, Humboldt-Universität zu Berlin, Newtonstr. 15, 12489 Berlin, Germany*

[a)]Electronic mail: haag@chemie.fu-berlin.de

[b)]Electronic mail: matthias.ballauff@helmholtz-berlin.de

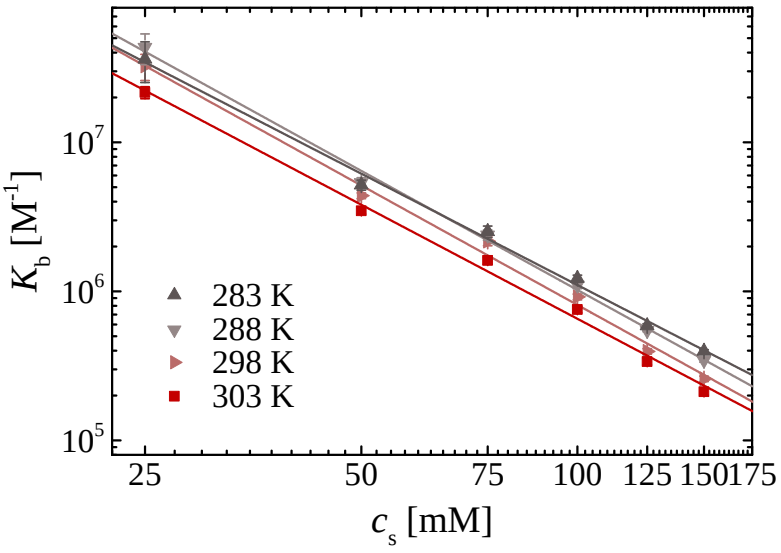

FIG. 1. The salt dependence of binding constant for dPGS-Lys interaction at different temperatures. The number of released counterions $\Delta N_{\rm ci}$ is 2.5±0.1, 2.7±0.1, 2.7±0.1, and 2.5±0.1 for 283 K, 288 K, 298 K, and 303 K, respectively.

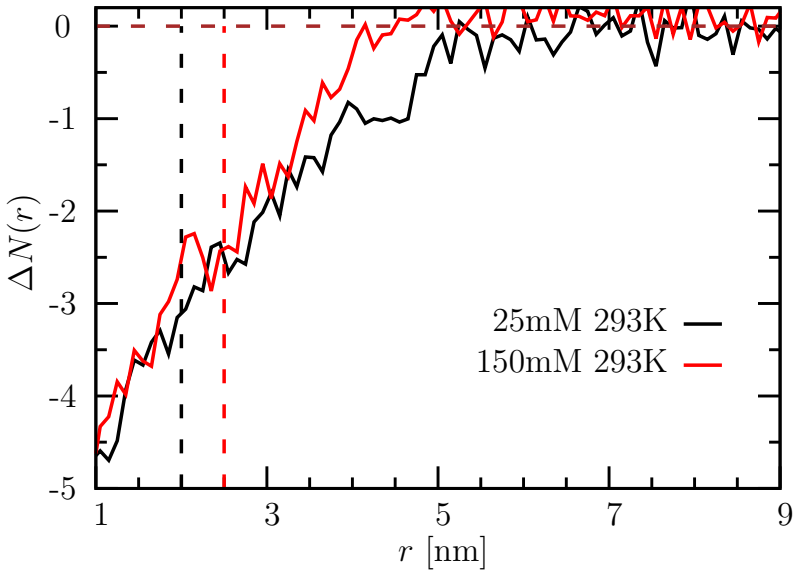

FIG. 2. The decrease of condensed counterions $\Delta N(r)$ on the dPGS surface upon binding with lysozyme according to computer simulations. r denotes the center-of-mass distance between dPGS and the first bound lysozyme. The number of released counterions can be read off at the distance $r_{\rm b}$ found with the bound state (dashed lines). $\Delta N(r_{\rm b})$ is 3.0 at $r_{\rm b}$=2.0 nm, and 2.5 at $r_{\rm b}$ = 2.5 nm.

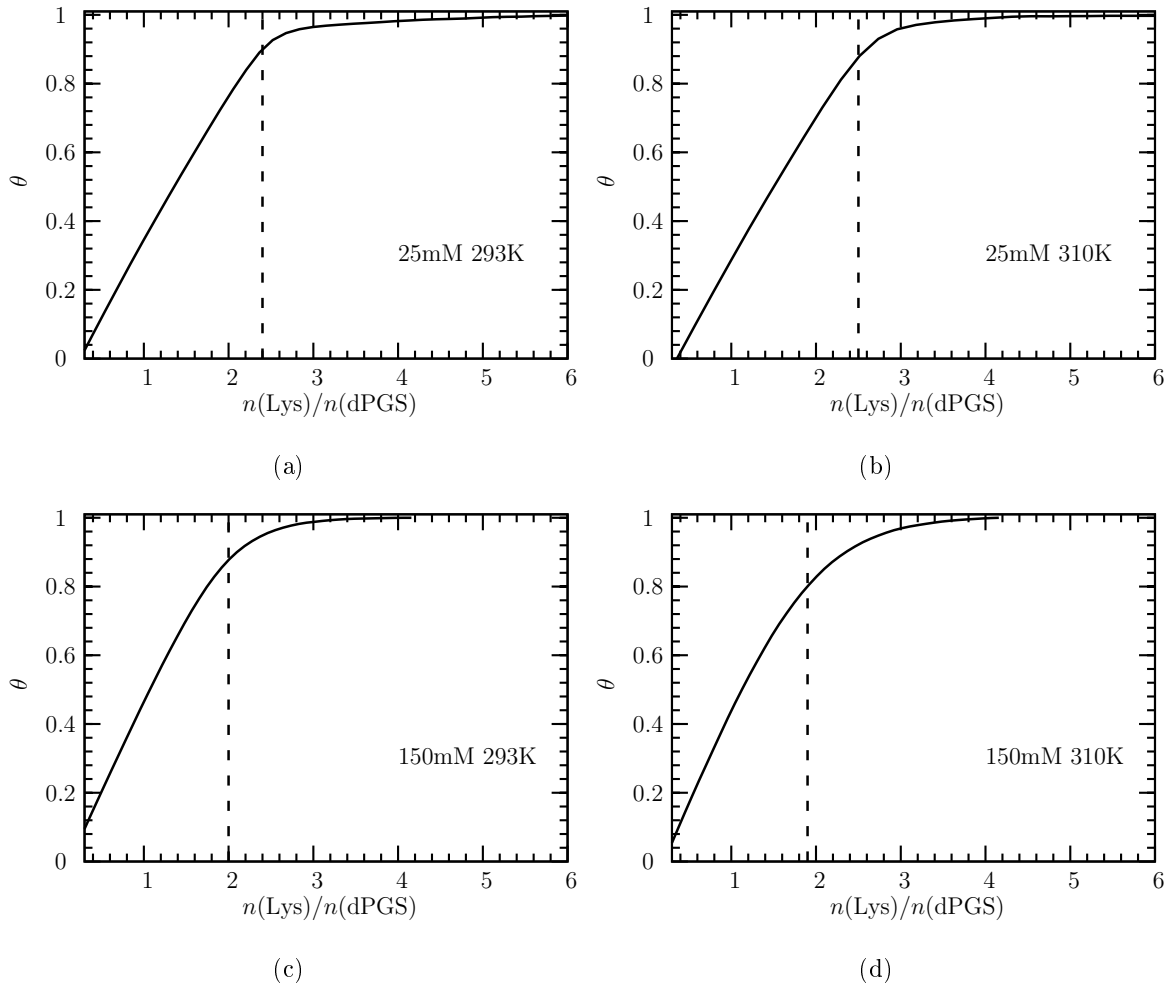

FIG. 3. The protein coverage θ as a function of the molar ratio n(Lys)/n(dPGS) in ITC measurements at different ionic strengths and temperatures. θ are plotted according to previous deviations (see the SI in ref.[1]). Each dashed line denotes the inflection point (binding number N) in the respective ITC isotherm. The intersection points with θ refer to the coverage θ^* at the inflection points.

REFERENCES

[1]X. Xu, Q. Ran, P. Dey, R. Nikam, R. Haag, M. Ballauff, and J. Dzubiella, Biomacromolecules **19**, 409 (2018).

4 Summary and Outlook

The interaction between proteins and polyelectrolytes has been studied intensively before. Most subjects are low-molecular-weight drug agents, biomolecules, and synthetic nanoparticles. The research on dendritic polyelectrolytes binding with proteins is mainly focused on polyamidoamine, however, some results show that it disturbs the secondary structure of the protein, which complicates the deviation of the binding affinity. Moreover, its binding mechanism with proteins is not clear until now. Thus a deep understanding of the driving forces for protein binding is of urgent demand. dPGS has high anti-inflammatory potential due to specific binding with L- and P-selectins. It has been explored in different areas of bioapplications such as therapeutics, diagnostics, and drug delivery. It is essential to study its interaction with native molecules, highly importantly proteins before further applications *in vivo*. Hence, dPGS was set as a model for dendritic polyelectrolyte to provide insight into the protein binding mechanism of the same sort.

Thermodynamic properties of protein complexation are important information for rational design of polyelectrolyte drug agents and carriers. The binding affinity and heat effect are most concerned properties. Here the interaction between dPGS and two model proteins, i.e. HSA and lysozyme were investigated by isothermal titration calorimetry combined with computer simulation. The two proteins are oppositely charged thus providing a good comparison in terms of electrostatic interaction. ITC is a powerful technique that reveals the stoichiometry, binding constant, and overall enthalpy change. Other quantities including binding free energy, heat capacity change, binding enthalpy, and binding entropy can also be derived accordingly. By varying the measuring condition, the dependence of all thermodynamic parameters on different factors gives indication on the determinants of the binding affinity and heat signal.

HSA with a net charge of -14 *e* at pH 7.4 is the most abundant serum protein and thus should be the first concern with dPGS. We measured the interaction with variants: temperature, ionic strength, and polymer size by ITC. Notably, the secondary structure of HSA in the presence of dPGS-G2 remained stable according to circular dichroism. Thus conformational change was ruled out in the contribution to the binding affinity. At 310 K and 150 mM ionic strength, the heat signal was too weak to be detected by

ITC. Molecular dynamics simulation also obtained very low affinity of -3.7 k_BT, which demonstrated that dPGS barely bound with HSA at physiological condition. At low salt concentration c_s=25 mM, dPGS bound to the positive site Sudlow II on HSA and the stoichiometry increased with polymer size. Namely, dPGS-G2, -G4, and -G5.5 absorbed 1, 2, and 4 proteins, respectively. The binding constant K_b decreased from 10^5 M^{-1} for -G2 to 10^3 M^{-1} for -G5.5 due to increasing electrostatic repulsion with polymer size. Interestingly, the measured enthalpy by ITC increased dramatically from negative to positive with temperature. All three dPGS-HSA complexes showed a large heat capacity change $\Delta C_{p,cal}$ of $\sim$8 kJ/(mol K). On the contrary, the binding free energy was stable with temperature. MD simulation with implicit water obtained comparable binding affinities for dPGS-G2 and the temperature dependence was again weak. The good agreement between experiments and simulations demonstrated that the binding was totally governed by electrostatics. Hydration effects had no contribution. Furthermore, ITC measured the binding constant K_b of dPGS-G2 at different ionic strengths. K_b decreased with salt, which followed the Record-Lohman relation, and thus led to the strength of counterion-release. ca. 4 released counterions brought an entropy gain to the system, which was the major part of electrostatic contributions to the binding free energy. The effect of counterion-release was temperature-independent, thus the binding free energy was slightly changed with temperature. Its temperature dependence led to binding enthalpy and entropy via the van't Hoff analysis. Both quantities changed largely with temperature and the corresponding heat capacity change $\Delta C_{p,vH}$ was of the similar magnitude ($\sim$6 kJ/(mol K)) with ITC result. Hence, the enthalpy-entropy compensation in our system was strong and practically total. All hydration contributions to the enthalpy were canceled out by a concomitant entropy contribution with the opposite sign.

Lysozyme with a net charge of +8 e at pH 7.4 is a good comparison to the negative HSA. Besides, its spherical shape and low molecular weight makes it easier for coarse-grained simulation and even atomistic simulation. The interaction between lysozyme and dPGS-G2, -G4, -G4.5, -G5.5 were investigated in MOPS buffer at 310 K by ITC. The binding number increased with polymer size as in the case of HSA. The binding constant was much higher than HSA due to electrostatic attraction. Surprisingly, K_b for all the dPGS at 10 mM ionic strength were in the similar scale of 10^8 M^{-1} according to experiments. Measurements on the electrophoretic mobility of dPGS showed that

the surface potential was stable even with increasing size and total charge. The binding affinities obtained by MD simulation agreed with the experimental results. Hence, for this hydrophilic polyelectrolyte electrostatic factors were responsible for binding while no hydrophobic contributions were involved. K_b for dPGS-G2 at different ionic strengths was measured, and the number of released counterions Δn_{ci} was obtained to be $\sim$3 which agreed with MD simulations. The corresponding entropy gain occupied more than 60% of the total free energy of binding. MD simulations demonstrated that Coulomb interaction provided the rest driving force. Δn_{ci} for other dPGS were also obtained by simulation. We found that for higher generations the entropy gain of counterion-release was also the dominant driving force for binding. The Gibbs free energy of binding weakly depended on polymer size (total charge) mainly due to two reasons: on the one hand, the effective charge density of dPGS renormalized by counterion condensation was stable for all dPGS, which led to a weak size dependence of the Coulomb interaction. On the other hand, the number of released ions only depended on the protein binding site so that the corresponding entropy gain was similar for dPGS of different sizes. The binding affinity of dPGS to L- and E-selectins was then compared in simulations. L-selectin with positive patch bound to dPGS with high affinity. Weak generation dependence of the Gibbs free energy was found and counterion-release entropy was again the major driving force. Besides, the coarse-grained simulation and atomistic simulation gave the same number of released ions and complex structure. E-selectin without positive patch did not bind with dPGS. With that, the selectivity on selectins and binding mechanism of dPGS was fully understood.

Then a systematic thermodynamic study was performed on the complexation of dPGS-G2 with lysozyme. The part above was done at a single temperature. Here the interaction was focused on one polymer and performed at six different ionic strengths each with seven temperatures. The aim was to discriminate the role of electrostatics from hydration effects at various conditions. Phosphate buffer was chosen so that the pH was stable with temperature. The salt dependence of K_b revealed the number of released counterions Δn_{ci} $\sim$3 the same as in MOPS. Δn_{ci} was found independent of temperature so that the entropy gain had a linear and weak dependence on T. At all the measured ionic strengths from 25 mM to 150 mM, the Gibbs free energy changed weakly with temperature. Van't Hoff analysis gave the binding enthalpy and entropy, which varied

largely with T showing strong enthalpy-entropy compensation over the entire range of salt concentrations. Different from HSA, here the heat capacity change $\Delta C_{\mathrm{p,vH}}$ was negative and $\Delta C_{\mathrm{p,cal}}$ was measured to be positive. Accordingly, the binding enthalpy ΔH_{vH} deviated largely from the calorimetric ΔH_{cal} indicating linked heat effects apart from binding. Combining the results from last part in MOPS buffer, ΔH_{cal} measured in two buffer solutions with different dissociation enthalpies indicated the occurrence of buffer deprotonation. Concomitantly, the released protons by the buffer were taken by protein residues at the binding site. The derived heat of protein protonation was in the similar magnitude as reported in literature, which demonstrated the contributions of linked equilibria in the measured overall enthalpy as well as heat capacity change.

In summary, we demonstrated that in the studied range of temperature and ionic strength the complexation of the two proteins with highly charged dendritic polyglycerol sulfate was wholly driven by electrostatics. The binding affinity was mainly determined by the released counterions of dPGS from the binding interface. dPGS did not disturb the structure of the protein so that conformational change was not involved in the binding mechanism. Hydration effects contributed to binding enthalpy and entropy, but they compensated each other and had no contribution in the Gibbs free energy. Linked equilibria in the binding mixture such as buffer/protein deprotonation/protonation also contributed to the overall heat effect, therefore the calorimetric enthalpy should not be taken as a measure for the strength of complexation.

Electrostatic interaction and hydrophobic interaction are regarded as the major driving forces for protein-polyelectrolyte binding. Experiments at various ionic strength and temperature estimate the role of electrostatics and water molecules in the thermodynamic properties. By the combination of ITC experiments with computer simulations, it is allowed to compare the contribution of electrostatics to the total free energy of binding and also give the complex structure. Thus, it is sufficient to reveal the binding mechanism with this approach. For our dPGS system and other structures where electrostatics is the driving force, computer simulation can be further applied to predict their binding affinity with related meaningful proteins for the sake of time and cost.

The conclusions here give insight to drug design of polyelectrolytes. Yet many questions are not fully resolved. The hydrophobicity of protein binding site is a crucial factor for the binding enthalpy and enthalpy-entropy compensation, whereas the hydra-

tion/dehydration of the residues is not clear yet. Accurate information can be obtained by atomistic simulation with explicit water, however, it is time-consuming to simulate big molecules in the box with water and the calculation of hydration/dehydration enthalpy is still under debate. Also the application of conclusions from this work to other drugs than highly charged hydrophilic agents requires further consideration. The dPGS used here were fully sulfated, while it is possible to prepare with different sulfation degrees for other applications. The influence of charge density on the concentration of condensed counterions and the effective charge of the polymer should be carefully considered for binding. Moreover, hydrophobic effect may become one of the driving forces for other dPGS derivatives and dendrimers with a hydrophobic scaffold.

5 Abstract

Here we investigate the interaction between proteins and dendritic polyglycerol sulfate with anti-inflammatory potential by ITC. The thermodynamic parameters of the complexation were measured to reveal the driving forces by varying temperature, ionic strength, and polymer size. Firstly, the binding enthalpy and entropy between human serum albumin and dPGS changed drastically with temperature without evident disturbance of the secondary structure. ITC experiments and MD simulations with implicit water agreed on the binding affinity, which demonstrated that the binding was totally governed by electrostatics, mainly, counterion-release. Thus the binding affinity was stable with temperature accompanied by strong enthalpy-entropy compensation.

Secondly, lysozyme with positive net charge showed high binding affinity to dPGS at low salt concentration. The binding number increased with the polymer size, whereas the binding affinity showed only a weak dependence due to similar effective charge densities of different dPGS renormalized by counterion condensation. Here again the binding was driven by electrostatics, mainly by counterion-release and the number of released ions determined by the interface at the protein binding site increased very slightly with the polymer size. The binding mechanism was found the same for dPGS with L-selectin. The number of released counterions was temperature-independent, thus the corresponding entropy gain increased slightly with temperature. The binding enthalpy was found largely different from the calorimetric enthalpy due to linked equilibria, i.e. buffer ionization and protein protonation, which contributed to the observed overall enthalpy and heat capacity change.

In all, this work demonstrated that the binding of hydrophilic dPGS with two different proteins was purely driven by electrostatics. Counterion-release from the dPGS surface was the major driving force. Hydration effects brought change to the binding enthalpy and entropy at different conditions; however, they compensated each other and thus did not contribute to the Gibbs free energy of binding. The discrepancy between the binding enthalpy and measured calorimetric enthalpy was originated from the linked equilibria in the binding mixture.

6 Kurzzusammenfassung

In dieser Arbeit wurde die Interaktion zwischen Proteinen und dendritischem poly glycerinsulfat mit entzündungshemmendem Potential mittels ITC untersucht. Die thermodynamischen Eigenschaften der Bindungskomplexe wurden durch Variation der Temperatur, Ionenstärke und Polymergröße bestimmt, um die Triebkräfte zu identifizieren. Dabei ändern sich zunächst Bindungsenthalpie und -entropie von dPGS zu Humanalbumin sehr stark mit der Temperatur ohne sichtbare Störung der Sekundärstruktur. Die mittels ITC bestimmte freie Bindungsenergie stimmt hierbei mit der durch MD Simulation unter Einbezug von Wasser ermittelten überein. Dies zeigt, dass die Bindung von elektrostatischen Effekten, hauptsächlich von der Freisetzung von Gegenionen, bestimmt wird. Folglich ist die freie Bindungsenergie gegen die Temperatur konstant, begleitet von starken Enthalpie-Entropie Kompensation.

Des Weiteren zeigt Lysozym mit positiver Nettoladung eine hohe Bindungsaffinität zu dPGS bei niedrigen Salzkonzentrationen. Die Koordinationszahl steigt mit der Polymergröße, während die freie Bindungsenergie nur eine schwache Abhängigkeit zeigt. Grund hierfür ist die Kondensation der Gegenionen auf den dPGS-Molekülen, die zu eine vergleichbaren Oberflächenladungsdichte bei allen Generationen führt. Auch hier wurde die Bindung durch Elektrostatik dominiert, hauptsächlich durch Freisetzung von Gegenionen und weil die Anzahl freigesetzter Ionen, die durch die Grenzfläche an der Bindungsstelle des Proteins bestimmt wird, sich mit der Polymergröße leicht erhöht. Für dPGS mit L-Selektin konnte hierbei derselbe Bindungsmechanismus identifiziert werden. Die Anzahl freigesetzter Gegenionen ist nicht temperaturabhängig, wodurch sich der zugehörige Entropiegewinn mit der Temperatur leicht erhöht. Wegen der gekoppelten Gleichgewichte, d.h. wegen der Ionisierung des Puffers und der Protonierung des Proteins, welche zur beobachteten Gesamtenthalpie und zur Änderung der Wärmekapazität beitragen, weicht die Bindungsenthalpie stark von der kalorimetrischen Enthalpie ab.

Zusammengefasst konnte gezeigt werden, dass die Bindung von hydrophilem dPGS mit zwei Proteinen rein elektrostatischer Natur ist. Dabei war die Freisetzung von Gegenionen von der dPGS Oberfläche die vorherrschende Triebkraft. Die Bindungsenthalpie und –entropie variiert aufgrund von Hydratationseffekten unter verschiedenen Bedingungen; dabei kompensieren sich jedoch die Änderungen von Enthalpie und

Entropie und tragen deshalb nicht zur freien Bindungsenergie bei. Die Diskrepanz zwischen Bindungsenthalpie und kalorimetrisch gemessener Enthalpie ergibt sich aus den gekoppelten Gleichgewichten in der Bindungsmischung.

7 References

[1] Jenkins, A.; Kratochvil, P.; Stepto, R.; Suter, U. *Pure Appl. Chem.* **1996**, *68*, 2287–2311.

[2] Cox, M. M.; Nelson, D. L. *Lehninger principles of biochemistry.*; WH Freeman, 2008.

[3] Chuang, Y.-J.; Swanson, R.; Raja, S. M.; Olson, S. T. *J. Biol. Chem.* **2001**, *276*, 14961–14971.

[4] Xiong, W.; Ren, C.; Tian, M.; Yang, X.; Li, J.; Li, B. *Food Hydrocolloids* **2017**, *73*, 41–50.

[5] Giri, J.; Diallo, M. S.; Simpson, A. J.; Liu, Y.; Goddard III, W. A.; Kumar, R.; Woods, G. C. *ACS Nano* **2011**, *5*, 3456–3468.

[6] Becker, A. L.; Welsch, N.; Schneider, C.; Ballauff, M. *Biomacromolecules* **2011**, *12*, 3936–3944.

[7] Welsch, N.; Becker, A. L.; Dzubiella, J.; Ballauff, M. *Soft Matter* **2012**, *8*, 1428–1436.

[8] Wang, S.; Chen, K.; Li, L.; Guo, X. *Biomacromolecules* **2013**, *14*, 818–827.

[9] Khandare, J.; Calderón, M.; Dagia, N. M.; Haag, R. *Chem. Soc. Rev.* **2012**, *41*, 2824–2848.

[10] Camarada, M.; Márquez-Miranda, V.; Araya-Durán, I.; Yévenes, A.; González-Nilo, F. *Phys. Chem. Chem. Phys.* **2015**, *17*, 19001–19011.

[11] Zhu, J.; Xiong, Z.; Shen, M.; Shi, X. *RSC Adv.* **2015**, *5*, 30286–30296.

[12] Manning, G. S. *J. Chem. Phys.* **1969**, *51*, 924–933.

[13] Manning, G. S. *J. Chem. Phys.* **1969**, *51*, 934–938.

[14] Huang, Q.; Dubin, P.; Moorefield, C.; Newkome, G. *J. Phys. Chem. B* **2000**, *104*, 898–904.

[15] Gurtovenko, A. A.; Lyulin, S. V.; Karttunen, M.; Vattulainen, I. *J. Chem. Phys.* **2006**, *124*, 094904.

[16] Chen, W.-R.; Porcar, L.; Liu, Y.; Butler, P. D.; Magid, L. J. *Macromolecules* **2007**, *40*, 5887–5898.

[17] Karatasos, K.; Krystallis, M. *J. Chem. Phys.* **2009**, *130*, 114903.

[18] Harries, D.; May, S.; Ben-Shaul, A. *Soft Matter* **2013**, *9*, 9268–9284.

[19] Minsky, B. B.; Atmuri, A.; Kaltashov, I. A.; Dubin, P. L. *Biomacromolecules* **2013**, *14*, 1113–1121.

[20] Xu, X.; Ran, Q.; Haag, R.; Ballauff, M.; Dzubiella, J. *Macromolecules* **2017**, *50*, 4759–4769.

[21] Iwasa, K. *J. Phys. Chem.* **1977**, *81*, 1829–1833.

[22] Manning, G. S. *J. Phys. Chem.* **1981**, *85*, 1506–1515.

[23] Garcia-Fernandez, E.; Paulo, P. M. *J. Phys. Chem. Lett.* **2014**, *5*, 1472–1478.

[24] Böhme, U.; Scheler, U. *Adv. Colloid Interface Sci.* **2010**, *158*, 63–67.

[25] Liu, Y.; Porcar, L.; Hong, K.; Shew, C.-Y.; Li, X.; Liu, E.; Butler, P. D.; Herwig, K. W.; Smith, G. S.; Chen, W.-R. *J. Chem. Phys.* **2010**, *132*, 124901.

[26] Ohshima, A.; Konishi, T.; Yamanaka, J.; Ise, N. *Phys. Rev. E* **2001**, *64*, 051808.

[27] Wu, B.; Chen, W.-R.; Egami, T.; Li, X.; Liu, Y.; Wang, Y.; Do, C.; Porcar, L.; Hong, K.; Liu, L.; Smith, G. S.; Smith, S. C. *J. Chem. Phys.* **2012**, *137*, 064902.

[28] Porcar, L.; Liu, Y.; Hong, K.; Butler, P. D.; Huang, E.-W.; Chen, W.-R. **2009**, *279*, 65–71.

[29] Paulo, P. M.; Lopes, J. N. C.; Costa, S. M. *J. Phys. Chem. B* **2007**, *111*, 10651–10664.

[30] Maiti, P. K.; Messina, R. *Macromolecules* **2008**, *41*, 5002–5006.

[31] Lee, I.; Athey, B. D.; Wetzel, A. W.; Meixner, W.; Baker, J. R. *Macromolecules* **2002**, *35*, 4510–4520.

[32] Maiti, P. K.; ÇaÇğın, T.; Lin, S.-T.; Goddard, W. A. *Macromolecules* **2005**, *38*, 979–991.

[33] Ibrahim, A.; Koval, D.; Kašička, V.; Faye, C.; Cottet, H. *Macromolecules* **2012**, *46*, 533–540.

[34] Tang, M. X.; Redemann, C. T.; Szoka, F. C. *Bioconjugate Chem.* **1996**, *7*, 703–714.

[35] Maiti, P. K.; Bagchi, B. *Nano Lett.* **2006**, *6*, 2478–2485.

[36] Vasumathi, V.; Maiti, P. K. *Macromolecules* **2010**, *43*, 8264–8274.

[37] Tomalia, D. A.; Naylor, A. M.; Goddard, W. A. *Angew. Chem. Int. Ed.* **1990**, *29*, 138–175.

[38] Murat, M.; Grest, G. S. *Macromolecules* **1996**, *29*, 1278–1285.

[39] Timoshenko, E. G.; Kuznetsov, Y. A.; Connolly, R. *J. Chem. Phys.* **2002**, *117*, 9050–9062.

[40] Ballauff, M.; Likos, C. N. *Angew. Chem. Int. Ed.* **2004**, *43*, 2998–3020.

[41] Tomalia, D. A. *New J. Chem.* **2012**, *36*, 264–281.

[42] Lee, C. C.; MacKay, J. A.; Fréchet, J. M.; Szoka, F. C. *Nat. Biotechnol.* **2005**, *23*, 1517.

[43] Dernedde, J.; Rausch, A.; Weinhart, M.; Enders, S.; Tauber, R.; Licha, K.; Schirner, M.; Zügel, U.; von Bonin, A.; Haag, R. *Proc. Natl. Acad. Sci.* **2010**, *107*, 19679–19684.

[44] Cheng, Y.; Zhao, L.; Li, Y.; Xu, T. *Chem. Soc. Rev.* **2011**, *40*, 2673–2703.

[45] Kannan, R.; Nance, E.; Kannan, S.; Tomalia, D. *J. Intern. Med.* **2014**, *276*, 579–617.

[46] Pourianazar, N. T.; Mutlu, P.; Gunduz, U. *J. Nanopart. Res.* **2014**, *16*, 2342.

[47] Maysinger, D.; Gröger, D.; Lake, A.; Licha, K.; Weinhart, M.; Chang, P. K.-Y.; Mulvey, R.; Haag, R.; McKinney, R. A. *Biomacromolecules* **2015**, *16*, 3073–3082.

[48] Sousa-Herves, A.; Würfel, P.; Wegner, N.; Khandare, J.; Licha, K.; Haag, R.; Welker, P.; Calderón, M. *Nanoscale* **2015**, *7*, 3923–3932.

[49] Bugno, J.; Hsu, H.-j.; Hong, S. *Biomater. Sci.* **2015**, *3*, 1025–1034.

[50] Khandare, J.; Mohr, A.; Calderón, M.; Welker, P.; Licha, K.; Haag, R. *Biomaterials* **2010**, *31*, 4268–4277.

[51] Sunder, A.; Hanselmann, R.; Frey, H.; Mülhaupt, R. *Macromolecules* **1999**, *32*, 4240–4246.

[52] Haag, R.; Sunder, A.; Stumbé, J.-F. *J. Am. Chem. Soc.* **2000**, *122*, 2954–2955.

[53] Türk, H.; Haag, R.; Alban, S. *Bioconjugate Chem.* **2004**, *15*, 162–167.

[54] Weinhart, M.; Gröger, D.; Enders, S.; Riese, S. B.; Dernedde, J.; Kainthan, R. K.; Brooks, D. E.; Haag, R. *Macromol. Biosci.* **2011**, *11*, 1088–1098.

[55] Paulus, F.; Steinhilber, D.; Welker, P.; Mangoldt, D.; Licha, K.; Depner, H.; Sigrist, S.; Haag, R. *Polym. Chem.* **2014**, *5*, 5020–5028.

[56] Weinhart, M.; Gröger, D.; Enders, S.; Dernedde, J.; Haag, R. *Biomacromolecules* **2011**, *12*, 2502–2511.

[57] Boreham, A.; Pikkemaat, J.; Volz, P.; Brodwolf, R.; Kuehne, C.; Licha, K.; Haag, R.; Dernedde, J.; Alexiev, U. *Molecules* **2015**, *21*, 22.

[58] Schneider, T.; Welker, P.; Licha, K.; Haag, R.; Schulze-Tanzil, G. *BMC musculoskeletal disorders* **2015**, *16*, 387.

[59] Schneider, T.; Welker, P.; Haag, R.; Dernedde, J.; Hug, T.; Licha, K.; Kohl, B.; Arens, S.; Ertel, W.; Schulze-Tanzil, G. *Inflamm. Res.* **2015**, *64*, 917–928.

[60] Zhong, Y.; Dimde, M.; Stöbener, D.; Meng, F.; Deng, C.; Zhong, Z.; Haag, R. *ACS Appl. Mater. Interfaces* **2016**, *8*, 27530–27538.

[61] Vonnemann, J.; Sieben, C.; Wolff, C.; Ludwig, K.; Böttcher, C.; Herrmann, A.; Haag, R. *Nanoscale* **2014**, *6*, 2353–2360.

[62] Vonnemann, J.; Liese, S.; Kuehne, C.; Ludwig, K.; Dernedde, J.; Böttcher, C.; Netz, R. R.; Haag, R. *J. Am. Chem. Soc.* **2015**, *137*, 2572–2579.

[63] Miura, N.; Dubin, P. L.; Moorefield, C.; Newkome, G. *Langmuir* **1999**, *15*, 4245–4250.

[64] De Luca, S.; Chen, F.; Seal, P.; Stenzel, M. H.; Smith, S. C. *Biomacromolecules* **2017**, *18*, 3665–3677.

[65] Nelson, D. L.; Lehninger, A. L.; Cox, M. M. *Lehninger principles of biochemistry*; Macmillan, 2008.

[66] Giehm, L.; Christensen, C.; Boas, U.; Heegaard, P. M.; Otzen, D. E. *Biopolymers* **2008**, *89*, 522–529.

[67] Moss, J. M.; Van Damme, M.-P. I.; Murphy, W. H.; Preston, B. N. *Arch. Biochem. Biophys.* **1997**, *348*, 49–55.

[68] Hattori, T.; Hallberg, R.; Dubin, P. L. *Langmuir* **2000**, *16*, 9738–9743.

[69] Marky, N. L.; Manning, G. S. *J. Am. Chem. Soc.* **2000**, *122*, 6057–6066.

[70] Seyrek, E.; Dubin, P. L.; Tribet, C.; Gamble, E. A. *Biomacromolecules* **2003**, *4*, 273–282.

[71] Bowman, W.; Rubinstein, M.; Tan, J. *Macromolecules* **1997**, *30*, 3262–3270.

[72] Steuber, H.; Heine, A.; Klebe, G. *J. Mol. Biol.* **2007**, *368*, 618–638.

[73] Carlsson, F.; Linse, P.; Malmsten, M. *J. Phys. Chem. B* **2001**, *105*, 9040–9049.

[74] Latt, S. A.; Sober, H. A. *Biochemistry* **1967**, *6*, 3293–3306.

[75] Riggs, A. D.; Bourgeois, S.; Cohn, M. *J. Mol. Biol.* **1970**, *53*, 401–417.

[76] Riggs, A. D.; Suzuki, H.; Bourgeois, S. *J. Mol. Biol.* **1970**, *48*, 67–83.

[77] Poliakow, M.; Champagne, M.; Daune, M. *Eur. J. Biochem.* **1972**, *26*, 212–219.

[78] Bujalowski, W.; Lohman, T. M. *J. Mol. Biol.* **1989**, *207*, 269–288.

[79] Yang, C.-C.; Huang, Y.-C.; Chen, C.-Y.; Su, C.-J.; Chen, H.-L.; Ivanov, V. A. *Macromolecules* **2014**, *47*, 3117–3127.

[80] Record, M. T.; Lohman, T. M.; De Haseth, P. *J. Mol. Biol.* **1976**, *107*, 145–158.

[81] Record, M. T.; Anderson, C. F.; Lohman, T. M. *Q. Rev. Biophys.* **1978**, *11*, 103–178.

[82] Mascotti, D. P.; Lohman, T. M. *Proc. Natl. Acad. Sci.* **1990**, *87*, 3142–3146.

[83] Fried, M. G.; Stickle, D. F. *FEBS J.* **1993**, *218*, 469–475.

[84] Waldron, T. T.; Schrift, G. L.; Murphy, K. P. *J. Mol. Biol.* **2005**, *346*, 895–905.

[85] Overman, L. B.; Bujalowski, W.; Lohman, T. M. *Biochemistry* **1988**, *27*, 456–471.

[86] He, S.-z.; Merlitz, H.; Sommer, J.-U.; Wu, C.-X. *Eur. Phys. J. E* **2015**, *38*, 101.

[87] Henzler, K.; Haupt, B.; Lauterbach, K.; Wittemann, A.; Borisov, O.; Ballauff, M. *J. Am. Chem. Soc.* **2010**, *132*, 3159–3163.

[88] Kyte, J. *Biophys. Chem.* **2002**, *100*, 193–203.

[89] Chen, W.-Y.; Huang, H.-M.; Lin, C.-C.; Lin, F.-Y.; Chan, Y.-C. *Langmuir* **2003**, *19*, 9395–9403.

[90] Chandler, D. *Nature* **2005**, *437*, 640–647.

[91] Dill, K. A.; Truskett, T. M.; Vlachy, V.; Hribar-Lee, B. *Annu. Rev. Biophys. Biomol. Struct.* **2005**, *34*, 173–199.

[92] Sedlmeier, F.; Horinek, D.; Netz, R. R. *J. Chem. Phys.* **2011**, *134*, 02B604.

[93] Freire, E. *Chem. Biol. Drug Des.* **2009**, *74*, 468–472.

[94] Martin, S. F.; Clements, J. H. *Annu. Rev. Biochem.* **2013**, *82*, 267–293.

[95] Glas, A.; Bier, D.; Hahne, G.; Rademacher, C.; Ottmann, C.; Grossmann, T. N. *Angew. Chem. Int. Ed.* **2014**, *53*, 2489–2493.

[96] Biela, A.; Sielaff, F.; Terwesten, F.; Heine, A.; Steinmetzer, T.; Klebe, G. *J. Med. Chem.* **2012**, *55*, 6094–6110.

[97] Klebe, G. *Nat. Rev. Drug Discov.* **2015**, *14*, 95–110.

[98] Cooper, C.; Dubin, P.; Kayitmazer, A.; Turksen, S. *Curr. Opin. Colloid Interface Sci.* **2005**, *10*, 52–78.

[99] Wienken, C. J.; Baaske, P.; Rothbauer, U.; Braun, D.; Duhr, S. *Nat. Commun.* **2010**, *1*, 100.

[100] Kayitmazer, A. B.; Seeman, D.; Minsky, B. B.; Dubin, P. L.; Xu, Y. *Soft Matter* **2013**, *9*, 2553–2583.

[101] Froehlich, E.; Mandeville, J.; Jennings, C.; Sedaghat-Herati, R.; Tajmir-Riahi, H. *J. Phys. Chem. B* **2009**, *113*, 6986–6993.

[102] Sekowski, S.; Buczkowski, A.; Palecz, B.; Gabryelak, T. *Spectrochim. Acta A* **2011**, *81*, 706–710.

[103] Ciolkowski, M.; Pałecz, B.; Appelhans, D.; Voit, B.; Klajnert, B.; Bryszewska, M. *Colloids Surf. B* **2012**, *95*, 103–108.

[104] Zhang, H.-M.; Lou, K.; Cao, J.; Wang, Y.-Q. *Langmuir* **2014**, *30*, 5536–5544.

[105] Szwed, A.; Milowska, K.; Ionov, M.; Shcharbin, D.; Moreno, S.; Gomez-Ramirez, R.; de la Mata, F.; Majoral, J.; Bryszewska, M.; Gabryelak, T. *RSC Adv.* **2016**, *6*, 97546–97554.

[106] Lindman, S.; Lynch, I.; Thulin, E.; Nilsson, H.; Dawson, K. A.; Linse, S. *Nano Lett.* **2007**, *7*, 914–920.

[107] Chanphai, P.; Froehlich, E.; Mandeville, J.; Tajmir-Riahi, H. *Colloids Surf. B* **2017**, *150*, 168–174.

[108] Haynie, D. T. *Biological thermodynamics*; Cambridge University Press, 2001; pp 73–100.

[109] Klajnert, B.; Stanisławska, L.; Bryszewska, M.; Pałecz, B. *Biochim. Biophys. Acta* **2003**, *1648*, 115–126.

[110] Mahtab, R.; Harden, H. H.; Murphy, C. J. *J. Am. Chem. Soc.* **2000**, *122*, 14–17.

[111] Yu, S.; Xu, X.; Yigit, C.; van der Giet, M.; Zidek, W.; Jankowski, J.; Dzubiella, J.; Ballauff, M. *Soft Matter* **2015**, *11*, 4630–4639.

[112] Kozlov, A. G.; Lohman, T. M. *J. Mol. Biol.* **1998**, *278*, 999–1014.

[113] Olsson, T. S.; Williams, M. A.; Pitt, W. R.; Ladbury, J. E. *J. Mol. Biol.* **2008**, *384*, 1002–1017.

[114] Yigit, C.; Welsch, N.; Ballauff, M.; Dzubiella, J. *Langmuir* **2012**, *28*, 14373–14385.

[115] Ladbury, J. E. *Chem. & Biol.* **1996**, *3*, 973–980.

[116] Niedzwiecka, A.; Stepinski, J.; Darzynkiewicz, E.; Sonenberg, N.; Stolarski, R. *Biochemistry* **2002**, *41*, 12140–12148.

[117] Datta, K.; LiCata, V. J. *Nucleic Acids Res.* **2003**, *31*, 5590–5597.

[118] Datta, K.; Wowor, A. J.; Richard, A. J.; LiCata, V. J. *Biophys. J.* **2006**, *90*, 1739–1751.

[119] Evans, D. F.; Wennerstrom, H. *Colloidal domain*; Wiley-Vch, 1999; pp 279–286.

[120] Liu, C.-C.; Richard, A. J.; Datta, K.; LiCata, V. J. *Biophys. J.* **2008**, *94*, 3258–3265.

[121] Becktel, W. J.; Schellman, J. A. *Biopolymers* **1987**, *26*, 1859–1877.

[122] Motono, C.; Oshima, T.; Yamagishi, A. *Protein Eng.* **2001**, *14*, 961–966.

[123] Lee, C.-F.; Allen, M. D.; Bycroft, M.; Wong, K.-B. *J. Mol. Biol.* **2005**, *348*, 419–431.

[124] Brown, H. S.; LiCata, V. J. *Biochim. Biophys. Acta* **2013**, *1834*, 2133–2138.

[125] Deutschman, W. A.; Dahlquist, F. *Biochemistry* **2001**, *40*, 13107–13113.

[126] Liu, C.-C.; LiCata, V. J. *Proteins* **2014**, *82*, 785–793.

[127] Gallagher, K.; Sharp, K. *Biophys. J.* **1998**, *75*, 769–776.

[128] Silverstein, K. A.; Haymet, A.; Dill, K. A. *J. Am. Chem. Soc.* **1998**, *120*, 3166–3175.

[129] Mancera, R. L. *J. Phys. Chem. B* **1999**, *103*, 3774–3777.

[130] Lukšič, M.; Urbic, T.; Hribar-Lee, B.; Dill, K. A. *J. Phys. Chem. B* **2012**, *116*, 6177–6186.

[131] Loladze, V. V.; Ermolenko, D. N.; Makhatadze, G. I. *Protein Sci.* **2001**, *10*, 1343–1352.

[132] Naghibi, H.; Tamura, A.; Sturtevant, J. M. *Proc. Natl. Acad. Sci.* **1995**, *92*, 5597–5599.

[133] Horn, J. R.; Russell, D.; Lewis, E. A.; Murphy, K. P. *Biochemistry* **2001**, *40*, 1774–1778.

[134] Geschwindner, S.; Ulander, J.; Johansson, P. *J. Med. Chem.* **2015**, *58*, 6321–6335.

[135] Baker, B. M.; Murphy, K. P. *Biophys. J.* **1996**, *71*, 2049–2055.

[136] Kozlov, A. G.; Lohman, T. M. *Proteins* **2000**, *41*, 8–22.

[137] Kozlov, A. G.; Lohman, T. M. *Biochemistry* **1999**, *38*, 7388–7397.

[138] Fukada, H.; Takahashi, K. *Proteins* **1998**, *33*, 159–166.

[139] Ferenczy, G. G.; Keserű, G. M. *Drug Discov. Today* **2010**, *15*, 919–932.

[140] Reynolds, C. H.; Holloway, M. K. *ACS Med. Chem. Lett.* **2011**, *2*, 433–437.

[141] Ladbury, J. E.; Klebe, G.; Freire, E. *Nat. Rev. Drug Discov.* **2010**, *9*, 23–27.

[142] Cooper, A.; Johnson, C. M.; Lakey, J. H.; Nöllmann, M. *Biophys. Chem.* **2001**, *93*, 215–230.

[143] Talhout, R.; Villa, A.; Mark, A. E.; Engberts, J. B. *J. Am. Chem. Soc.* **2003**, *125*, 10570–10579.

[144] Lafont, V.; Armstrong, A. A.; Ohtaka, H.; Kiso, Y.; Mario Amzel, L.; Freire, E. *Chem. Biol. Drug Des.* **2007**, *69*, 413–422.

[145] Lumry, R.; Rajender, S. *Biopolymers* **1970**, *9*, 1125–1227.

[146] Dunitz, J. D. *Chem. Biol.* **1995**, *2*, 709–712.

[147] Ford, D. M. *J. Am. Chem. Soc.* **2005**, *127*, 16167–16170.

[148] Brandt, T.; Holzmann, N.; Muley, L.; Khayat, M.; Wegscheid-Gerlach, C.; Baum, B.; Heine, A.; Hangauer, D.; Klebe, G. *J. Mol. Biol.* **2011**, *405*, 1170–1187.

[149] Breiten, B.; Lockett, M. R.; Sherman, W.; Fujita, S.; Al-Sayah, M.; Lange, H.; Bowers, C. M.; Heroux, A.; Krilov, G.; Whitesides, G. M. *J. Am. Chem. Soc.* **2013**, *135*, 15579–15584.

[150] Chodera, J. D.; Mobley, D. L. *Annu. Rev. Biophys.* **2013**, *42*, 121–142.

[151] Olano, L. R.; Rick, S. W. *J. Am. Chem. Soc.* **2004**, *126*, 7991–8000.

[152] Liang, Y. *Acta Biochim. Biophys. Sin.* **2008**, *40*, 565–576.

[153] Huang, R.; Lau, B. L. *BBA General Subjects* **2016**, *1860*, 945–956.

[154] Wiseman, T.; Williston, S.; Brandts, J. F.; Lin, L.-N. *Anal. Biochem.* **1989**, *179*, 131–137.

[155] Fasano, M.; Curry, S.; Terreno, E.; Galliano, M.; Fanali, G.; Narciso, P.; Notari, S.; Ascenzi, P. *IUBMB Life* **2005**, *57*, 787–796.

[156] Woelke, A. L.; Kuehne, C.; Meyer, T.; Galstyan, G.; Dernedde, J.; Knapp, E.-W. *J. Phys. Chem. B* **2013**, *117*, 16443–16454.

[157] Xu, X.; Ran, Q.; Dey, P.; Nikam, R.; Haag, R.; Ballauff, M.; Dzubiella, J. *Biomacromolecules* **2018**, *19*, 409–416.

Appendix A

Publications and Presentations

Publications

Qidi Ran, Xiao Xu, Pradip Dey, Shun Yu, Yan Lu, Joachim Dzubiella, Rainer Haag*, Matthias Ballauff*. Interaction of human serum albumin with dendritic polyglycerol sulfate: Rationalizing the thermodynamics of binding. **2018** (Submitted).

Qidi Ran, Xiao Xu, Joachim Dzubiella, Rainer Haag*, Matthias Ballauff*. Thermodynamics of the binding of lysozyme to a dendritic polyelectrolyte: Counterion-release vs. hydration. **2018** (To be submitted).

Xiao Xu, **Qidi Ran**, Pradip Dey, Rohit Nikam, Rainer Haag, Matthias Ballauff, Joachim Dzubiella*. Counterion-release entropy governs the inhibition of serum proteins by polyelectrolyte drugs. *Biomacromolecules*, **2018**, 19 (2), 409-416.

Xiao Xu, **Qidi Ran**, Rainer Haag, Matthias Ballauff, Joachim Dzubiella*. Charged dendrimers revisited: Effective charge and surface potential of dendritic polyglycerol sulfate. *Macromolecules*, **2017**, 50 (12), 4759-4769.

Leixiao Yu, Chong Cheng, **Qidi Ran**, Christoph Schlaich, Paul-Ludwig Michael Noeske, Wenzhong Li, Qiang Wei*, Rainer Haag*. Bioinspired universal monolayer coatings by combining concepts from blood protein adsorption and mussel adhesion. *ACS Appl. Mater. Interfaces*, **2017**, 9 (7), 6624-6633.

Shilin Mei, Charl J. Jafta, Iver Lauerman, **Qidi Ran**, Martin Kärgell, Matthias Ballauff, Yan Lu*. Porous Ti_4O_7 particles with interconnected-pore structure as a high-efficiency polysulfide mediator for lithium-sulfur batteries. *Adv. Funct. Mater.*, **2017**, 27, 26.

Jie Cao, Charl J. Jafta, Jiang Gong, **Qidi Ran**, Xianzhong Lin, Roberto Félix, Re-

gan G. Wilks, Marcus Bär, Jiayin Yuan, Matthias Ballauff, Yan Lu*. Synthesis of dispersible mesoporous nitrogen-doped hollow carbon nanoplates with uniform hexagonal morphologies for supercapacitors. *ACS Appl. Mater. Interfaces*, **2016**, 8 (43), 29628-29636.

Oral Presentation

Qidi Ran, Matthias Ballauff, Rainer Haag
Interaction of hyperbranched polyglycerol sulfate with serum proteins
30th Conference of The European Colloid and Interface Society, Sep. 4-9 2016, Rome, Italy

Poster Presentations

Qidi Ran, Rainer Haag, Matthias Ballauff
Interaction of hyperbranched polyglycerol sulfate with proteins: calorimetry versus computer simulations
HVI Symposium on Multifunctional Biomaterials for Medicine, Nov. 27-29 2016, Berlin, Germany

Qidi Ran, Rainer Haag, Matthias Ballauff
Thermodynamics of dendritic polyglycerol sulfate binding with proteins
4th International Symposium of the Collaborative Research Center (SFB) 765 on "Multivalent Interactions of Pathogens with Biological Surfaces", Oct. 4-6 2017, Berlin, Germany

Appendix B

Curriculum Vitae

For the reason of privacy,
the CV is not included in the online version.